FONDO SOCIALE EUROPEO PROGRAMMA OPERATIVO NAZIONALE 2000/2006
"Ricerca Scientifica, Sviluppo Tecnologico, Alta Formazione"
Regioni dell'Obiettivo 1 – Misura III.4 - "Formazione superiore ed universitaria"

DOTTORATO DI RICERCA IN INGEGNERIA
CIVILE PER L'AMBIENTE ED IL TERRITORIO

Università degli Studi di Salerno

VIII Ciclo Nuova Serie (2006-2009)

TESI DI DOTTORATO

WAVE ACTION ON SHALLOW WATER AND APPLICATIONS TO COASTAL HAZARD

MARINA MONACO

Coordinatore del Dottorato
PROF. ING. RODOLFO M.A. NAPOLI

Relatore
PROF. ING. EUGENIO PUGLIESE CARRATELLI

Correlatore
PROF. ING. ENRICO FOTI

DOTT. ING. FABIO DENTALE

WAVE ACTION ON SHALLOW WATER
AND APPLICATIONS TO COASTAL HAZARD

Finito di stampare il 27/03/2010

CONTENTS

CONTENTS i

List of Symbols v
List of Abbreviations vii
List of Figures ix
List of Tables xiii

SOMMARIO xv
ABSTRACT xix
RESUME' xxiii
RESUMEN xxvii

ACKNOWLEDGEMENTS xxxi

ABOUT THE AUTHOR xxxiii

1 INTRODUCTION 1
1.1 Context and aim of study 1
1.2 Outline of the thesis 2

2 MODELING FLUID FLOW 5
2.1 Numerical methods 5
2.2 Turbulence 7
2.3 RANS Equations 10
2.4 Turbulence models 12
2.4.1 K-ε model 13
2.4.2 RNG model 15
2.4.3 Wall function 15
2.5 Free surface displacement 17
2.5.1 Volume-of-Fluid (VOF) Method 18
2.6 Boundary conditions 20

2.7 Numerical implementation 21
2.7.1 Grid based systems 21
2.7.2 Stability condition 23
2.7.3 Numerical Viscosities 23

3 NUMERICAL METHODOLOGY of RANS/VOF MODELS 25
3.1 General Description of RANS/VOF models 25
3.2 Procedure of Simulation 27
3.3 Wave generation 28
3.3.1 Generation of waves using wave description theory 29
3.3.2 Generation of waves using a wave maker 31

4 SIMULATION OF REGULAR WAVES ON BEACH 33
4.1 Validation of the numerical model 33
4.2 Numerical setup 35
4.3 VOF and TrueVOF methods 37
4.4 Comparison between wave makers 41
4.5 Convergence analysis on computational discretization 43
4.5.1 Spatial discretization 43
4.5.2 Temporal discretization 50
4.6 Convergence analysis on turbulence models 51
4.6.1 Characteristic length scale 53
4.6.2 Turbulence Models 56

5 WAVE PROPAGATION ANALYSIS 59
5.1 Spilling on long sloping beach 59
5.2 Stokes drift 65
5.3 Reflection and Seiching 66
5.4 Breaking: types and criteria 69
5.5 Evaluation of Run-Up Length 78

6 THE SCALE EFFECT....81
6.1 Hydraulic Similitude Theory....84
6.2 Limitations of Physical Modeling: the Scale Effects....85
6.3 The importance of scale effects on experimental results....86
6.4 Analysis on the scale effect....88

7 ENERGY AND MOMENTUM FLUX....99
7.1 General formulae for progressive waves....99
7.2 Wave energy for small amplitude theory....101
7.3 Numerical applications to non-breaking, breaking and reformed wave....104
7.4 Wave actions on a schematic structure....109

8 WAVE ACTION ON VERTICAL STRUCTURES....118
8.1 Hydraulic Pressures on Structures....118
8.2 Impact of Waves on Vertical Structures....123

9 CONCLUDING REMARKS....126

REFERENCES....130

APPENDIX I....139

LIST OF SYMBOLS

A	wave amplitude
C	propagation speed
C_g	group velocities
d	still water depth
E	mean wave energy density per unit horizontal area
e(t)	energy density
F	volume of fluid function
f	general function
Fe	energy flux
F_h	horizontal force per unit extension of wall
F_{qdm}	momentum flux
g	acceleration of gravity
h	local water depth
H	wave height
H_0	deep water wave height
H_s	significant wave height
K	turbulent kinetic energy
k	wave number
L	wave length
L_0	deep water wave length
m	slope
p	pressure
Q	volume flow rate
R	run-up
S_{ij}	radiation stress tensor
t	time in the physical domain
T	wave period
u	horizontal particle velocity along x axis
u'	turbulence velocity
<u>	averaged velocity

V	horizontal particle velocity along y axis
V_c	volume of the cell
V_w	volume of water inside a cell
w	vertical particle velocity
x	horizontal coordinate in the cross-shore direction
y	horizontal coordinate in the long-shore direction
z	vertical coordinate
γ_b	breaking parameter
$\Delta x, \Delta y, \Delta z$	grid size
$\mathcal{K}$	Turbulent Kinetic Energy
ε	Turbulent Kinetic Energy Dissipation Rate
η	surface elevation with respect to the mean level
η^*	Kolmogorov length scale
θ	slope angle
λ	geometrical scale
μ	dynamic viscosity
ν	kinematic viscosity
ν_t	turbulent kinematic viscosity
ξ	surf similarity parameter
$\xi(t)$	wave-maker displacement
ϱ	water density
φ	phase shift angle
Φ	velocity potential
ω	wave frequency

LIST OF ABBREVIATIONS

CFD	Computational Fluid Dynamics
CFL	Courant-Friedrichs-Levy
DNS	Direct Numerical Simulation
FAVOR	Fractional Area/Volume Obstacle Representation
Fr	Froude Number
LES	Large Eddy Simulation
Ma	Mach Number
MAC	Marker And Cell
NS	Navier Stokes
RANS	Reynolds-Averaged Navier Stokes
Re	Reynolds Number
RNG	Renormalization-Group
SPH	Smoothed Particle Hydrodynamics
srfht	Surface height
SWL	Still water level
TKE	Turbulent Kinetic Energy
VOF	Volume-Of-Fluid
VPN	Virtual Private Networking
We	Weber Number

LIST OF FIGURES

Figure 2.1 : Energy cascade....9
Figure 2.2 : Approaches for the computation of turbulent flow....10
Figure 2.3 : Decomposition of a statistically stationary signal....11
Figure 2.4 : Decomposition of a not statistically stationary signal....11
Figure 2.5 : Wall bounded flow....16
Figure 2.6: Logarithmic velocity profile in a turbulent boundary layer....17
Figure 2.7: Free surface elevation as function of time....18
Figure 2.8: Typical values of the VOF function near free surface....19
Figure 2.9: Mesh arrangement and labeling convention....22
Figure 3.1: Location of variables in a mesh cell....26
Figure 3.2: Different types of wave generators....28
Figure 3.3: Schematic diagram showing a linear wave coming from a flat bottom reservoir on the right into the computational domain through the mesh boundary. 29
Figure 3.4: Wave generated by piston motion 32
Figure 4.1: General numerical set-up 33
Figure 4.2: Experimental images from Ting & Kirby (1996): a) spilling; b) plunging....34
Figure 4.3: Correlation between numerical and experimental wave heights at different probes....34
Figure 4.4: Comparison between instantaneous water height η, from experimental data, FLOW-3D numerical results and 2D SPH (from De Padova 2008a)....35
Figure 4.5: Numerical set up....37
Figure 4.6: Three steps of the Lagrangian interface tracking method: a) piecewise linear interface reconstruction with the normal n; b) moving the control volume; c) overlaying the advected volume onto the grid. 38
Figure 4.7: Volume of Fluid as function of time....39
Figure 4.8: Surface Height as function of time in the probes P1, P2 and P3....40
Figure 4.9: Wave height in the tree probes by internal and external wave makers....42
Figure 4.10: Sketch of different grid size....44

Figure 4.11: Comparison between wave height at different grid size: coarser grid; medium grid; finer grid.....45
Figure 4.12: Vertical profile of horizontal velocity (Vx), turbulent kinetic energy (TKE) and dynamic viscosity (Mu) at different grid sizes (coarse grid on the left and medium grid on the right) in the probe P1 47
Figure 4.13: Vertical profile of horizontal velocity (Vx), turbulent kinetic energy (TKE) and dynamic viscosity (Mu) at different grid sizes (coarse grid on the left and medium grid on the right) in the probe P2 48
Figure 4.14: Vertical profile of horizontal velocity (Vx), turbulent kinetic energy (TKE) and dynamic viscosity (Mu) at different grid sizes (coarse grid on the left and medium grid on the right) in the probe P3 49
Figure 4.15: Input velocity with different temporal increment 51
Figure 4.16: Influence of different TLEN on wave height in probes P1, P2, P3.....54
Figure 4.17: Influence of different TLEN on horizontal velocity, turbulent kinetic energy and dynamic viscosity vertical profiles in probe P3.....55
Figure 4.18: Influence of turbulence models on the wave height in P1, P2 and P3.....56
Figure 4.19: Influence of turbulence models on the horizontal velocity in P3 (broken wave) 57
Figure 5.1: Numerical set-up of long sloping beach 59
Figure 5.2: Comparison between wave height in different probes: variable grid size; constant grid size.....61
Figure 5.3: Comparison between wave height in different probes with a constant grid size: 20cm; 15cm. 62
Figure 5.4: Wave elevation in the constant depth zone as function of place: a) short sloping beach; b) long sloping beach. 64
Figure 5.5: Left boundary volume flow rate.....65
Figure 5.6: Incident, Reflected and Total wave 67
Figure 5.7: Wave elevation as function of time in the probe 170 for the short sloping beach.....68
Figure 5.8: Surface height at t=96.60s.....70
Figure 5.9: Surface height for different breaking wave: a) spilling; b) plunging.....72

Figure 5.10: Surface height for a natural beach. a) field data; b) numerical results 73
Figure 5.11: Verification of the classical breaking criterion 73
Figure 5.12: Horizontal velocity at breaking point 74
Figure 5.13: Turbulence generation and localization at different time: 1-2-3-4) spilling; 5-6-7-8) plunging (photos by Ting and Kirby laboratory experiments) 75
Figure 5.14: Turbulent Kinetic Energy amount and localization at different time and for different breaking types: a) spilling; b) plunging 76
Figure 5.15: Turbulent Kinetic Energy amount and localization at different time and for different breaking types: a) spilling; b) plunging 77
Figure 5.16: Definition of wave runup 78
Figure 5.17: Numerical results: (1) free surface elevation above bottom; (2) free surface elevation above still water level 80
Figure 6.1: Processes and relevant similitude laws for wave motions 87
Figure 6.2: Scale effect on the wave height at different probes P1, P2 and P3: / full scale; / scale 1:40; /scale 1:80 90
Figure 6.3: Scale effect on the horizontal velocity at different probes P1, P2 and P3 91
Figure 6.4: Scale effect on the turbulent kinetic energy at different probes 93
Figure 6.5: Scale effect on the eddy viscosity at probe P1 94
Figure 6.6: Scale effect on the eddy viscosity at probe P2 95
Figure 6.7: Scale effect on the eddy viscosity at probe P3 96
Figure 6.8: Scale effect on the undertow profiles at different probes 97
Figure 7.1: Flux for a sinusoidal wave 103
Figure 7.2: Numerical set-up 104
Figure 7.3: Time history of momentum flux in probe P1 (linear wave), P2 (breaking wave) and P3 (reformed wave) 106
Figure 7.4: Wave height and momentum flux time histories in probe P1 for different H 107
Figure 7.5: Wave height and momentum flux time histories in probe P3 for different H 108
Figure 7.6: Numerical set-up with schematic structure, waters height and momentum fluxes at the wall as function of time: scheme A 110

Figure 7.7: Numerical set-up with schematic structure, waters height and momentum fluxes at the wall as function of time: scheme B 111
Figure 7.8: Surface elevations and momentum fluxes at the wall for different incident waves: a) T=4.8s.....112
Figure 7.9: Surface elevations and momentum fluxes at the wall for different incident waves: b) T=10s 113
Figure 7.10: Pressure vertical profiles at the wall for different wave height (H=1, 2, 3, 4 m - T=4.8 s) 114
Figure 7.11: Pressure vertical profiles at the wall for different wave height (H=1, 2, 3, 4 m - T=10 s) 115
Figure 7.12: Horizontal force at the wall for different incident waves: a) T=4.8 s b) T=10 s.....116
Figure 8.1: Proverbs Parameter Map.....120
Figure 8.2: Identification of wave impact loading.....121
Figure 8.3: Typical slamming pressure as computed by RANS/VOF (dt=0.4 s; dz=0.1 m).....122
Figure 8.4: Typical slamming pressure as computed by RANS/VOF (dt=0.001 s; dz=0.05 m) 122
Figure 8.5: Slamming pressure comparison for different wave.....123
Figure 8.6: Pressure and forces at the wall for different wave heights (H=1-2-3-4m) and periods (T=4.8s; T=10s) RANS/VOF numerical simulation - GT Goda Takahashi procedure 125

LIST OF TABLES

Table 4.1: Geometrical and numerical parameters 37
Table 4.2: Different grid size 43
Table 5.1: Geometrical and numerical parameters 60
Table 5.2: Numerical variable grid 60
Table 5.3: Breaking type limits 71
Table 5.4: Wave parameters 72
Table 5.5: Applied Run-up formulas 79
Table 5.6: Values for run-up calculation 79
Table 6.1: Some published work on wave breaking over beaches with Numerical NS/VOF integration 82
Table 6.2: Similarity ratios 84
Table 6.3: Dimensionless similitude parameters 85
Table 6.4: Processes, relevant similitude laws and critical limits for wave motions 88
Table 7.1: Results for the comparison between the formulas 103
Table 8.1: Overview of design methods for wave loading (PROVERBS) 119

SOMMARIO

Il fenomeno della rottura delle onde su bassi fondali è stata per molti anni uno degli argomenti di ricerca maggiormente investigati e molte pubblicazioni a riguardo sono disponibili in letteratura. Scopo della presente tesi non è fare una rassegna dei lavori presentati, ma è doveroso citare alcune pubblicazioni interessanti – anche se datate – sulla descrizione della rottura delle onde su spiaggia, come quelle proposte da Peregrine (1983), Battjes (1988) e Liberatore-Petti (1992).

Infatti, la rottura è il più importante processo che influenza le dinamiche costiere: in alcuni casi le onde frangono su bassi fondali, altre volte direttamente sulla battigia, altre ancora non sono proprio interessate dalla rottura (ad esempio in presenza di fondali con forte pendenza o per onde molto lunghe). La tipologia di rottura più frequente è quella in acque basse, dovuta all'interazione del moto ondoso col fondale; essa risulta anche quella maggiormente prevedibile, tuttavia l'individuazione univoca del punto di rottura non è ancora un argomento chiuso, neanche negli esperimenti fisici controllati. I tipi di rottura sono classicamente classificati come: spilling (con cresta simmetrica rispetto all'asse verticale e schiuma che "spilla" dalla parte del verso di propagazione del moto ondoso), plunging (con cresta non simmetrica e con la presenza di un getto e di un successivo "tuffo" dalla parte del verso di propagazione del moto ondoso), surfing (caratterizzato da un innalzamento della superficie dell'acqua prima della rottura) e collapsing (tipologia intermedia tra plunging e surging).

La dinamica dei fluidi in assenza di frangimento può essere descritta utilizzando la teoria del moto a potenziale nella maggior parte del campo di moto, tranne in prossimità del fondale e della superficie libera, dove si sviluppa la vorticità limitatamente ad uno strato limite. Nei casi in cui le particolarità in prossimità della superficie libera (necessarie, ad esempio, per l'interazione vento-onde) e/o in prossimità del fondo (necessarie, ad esempio, per l'analisi del trasporto solido) non sono di interesse, la teoria del moto a potenziale è sufficiente. Dopo la rottura, invece, 'onde' e

'vortici' (e quindi un componente potenziale e uno rotazionale del campo di moto in un flusso) sono intimamente mescolati.
La surf e swash zone sono caratterizzate dalla completa trasformazione del moto organizzato delle onde incidenti in moti di tipologie e scale diverse, comprendenti sia la turbolenza su piccole scale (meno di un periodo d'onda) che le caratteristiche medie del moto su scale più grandi (di gran lunga superiore al periodo d'onda) [Battjes, 1988].
E 'ovvio che [Stive e Wind, 1982; Lin e Liu, 1998a; Svendsen et al., 2000; Svendsen, 2005] anche il contributo di termini - notoriamente trascurati nelle tradizionali ipotesi di pressione idrostatica, profilo di velocità uniforme sulla profondità e turbolenza trascurabile - sono importanti e devono essere tenuti nella massima considerazione qualora si voglia modellare l'idrodinamica della surf zone.

Le equazioni non lineari delle acque basse NLSE ('800) e i modelli di Boussinesq [Peregrine, 1967] hanno limiti intrinseci e possono solo simulare il processo di rottura delle onde e la sua evoluzione, introducendo ipotesi semi-empiriche ad hoc e valori limiti di soglia per rappresentare la dissipazione delle onde. Inoltre, questi modelli non hanno la capacità di determinare la distribuzione spaziale della energia cinetica turbolenta, che è di grande importanza negli studi di trasporto solido [Lin e Liu, 1998b].
Considerato tutto questo, era naturale che la risoluzione delle equazioni di Navier-Stokes, ormai ampiamente testata e sviluppata in altri campi della meccanica dei fluidi, diventasse presto uno dei principali approcci per descrivere i processi di idrodinamica costiera, grazie al vantaggio di avere meno ipotesi limitative, nessuna teoria delle onde imposta a priori e la capacità di simulare i complessi processi di turbolenza.

La modellazione numerica tridimensionale della rottura delle onde è estremamente difficile. Si devono infatti risolvere diverse problematiche: prima di tutto, bisogna essere in grado di localizzare con precisione la posizione della superficie libera durante il processo di rottura, in modo che la dinamica della superficie sia ben riprodotta. In secondo luogo, si deve modellare correttamente il processo fisico della produzione di turbolenza, il suo trasporto e la sua dissipazione durante l'intero processo di rottura. In terzo luogo, si ha la necessità di ovviare all'enorme richiesta computazionale.

Alcuni buoni risultati nell'ambito della modellazione bidimensionale si sono avuti riguardo al tracciamento della superficie libera per l'approccio di tipo euleriano: il metodo "Marker And Cell" (MAC) (ad esempio, Johnson et al.1994) e il metodo del "Volum Of Fluid" (VOF) (ad esempio, Ng e Kot 1992, Lin e Liu, 1998a), che sembra ormai prevalere.

L'approccio più comune per la simulazione del moto ondoso in presenza di frangimento è attualmente l'applicazione delle equazioni 2D di Navier Stokes mediate alla Reynolds (RANS) congiuntamente al metodo del Volume di Fluid (VOF) per il calcolo della superficie libera ed a un modello di chiusura della turbolenza. Tale approccio, pur essendo stato testato per molti anni da diversi autori (si veda ad esempio Bovolin et al, 2004) ha raggiunto la piena efficacia con un articolo fondamentale di Lin e Liu (1998a). Questa linea di ricerca è andata avanti con successo per molti anni, tanto che oggi esistono procedure affidabili per la simulazione della rottura delle onde, del run-up e dell'interazione con le strutture.

Il più ovvio passo successivo, vale a dire l'applicazione dei modelli Large Eddy Simulation (LES), non ha dato ancora risultati di altrettanto successo [Watanabe e Saeki, 1999; Christensen e Deigaard, 2001; Lubin et al, 2006; Christensen, 2006]. I modelli LES richiedono necessariamente una completa soluzione nelle 3-dimensioni e gli effetti tridimensionali della turbolenza potrebbero essere davvero importanti nella previsione delle velocità all'interno della surf zone, in particolare nel caso di rottura di tipo plunging [Watanabe e Saeki, 1999]. Tali modelli sono certamente uno strumento promettente per lo studio dell'idrodinamica della surf zone, tuttavia, l'approccio LES richiede la risoluzione su griglie molto più fitte e su un dominio molto più vasto rispetto all'approccio RANS, con conseguente troppo forte richiesta computazionale, almeno per il momento. Essi restano perciò una buona prospettiva per il futuro.

Il metodo Smoothed Particle Hydrodynamics (SPH), importato dal settore astrofisico in una serie di altri campi, è un metodo relativamente nuovo per l'esame della propagazione delle onde fortemente non lineari e del frangimento [Monaghan et al, 1977; Dalrymple et al, 2005; Viccione et al, 2007-2008].

L'SPH offre una varietà di vantaggi per la modellazione dei fluidi, in particolare quelli con una superficie libera: il metodo, secondo l'approccio Lagrangiano, è meshfree e l'equivalente dei nodi della griglia sono le particelle di fluido che si muovono con il flusso. La superficie libera non richiede dunque approcci particolari, come ad esempio il metodo VOF o una localizzazione lagrangiana della superficie. L'SPH è una tecnica basata sul calcolo delle traiettorie delle particelle di fluido, che interagiscono tra di loro in base alle equazioni di Navier-Stokes. Ciascuna di queste particelle trasporta con se informazioni scalari, densità, pressione, componenti della velocità, etc.

Il lavoro qui presentato si basa principalmente sull'applicazione bidimensionale delle equazioni RANS/VOF allo studio dei processi relativi alla surf zone e mira a dimostrare la loro capacità di migliorare l'attuale modellazione idrodinamica della surf zone su una spiaggia a pendenza naturale e nella zona di fronte a strutture costiere imbasate in acque basse, confrontando le prestazioni di tale metodo con osservazioni di laboratorio e con risultati teorici e numerici di altri studi presenti in letteratura.

Parole chiave: onde regolari, modellazione numerica, metodo euleriano RANS/VOF, modelli di turbolenza, effetti di scala, frangimento, impatto su strutture verticali.

ABSTRACT

The mechanics of wave breaking in shallow water has been a major research field for many years, and a very large number of published results are available. No attempt is made here to review the whole literature. Some interesting – if somewhat outdated - descriptions of waves breaking on beaches are presented by Peregrine (1983), Battjes (1988) or Liberatore-Petti (1992).

In fact, the most important process in the near coast zone of the shoreline motion is wave breaking. Some waves break in shallow water, some of them break at the water's edge and in other circumstances waves do not break at all (with steep beach slopes, incident waves with low steepness - or long waves). In general, breaking in deep water is rarer than breaking in shallow water. The latter is triggered by the bottom and is more predictable, although the simple question 'where breaking starts' is far from having a unique answer, even in controlled physical experiments. The breaker types are, generally, classified as spilling (where the water spills down the front face), plunging (with a jet emanating from the front crest), surging (characterized by a rise in water surface before the breaking) and collapsing (between plunging and surging).

The fluid dynamics of non-breaking waves can be described using potential theory in most of the flow field except near the bottom and near the free surface, where vorticity develops and is confined to a boundary layer. As long as the details near the free surface (e.g. necessary for wind–wave interaction) and/or near the bottom (e.g. necessary for sediment transport analysis) are not of interest, the potential theory approach is sufficient. After breaking, 'waves' and 'eddies', essentially a potential component and a rotational component of the flow field, are intimately mixed.

The surf and swash zones are characterized by the complete transformation of the organized motion of the incident, sea-swell, waves into motions of different types and scales, including small-scale (less than

a wave period) turbulence, and large-scale (much greater than the wave period) mean flows [Battjes, 1988].
It is obvious that [Stive and Wind, 1982; Lin and Liu, 1998a; Svendsen et al., 2000; Svendsen, 2005] contributions from terms which have traditionally been neglected in the traditional assumptions of hydrostatic pressure, depth uniform velocity profile, and negligible turbulence, are important and must be taken into full account in surf zone hydrodynamics.
Non Linear Shallow Water equations ('800) and Boussinesq models [Peregrine, 1967] have intrinsic limitations and can only simulate wave breaking and its evolution by assuming on semi-empirical ad hoc assumptions and threshold values to represent wave dissipation. Moreover, these models lack the capability to determine spatial distribution of the turbulent kinetic energy, which is of great importance for sediment transport studies [Lin and Liu, 1998b].
Given all this, it was only natural that the Navier-Stokes solvers now widely tested and developed in other fields of fluid mechanics, with less restricted assumptions involved, no wave theory assumed beforehand, and the capability to simulate complex turbulent processes, should soon become one of the main approaches to describe nearshore processes.

Numerical modeling of three-dimensional breaking waves is extremely difficult. Several challenging tasks must be overcome. First of all, one must be able to track accurately the free surface location during the wave breaking process so that the near surface dynamics is captured. Secondly, one must properly model the physics of turbulence production, transport and dissipation throughout the entire wave breaking process. Thirdly, one needs to overcome the huge demand in computational resources.
There have been some successful two-dimensional results. For instance, more recent is the treatment of the free surface within such an Eulerian framework with the marker and cell (MAC) method [e.g., Johnson et al.1994] and the volume of fluid method (VOF) [e.g., Ng and Kot 1992, Lin and Liu, 1998a].

The most common approach for simulating breaking waves is presently the application of 2D-Reynolds Averaged Navier-Stokes (RANS) equations with a Volume of Fluid (VOF) surface computation and a turbulence closure model. Such an approach, while being often tested for many years by many various Authors (see for instance Bovolin et al,

2004) only reached full maturity with a fundamental paper by Lin and Liu (1998a). This line of research has been going on successfully for many years to the point that reliable procedures now exist to simulate wave breaking, run up and interaction with structures.

The next obvious step. i.e. the application of Large Eddy Simulation (LES) models has so far not been equally successful [Watanabe and Saeki, 1999; Christensen and Deigaard, 2001; Lubin et al, 2006; Christensen, 2006].
LES models necessarily require a fully three-dimensional solution and three-dimensional turbulence effects might be indeed important in the prediction of velocity within the surf zone, especially in the case of plunging breaker [Watanabe and Saeki, 1999]. Such models certainly are a promising tool in the study of surf zone hydrodynamics; however, the LES approach requires much finer grid resolution and a lager computational domain than the RANS approach, resulting in the very high demand on computational resource, at least for the time being. They are however a definite perspective for the future.

Smoothed Particle Hydrodynamics (SPH) method, adapted from astrophysics into a number of fields, is a relatively new method for examining the propagation of highly nonlinear and breaking waves [Monaghan et al, 1977; Dalrymple et al, 2005; Viccione et al, 2007-2008].
SPH offers a variety of advantages for fluid modeling, particularly those with a free surface.
The Lagrangian method is meshfree; the equivalents of mesh points are the fluid particles moving with the flow. The free surface requires no special approaches, such as the volume-of-fluid method or a Lagrangian surface tracking. Furthermore, the method can treat rotational flows with vorticity and turbulence.
SPH is a technique based on computing the trajectories of particles of fluid, which interact according to the Navier–Stokes equations. Each of such particles carries scalar information, density, pressure, velocity components, etc.

The work presented here is therefore mainly based on the application of the Eulerian 2-dimensional RANS/VOF equations to the study of surf zone processes on a beach. In particular the work is aimed at demonstrating the capability of RANS/VOF to improve the current modeling of surf zone hydrodynamics on sloping natural beach and in front of shallow water coastal structures , comparing its performance with laboratory observations and other theoretical and numerical results.

Keywords: regular waves, numerical modelling, Eulerian RANS/VOF method, turbulence models, scale effects, breaking, impact on vertical structures.

RESUME'

Le phénomène de la rupture des vagues sur bas fonds a été pendant pluisieres d'années un des sujets de recherche le plus étudié et beaucoup de publications à ce sujet sont disponibles en littérature. Objectif de cette thèse n'est pas de faire une revue des travaux présentés, mais il est juste de citer quelques publications intéressantes - même si elles ne sont pas très récentes - sur la description de la rupture des vagues sur la plage, comme celles proposées par Peregrine (1983), Battjes (1988) et Liberatore-Petti (1992).

En effet, la rupture est le plus important phénomène qu'il influence les dynamiques côtières: en certains cas les vagues écrasent sur bas fonds, d'autres fois directement sur la ligne de brisement, d'autres aussi ne sont pas vraiment concernés par la rupture (par exemple en présence de fonds avec de forte pente ou par des vagues très longues). La typologie de rupture plus fréquente est celle en eaux bas, dû à l'interaction du mouvement houleux avec le fond; elle reste la plus prévisible, toutefois, la détermination univoque du point de rupture n'est pas encore un argument dépassé, même pas dans les expériences physiques contrôlées.
Les types de rupture sont généralement classifiés comme : spilling (avec une crête symétrique par rapport à l'axe vertical et l'écume qui "épingle" du côté de la propagation du mouvement houleux), plunging (avec une crête pas symétrique et avec la présence d'un jet et d'un "plongeon" successif du côté de la propagation du mouvement houleux), surfing (caractérisé d'une élévation de la superficie de l'eau avant la rupture) et collapsing (typologie intermédiaire entre plunging et surging).

La dynamique des fluides en absence de rupture peut être décrite en utilisant la théorie du mouvement à potentiel dans la plupart du champ de mouvement, sauf à proximité du fond et de la surface libre, où il y a la présence de tourbillons dans une couche limite. Dans les cas ou les particularités en proximités de la superficie libre (nécessaires, par exemple, pour l'interaction vent-vagues) et/ou en proximités du fond (nécessaires, par exemple, pour l'analyse du transport solide) ne sont pas

d'intérêt, la théorie du mouvement à potentiel est suffisante. Par contre, après la rupture, 'vagues' et 'tourbillons' (qui est donc un composant potentiel et un composant rotationnel du champ de mouvement dans un flux) sont ensuite bien mélangés.
Le surf et swash zones sont caractérisés par la transformation complète du mouvement organisé des vagues incidents en mouvements de typologies et d'escaliers différents, comprenant soit la turbulence sur des petits escaliers (moins d'une période de flot) soit les moyennes caractéristiques du mouvement sur des escaliers plus grands (de loin supérieur à la période de vague)[Battjes, 1988].
Il est évident que [Stive e Wind, 1982; Lin e Liu, 1998a; Svendsen et al., 2000; Svendsen, 2005] aussi la contribution de termes - notoirement négligés dans les hypothèses traditionnelles de pression hydrostatique, profil de vitesse uniforme sur la profondeur et turbulence négligeable - sont importants et ils doivent avoir une grande importance s'ils veulent modeler l'hydrodynamique du surf zones.

Les équations pas linéaires des eaux basses NLSE ('800) et les modèles de Boussinesq [Peregrine, 1967] ont des limites intrinsèques et ils peuvent simuler seulement le procès de rupture des vagues et son évolution, en introduisant des hypothèses semi-empiriques ad hoc et des valeurs limites de seuil pour représenter la dissipation des vagues. En outre, ces modèles n'ont pas la capacité de déterminer la distribution spatiale de l'énergie cinétique turbulente, qu'il est de grande importance dans les études de transport solide [Lin et Liu, 1998b].
En considérant tout cela, c'était naturel que la résolution des équations de Navier-Stokes, maintenant amplement développée en autres secteurs de la mécanique des fluides, devenait vite un des approches principales pour décrire les procès de hydrodynamique côtière, grâce l'avantage d'avoir moins hypothèses limitatives, aucune théorie des vagues à priori imposée et la capacité de simuler les complexes procès de turbulence.

Le modelage numérique tridimensionnel de la rupture des vagues est extrêmement difficile. On doit, en effet, résoudre différentes problématiques: avant tout, il faut être capable de localiser avec précision la position de la surface libre pendant le procès de rupture, de manière que la dynamique de la surface soit bien reproduite. En deuxième lieu, on doit modeler correctement le processus physique de la production de turbulence, son transport et sa dissipation pendant le procès entier de

rupture. En troisième lieu, on a la nécessité d'obvier à l'énorme demande computationnelle. Quelques bons résultats dans le cadre du modelage bidimensionnel on a obtenu au traçage de la surface libre pour l'approche d'Eulerian type: la méthode "Marker And Cell" (MAC) [par exemple, Johnson et al.1994] et la méthode du « Volum Of Fluid » (VOF) [par exemple, de Ng et de Kot 1992, de Lin et de Liu, 1998a].

L'approche plus commune pour la simulation du mouvement houleux en présence de rupture est actuellement l'application des équations 2D de Navier Stokes mediée à la Reynolds (RANS) conjointement à la méthode du Volume de Fluide (VOF) pour le calcul de la surface libre et à un modèle de fermeture de la turbulence. Telle approche ayant aussi été testée pendant beaucoup d'années par différents auteurs (on remarque, par exemple, Bovolin et en, 2004) il a atteint efficacité avec un article fondamental de Lin et Liu, 1998a. Cette ligne de recherche à fait son chemin avec succès pendant beaucoup d'années, au point qu'aujourd'hui ces procédures fiables existent pour la simulation de la rupture des vagues, du run-up et de l'interaction avec les structures.

Le pas successif le plus évident, c'est à dire l'application des modèles Large Eddy Simulation (LES), il n'a pas encore donné de résultats avec autant de succès [Watanabe e Saeki, 1999; Christensen e Deigaard, 2001; Lubin et al, 2006; Christensen, 2006].
Les modèles LES demandent nécessairement une solution complète en 3-dimension et les effets tridimensionnels de la turbulence pourraient être vraiment importants dans la prévision des vitesses à l'intérieur du surf zones, en particulier en cas de rupture de type plunging [Watanabe et Saeki, 1999]. Tels modèles sont certainement un instrument prometteur pour l'étudie de l'hydrodynamique de la surf zone, toutefois, l'approche LES demande la résolution sur grilles plus épaisses par rapport à l'approche RANS, avec comme conséquent une trop fort demandé computationnelle, au moins pour le moment. Ils restent donc une bonne perspective pour l'avenir.

La méthode Smoothed Particle Hydrodynamics (SPH), importé par le secteur astrophysique dans une série d'autres secteurs, est une méthode relativement nouvelle pour l'examen de la propagation des vagues fortement pas linéaires et de la rupture [Monaghan et en, 1977; Dalrymple et en, 2005; Viccione et en, 2007 -2008].

Le SPH offre une variété d'avantages pour le modelage des fluides, en particulier ceux avec une surface libre: la méthode, selon l'approche Lagrangian est meshfree et l'équivalent des noeuds de la grille ce sont les particules de fluide qu'ils se remuent avec le flux. La surface libre ne demande pas des approches spéciales, comme par exemple la méthode VOF ou une localisation Lagrangian de la surface. En outre, la méthode peut traiter les flux rationnels, avec la présence de tourbillons et de turbulence.
Le SPH est une technique basée sur le calcule des trajectoires des particules de fluide, qui interagissent entre eux sur la base des équations de Navier-Stokes. Chaque particules transporte avec eux des indications numériques, la densité, la pression, les composantes de la vitesse, etc.

Le travail présenté se base principalement sur l'application bidimensionnelle des équations RANS/VOF à l'étude des procès relatifs au surf zones et vise à montrer leur capacité d'améliorer le modelage hydrodynamique actuelle du surf zones sur une plage à pente naturelle et dans la zone devant les structures côtières construites en eaux basses, en comparant les performances de telle méthode avec des observations de laboratoire et avec des résultats théoriques et numériques d'autres études présentes en littérature.

Mots-clés: vagues réguliers, modelage numérique, RANS/VOF Eulerian méthode, modèles de turbulence, effets d'escalier, pression, impact sur des structures verticales.

RESUMEN

El fenómeno de la rotura de las olas en aguas poco profundas, ha sido por muchos años uno de los argumentos de búsqueda principalmente investigado y muchas publicaciones están disponibles en literatura sobre el tema. El objetivo de esta tesis no es hacer una inspección de los trabajos presentados, pero cabe mencionar algunas publicaciones de interés - aunque fecháis - sobre la descripción de la rotura de las olas en la playa, como aquellos propuestos por Peregrine (1983), Battjes (1988) y Liberatore-Petti (1992).

En efecto, la rotura es el más importante proceso que influencia las dinámicas litorales: en algunos casos las olas se rompen sobre bajos fondos, otras veces directamente sobre la playa, otras no están realmente afectadas por la rotura (por ejemplo en presencia de fondos con fuerte inclinación o de olas muy largas). La tipología de rotura más comun se tiene en aguas bajas, debida a la interacción del movimiento de olas con el fondo; esta también resulta la principalmente previsible, pero la individuación unívoca del punto de rotura no es todavía un motivo zanjado, tampoco en los experimentos físicos controlados.
Los tipos de rotura generalmente son clasificados como: spilling (con cresta simétrica con respecto del eje vertical y espuma que "enganche" en el lado de la línea de propagación de las ondas), plunging (con cresta no simétrica y con la presencia de un chorro y una siguiente "zambullida" de la parte de la línea de propagación de las ondas), surfing (caracterizado por un aumento de la superficie del agua antes de la rotura) y collapsing (tipología intermedia entre plunging y surging).

La dinámica de los fluidos en ausencia de quebrantaolas puede ser descrita utilizando la teoría del movimiento a potencial en la mayor parte del campo de movimiento, excepto en proximidad del fondo y la superficie libre, dónde se desarrolla la vorticidad limitadamente a una capa límite. En los casos en que las caracteristicas en proximidad de la superficie libre (necesarias, por ejemplo, por la interacción viento-olas) e/o en proximidad del fondo (necesarias, por ejemplo, para el análisis del transporte sólido) no son de interés, la teoría del movimiento a potencial

es suficiente. Después de la rotura, sin embargo, "olas" y "remolinos"(por lo tanto un componente potencial y uno rotacional del campo de movimiento en un flujo) están ocultamente envueltas.
Las surf y las swash zonas son caracterizadas por la completa transformación del movimiento organizado de las olas incidentes en movimientos de tipologías y escalas diferentes, incluyendo tanto la turbulencia sobre pequeñas escalas (menos que un período de ola) que las características medias del movimiento sobre escalas más grandes (mucho superior al período de ola) [Battjes, 1988].
Es obvio que [Stive e Wind, 1982; Lin e Liu, 1998a; Svendsen et al., 2000; Svendsen, 2005] también el aporte de términos - notoriamente descuidados en las tradicionales hipótesis de presión hidrostática, perfil de velocidad uniforme sobre la profundidad y turbulencia irrelevante - son importantes y tienen que ser consideratos al máximo en el caso de que se quiera modelar la hidrodinámica de la surf zona.

Las ecuaciones no lineales de las aguas bajas NLSE ('800) y los modelos de Boussinesq [Peregrine, 1967] tienen límites intrínsecos y sólo pueden simular el proceso de rotura de las olas y su evolución, introduciendo hipótesis semi-empíricas ad hoc y valores límites de umbral para representar la disipación de las olas. Además, estos modelos no tienen la capacidad de determinar la distribución espacial de la energía cinética turbulenta, que es de gran importancia en los estudios de transporte sólido [Lin y Liu, 1998b].
Considerado todo esto, es natural que la resolución de las ecuaciones de Navier-Stokes, ya extensamente probada y desarrollada en otros campos de la mecánica de los fluidos, se convirtiera pronto en uno de los principales aproches para describir los procesos de la hidrodinámica costera, gracias a la ventaja de tener menos hipótesis definidas, ninguna teoría de las olas impuesta a priori y la capacidad de simular los complejos procesos de turbulencia.

El modelado numérico tridimensional de la rotura de las olas es gravemente difícil. Se deben en efecto solucionar diferentes problemáticas: en primer lugar, hace falta ser capaz de localizar con precisión la posición de la superficie libre durante el proceso de rotura, de modo que la dinámica de la superficie se repida bien. En segundo lugar, se tiene que moldear correctamente el proceso físico de la producción de turbulencia, su transporte y su disipación durante el

entero proceso de rotura. En tercer lugar, hay que superar la gran demanda computacional. Algunos buenos resultados en el ámbito del modelado bidimensional se han tenido respeto al seguimiento de la superficie libre por el aproche de tipo euleriano: el método "Marker And Cell" (MAC) [por ejemplo, Johnson et al, 1994] y el método del "Volum Of Fluid" (VOF) [por ejemplo, Ng y Kot - 1992, Lin y Liu – 1998a].

El método más común para la simulación del movimiento de las olas en presencia de ruptura es actualmente la aplicación de las ecuaciones 2D de Navier Stokes mediatas al Reynolds (RANS) conjuntamente al método del Volum of Fluid (VOF) para el cálculo de la superficie libre y a un modelo de cierre de la turbulencia. Tal aproche, habiendo sido probado durante muchos años por varios autores (se vea, por ejemplo, Bovolin et al, 2004) ha alcanzado la plena eficacia con un artículo fundamental de Lin y Liu (1998a). Esta línea de búsqueda ha ido adelante con éxito durante muchos años, tantos que hoy existen procedimientos confiables para la simulación de la rotura de las olas, del run-up y de la interacción con las estructuras.

El siguiente paso más evidente, es decir la aplicación de los modelos Large Eddy Simulation (LES), no ha dado todavía resultados de igualmente éxito [Watanabe e Saeki, 1999; Christensen e Deigaard, 2001; Lubin et al, 2006; Christensen, 2006]. Los modelos LES necesariamente requieren una completa solución en los 3-dimensiónes y los efectos tridimensionales de la turbulencia podrían ser muy importantes en la previsión de las velocidades dentro la surf zona, en particular en el caso de rotura de tipo plunging [Watanabe y Saeki, 1999]. Tales modelos son ciertamente un instrumento prometedor por el estudio de la hidrodinámica de la surf zona, sin embargo, el aproche LES solicita mucho la resolución sobre parrillas mucho más densas respecto al aproche RANS, dando lugar a una alta demanda computaciónal, al menos momentáneamente. Estos son por lo tanto una buena perspectiva para el futuro.

El método Smoothed Particle Hydrodynamics (SPH), importado por el sector astrofísico en una serie de otros campos, es un método relativamente nuevo para el examen de la propagación de las olas fuertemente no lineales y de la ruptura [Monaghan et al, 1977; Dalrymple et al, 2005; Viccione et al, 2007-2008]. El SPH ofrece una variedad de ventajas para la modelación el modelado de los fluidos, en particular de aquellos con una superficie libre: el método, según el aproche de Lagrange, es meshfree y el equivalente de los nudos de la parrilla son las partículas de fluido que se mueven con el flujo.
La superficie libre no requiere aproches caracteristicos, como por ejemplo el método VOF o una localización lagrangiana de la superficie. Además, el método puede tratar los flujos rotacionales, con vorticidad y turbulencia.
EL SPH es una técnica que se basa en el cálculo de las trayectorias de las partículas de fluido, que interaccionan entre de ellas sobre la base de ecuaciones de Navier-Stokes. Cada una de estas partículas transporta con si informaciones escalares, densidad, presión, componentes de la velocidad, etc.

El trabajo aquí presentado se basa principalmente en la aplicación bidimensional de las ecuaciones RANS/VOF al estudio de los procesos relativos al surf zona y quiere demostrar la capacidad de mejorar la modelación hidrodinámica actual de la surf zona sobre una playa a inclinación natural y en la zona en frente a estructuras costeras poseídas en aguas bajas, comparando las prestaciones de este método con observaciones de laboratorio y con resultados teóricos y numéricos de otros estudios presentes en literatura.

Palabras clave: olas regulares, modelismo numérico, Eulerian método RANS/VOF, modelos de turbulencia, efectos de escala, rotura, impacto sobre estructuras verticales.

ACKNOWLEDGEMENTS

Writing these pages represents for me a great emotion in remembering all the persons that helped me in my research and contributed to make these three years a wonderful experience.

First and most of all I would like to express sincere and deep gratitude to my Prof. E. Pugliese Carratelli for having induced me to love Hydraulics and for the opportunities he gave me. He has led me with affectionate patience, continuous encouragement and valuable suggestions.
Then, many thanks to Prof. Enrico Foti and Ing. Fabio Dentale, for their precious suggestions.

I'm grateful to C.U.G.RI for having placed the Parallel Computing Laboratory (LACP) at my disposal and to all my colleagues and friends of LIDAM and MEDUS, present and former, who greatly contributed to the pleasure of working at University. I feel very fortunate of having spent such a long, wonderful, pleasant time with them!

My last word is for my family, always present in my life with unfailing love.

ABOUT THE AUTHOR

MARINA MONACO è nata ad Eboli (Salerno, Italia) l' 11/11/1980.
Si è laureata nel 2005 presso la Facoltà di Ingegneria dell'Università degli Studi di Salerno, in Ingegneria Civile per l'Ambiente e il Territorio (V.O.), con una tesi in Idraulica Marittima riguardante l'analisi dell'erosione trasversale di una spiaggia.
Tra il 2006-2007 è stata contrattista del Centro di Competenza Regionale A.M.R.A. (Analisi e Monitoraggio del Rischio Ambientale), nell'ambito del progetto della Regione Campania (Settore Programmazione Interventi di Protezione Civile sul territorio) finalizzato alla determinazione degli scenari di rischio di erosione ed allagamento delle coste e relativi modelli.
Nel Novembre 2006 ha cominciato il Dottorato di Ricerca in Ingegneria Civile per l'Ambiente e il Territorio, presso l'Università degli Studi di Salerno, portando avanti un argomento di ricerca dal titolo "Azione del Moto Ondoso su Bassi Fondali ed Applicazioni al Rischio Costiero".

MARINA MONACO was born in Eboli (Salerno, Italy) on November 11th 1980.
She graduated in 2005 at the University of Salerno, Faculty of Engineering, in Civil Engineering for Environment and Land Use (a 5-year University Course), with a thesis on Maritime Hydraulics aimed at analyzing cross-shore erosion on a beach.
Between 2006-2007 worked under a contract by AMRA (Campania Regional Centre of Competence) on a EU funded activity for the Analysis and Monitoring of Environmental Hazards aimed at determining the risk scenarios of coastal erosion and flooding and related models.
In November 2006 she started her PhD research in Civil Engineering for for Environment and Land Use at the University of Salerno. The title of the research is "Wave Action On Shallow Water And Application To Coastal Hazard".

1 INTRODUCTION

1.1 CONTEXT AND AIM OF STUDY

In this work, we examine how the now standard computational fluid dynamics (CFD) model based on the Reynolds-averaged Navier Stokes (RANS) equations, combined with a turbulence closure model and free surface scheme, can compute cross-shore wave transformation and wave breaking.

One of the advantages of dealing with the full RANS equations rather than using simpler models is that no breaking criterion is to be specified beforehand, as wave breaking is a consequence of the fluid dynamics described by the general equations.
CFD models solve fundamental fluid dynamic equations combined with a fluid tracking method, and require a turbulence closure scheme to properly account for sub grid scale turbulence production, transport, and dissipation during the wave breaking process.
Fluid tracking schemes enable CFD models to keep track of complex free surface interfaces. Wave breaking can be interpreted from resulting fluid properties, such as velocity, turbulence, or free surface structures, without having to specify wave breaking conditions before hand.

Lin and Liu (1998) and Bradford (2000) successfully simulated Ting and Kirby (1995, 1996) laboratory data using a similar two-dimensional CFD approach. Ting and Kirby studied spilling and plunging in an experimental tank 40 m long, 0.6 m wide, and 1m deep with a linear beach profile with 1:35 slope and waves driven by a mechanical paddle prescribed to generate cnoidal waves.
Lin and Liu (1998) compared their CFD model at individual locations with the experimental results and found the model performed well in simulating detailed flow in a single wave breaking event.

Bradford (2000) further studied instantaneously as well as ensemble-averaged model results, also with good success. Both models simulated 20s of data citing computational and numerical limitations.
The studies strongly support the possibility that CFD models can be used to simulate wave breaking processes.

The main objective of the present work is to verify that CFD models can be used to simulate wave transformation and wave breaking at prototype field scales and to create a numerical laboratory that can be used to improve our understanding of the wave breaking process.

The flow field is governed by the RANS and continuity equations. The basic idea is, of course, to numerically integrate Navier-Stokes equations on a fixed Cartesian grid by using a finite volume method. A turbulence closure scheme is required to resolve sub grid scale turbulence and dissipation and is used to solve turbulence kinetic energy and dissipation transport equations. Free surfaces are tracked using the volume-of-fluid (VOF) approach (Hirt and Nichols, 1981).
While all the computations carried out for this work were made by using the "FLOW-3d" software system, by Flow Science, most current CFD programs follow more or less the same structure and criteria.

The main model and boundary conditions problems and features of such programs are briefly described in the following.

1.2 OUTLINE OF THE THESIS

The thesis is organized as follows: in section 2 numerical methods to simulate fluid flow are presented, while section 3 describes the numerical methodology of RANS/VOF and the wave generation process.
Section 4 presents some numerical simulations of regular waves on beach, with attention to the numerical model validation and to the convergence analysis on computational discretization and turbulence models.

In section 5, the model is applied to simulate wave propagation, wave run-up, breaking types and criteria.
Section 6 investigates the limitations of hydraulic similitude theory and the influence of the scale effects on results; in section 7 energy and momentum fluxes are evaluated using the model results and compared with the existing formulations from linear wave theory. The results are confronted for non-breaking, breaking and reformed waves, on a free sloping beach and in presence of a schematic structure.
Section 8 is about the wave impact on a vertical structures, with the calculation of pressures, forces and momentum fluxes on the wall and the comparison with the experimental design formula.
Finally, the concluding remarks of this study are presented in section 9.

2 MODELING FLUID FLOW

2.1 NUMERICAL METHODS

In 1822, Navier derived the equations for the motion of fluid. These equations are now known as the **Navier-Stokes equations** (Stokes independently rederived the equations in 1845). The Navier-Stokes equations represent the conservation of mass and momentum per unit mass:

$$\frac{\partial u}{\partial x}+\frac{\partial v}{\partial y}+\frac{\partial w}{\partial z}=0$$

$$\rho\left(\frac{\partial u}{\partial t}+u\frac{\partial u}{\partial x}+v\frac{\partial u}{\partial y}+w\frac{\partial u}{\partial z}\right)=-\frac{\partial p}{\partial x}+\mu\left(\frac{\partial^2 u}{\partial x^2}+\frac{\partial^2 u}{\partial y^2}+\frac{\partial^2 u}{\partial z^2}\right)=0$$

$$\rho\left(\frac{\partial v}{\partial t}+u\frac{\partial v}{\partial x}+v\frac{\partial v}{\partial y}+w\frac{\partial v}{\partial z}\right)=-\frac{\partial p}{\partial y}+\mu\left(\frac{\partial^2 v}{\partial x^2}+\frac{\partial^2 v}{\partial y^2}+\frac{\partial^2 v}{\partial z^2}\right)=0$$

$$\rho\left(\frac{\partial w}{\partial t}+u\frac{\partial w}{\partial x}+v\frac{\partial w}{\partial y}+w\frac{\partial w}{\partial z}\right)=-\frac{\partial p}{\partial z}-\rho g+\mu\left(\frac{\partial^2 w}{\partial x^2}+\frac{\partial^2 w}{\partial y^2}+\frac{\partial^2 w}{\partial z^2}\right)=0$$

where the z axis is vertical, so that the gravitational body force, only appears in the z equation.
However, despite the existence of powerful computers, it is not possible, and it will not be possible in the near future, to compute most of the mentioned flow problems, as 'real life' flow is often too complicated. For solving a flow problem, the Navier-Stokes equations and the continuity equation (describing conservation of mass) have to be solved simultaneously. This is done by discretising this set of equations, which in principle can be done by any of the following methods:

- finite element method;
- finite difference method;
- finite volume method.

The **finite element method** is most commonly used in combination with unstructured grids. An unstructured grid is constructed by dividing the geometry into small cells that can have different shapes. In combination with a chosen basis function such a cell is called an element. The approximate solution is built by combining all these functions.
The lack of structure makes simple computations more time (and memory) consuming than on a structured grid with the same number of cells. This is probably the reason that this method is not so often used for DNS; the strength of unstructured grids lies in its flexibility for very complex geometries.

The **finite difference method** discretises a differential equation to a difference equation.
It is especially suited for (curvilinear) structured grids where unknowns are all aligned with each other. The accuracy can be increased where this is required. A disadvantage is that the conservation form the Navier-Stokes equation is numerically not maintained such that the total momentum is usually not conserved.

The **finite volume method**, which is the method used in this thesis, discretises a mathematical model from its conservation form.
Although the Navier-Stokes and continuity equations are often shown as differential equations, they are actually physical conservation laws, which give the balance of momentum (and mass) that holds for any volume.
If the conservation laws are applied to an arbitrarily small volume around an arbitrary point in the flow domain, the differential equations are, provided a sufficient smooth solution, obtained.
When applying the finite volume method to the Navier-Stokes equations, the geometry has to be covered with cells; as for the finite element method, this can be a structured as well as an unstructured grid. Without going into detail, discretising in a finite volume manner means that for each cell locally the conservation law is applied, for all variables, such as for momentum, thermal energy, turbulent kinetic energy, ect. For each time step, the inflow of momentum through the cell boundary is computed, with contributions from convection, diffusion, and pressure differences. When the net inflow through the cell boundary is positive, the momentum in the cell increases which means that the velocity increases.

A cell face is always part of the boundary of its two adjacent cells; when the flux through the face is equal for both cells, then the (numerical) momentum is exactly conserved.

2.2 TURBULENCE

The main difficulty in studying turbulence is the simultaneous presence into the fluid of a large number of vortical structures with different characteristic size that mutually interact each other; they are due to non-linear terms in the Navier-Stokes equations and make difficult the analytical implementation.
In 1941, Kolmogorov presented his turbulence theory, based on a statistical approach, which described the energy spectrum. The basic idea of this theory is that the turbulence consists in the transfer of turbulent kinetic energy from larger whirling structures toward smaller, where it is dissipated in heat.
The sizes define a characteristic length scale for the eddies, which are also characterized by velocity scales and time scales (turnover time) dependent on the length scale. The large eddies are unstable and eventually break up originating smaller eddies, and the kinetic energy of the initial large eddy is divided into the smaller eddies that stemmed from it. These smaller eddies undergo the same process, giving rise to even smaller eddies which inherit the energy of their predecessor eddy, and so on. In this way, the energy is passed down from the large scales of the motion to smaller scales until reaching a sufficiently small length scale such that the viscosity of the fluid can effectively dissipate the kinetic energy into internal energy (energy cascade).
Kolmogorov postulated that for very high Reynolds number, the small scale turbulent motions are statistically isotropic (i.e. no preferential spatial direction could be discerned). In general, the large scales of a flow are not isotropic, since they are determined by the particular geometrical features of the boundaries (the size characterizing the large scales will be denoted as L^*); in energy cascade this geometrical and directional information is lost, while the scale is reduced, so that the statistics of the small scales has a universal character: they are the same for all turbulent flows when the Reynolds number is sufficiently high.

Thus, Kolmogorov introduced a second hypothesis: for very high Reynolds numbers the statistics of small scales are universally and uniquely determined by the viscosity (ν) and the rate of energy dissipation (ε). With only these two parameters, the unique length that can be formed by dimensional analysis is:

$\eta^* = \left(\frac{\nu^3}{\varepsilon}\right)^{1/4}$ this is today known as the **Kolmogorov length scale**.

A turbulent flow is characterized by a hierarchy of scales through which the energy cascade takes place.
Dissipation of kinetic energy takes place at scales of the order of Kolmogorov length η*, while the input of energy into the cascade comes from the decay of the large scales, of order L*.
These two scales at the extremes of the cascade can differ by several orders of magnitude at high Reynolds numbers. In between there is a range of scales (each one with its own characteristic length *r**) that has formed at the expense of the energy of the large ones. These scales are very large compared with the Kolmogorov length, but still very small compared with the large scale of the flow (i.e. $\eta^* << r^* << L^*$).
Since eddies in this range are much larger than the dissipative eddies that exist at Kolmogorov scales, kinetic energy is essentially not dissipated in this range, and it is merely transferred to smaller scales until viscous effects become important as the order of the Kolmogorov scale is approached. Within this range inertial effects are still much larger than viscous effects, and it is possible to assume that viscosity does not play a role in their internal dynamics (for this reason this range is called "inertial range").
Hence, a third hypothesis of Kolmogorov was that at very high Reynolds number the statistics of scales in the range $\eta^* << r^* << L^*$ are universally and uniquely determined by the scale r and the rate of energy dissipation ε.

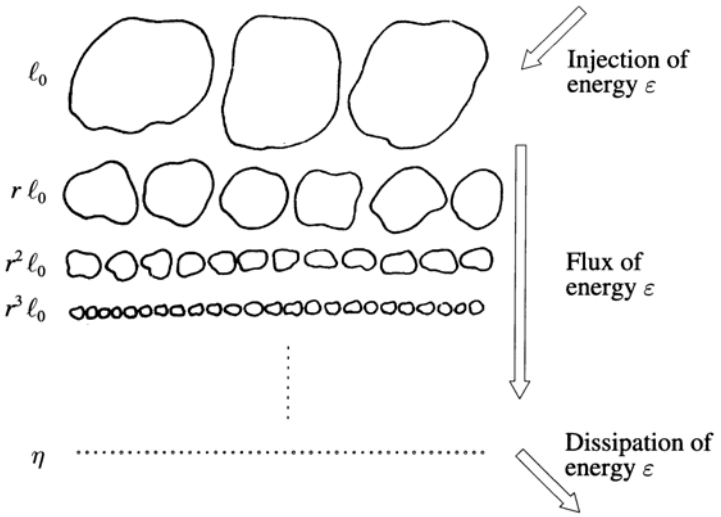

Figure 2.1 : Energy cascade

From a mathematical point of view, the concept of turbulence is identical with the chaotic behavior of the solutions of the Navier-Stokes equations. The feature which makes the random turbulent motions is a strong sensitivity to initial conditions presented by Navier-Stokes equations, in the size as greater as the larger the number of Reynolds is.
In fact, from the is dimensional analysis, the dimensionless group that governs the transition from a laminar to a turbulent flux is the number of Re, which expresses the relationship between inertial forces and viscous forces. Seems natural to think that for low Reynolds number there are situations of laminar flow while high values of Re agree with turbulent flow.
The equations of Navier-Stokes are therefore able to represent any turbulent flow field, but their digital direct resolution (Direct Numerical Simulation, DNS), requires a grid with a spatial resolution of about of size of the smallest turbulent structures (so-called Kolmogorov structures).
For these reasons, the DNS method applied to the problem under consideration (Re = $10^{6\text{-}9}$) would require a too high computational cost. It was therefore necessary to make use of an alternative method based on the numerical solution of the average motion and the implementation of turbulent models.

In general, three computational approaches exist for the computation of turbulent flow: Direct Numerical Simulation (**DNS**), Large Eddy Simulation (**LES**), and Reynolds Averaged Navier-Stokes (**RANS**).

In case of DNS, turbulence is not modeled and all details need to be resolved from the Navier-Stokes equations in the simulation; in the second case, a localized spatial filter is applied, which removes the small-scale details; and in the latter case, a long-time temporal filter is applied resulting in computation of the mean flow which is steady in time.

The computational effort for LES lies in between that for DNS and RANS. For both LES and RANS a closure model needs to be specified describing the influence of the turbulence on the computed flow.

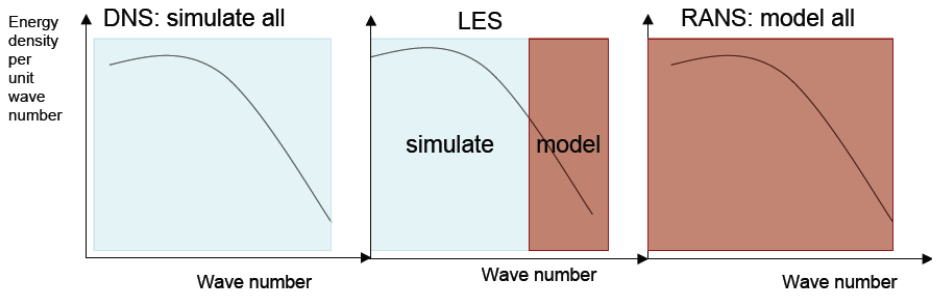

Figure 2.2 : Approaches for the computation of turbulent flow

2.3 RANS EQUATIONS

In general, all dependent time signal (in this case velocity) can be decomposed into a mean term and a fluctuating term. If the average term is constant over time, then we have:

$$u(x,t) = U(x) + u'(x,t)$$

$$U(x) = < u(x,t) > = \lim_{T\to\infty} \frac{1}{T} \int_0^T u(x,t)dt \qquad u'(x,t) = u(x,t) - U(x)$$

In this case, obviously $< u'(x,t) > \equiv 0$

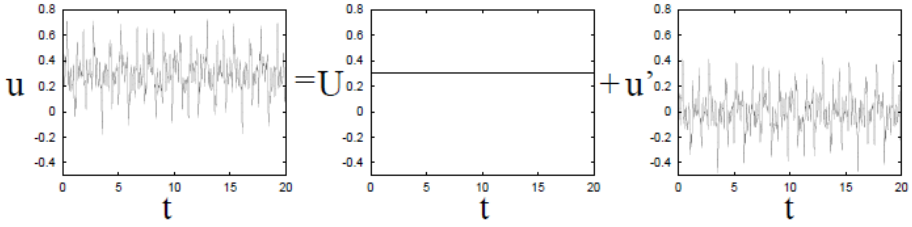

Figure 2.3 : Decomposition of a statistically stationary signal

If the average term is also a function of time, then the averaged operation should not be made for a infinite time but on a finite time interval that is very large compared to the time scale of fluctuations but short enough compared with time variation of mean field.

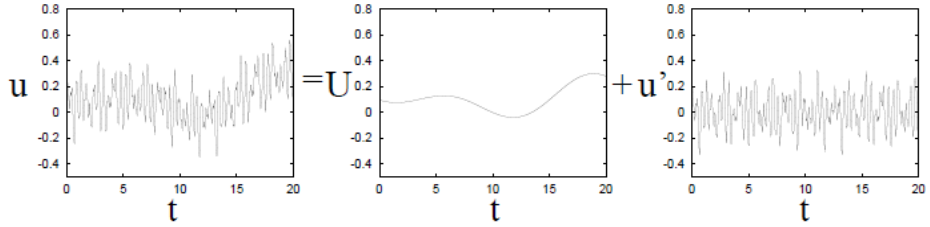

Figure 2.4 : Decomposition of a not statistically stationary signal

For a turbulent flow, the velocity field and the pressure field can be decomposed into two parts: the averaged velocity and pressure, $\langle u_i \rangle$ and $\langle p \rangle$, and the turbulence velocity and pressure, u_i' and p'. Thus,

$$u_i = \langle u_i \rangle + u_i'; \qquad p = \langle p \rangle + p'$$

in which i = 1,2,3 for a three-dimensional flow.

If the fluid is assumed to be incompressible, the mean flow field is governed by the follow **Reynolds Averaged Navier Stokes equations**:

$$\frac{\partial \langle u_i \rangle}{\partial x_i} = 0$$

$$\frac{\partial \langle u_i \rangle}{\partial t} + \langle u_j \rangle \frac{\partial \langle u_i \rangle}{\partial x_j} = -\frac{1}{\rho}\frac{\partial \langle p \rangle}{\partial x_i} + g_i + \frac{1}{\rho}\frac{\partial \langle \tau_{ij} \rangle}{\partial x_j} - \frac{\partial \langle u_i' u_j' \rangle}{\partial x_j}$$

where ρ is the density of the fluid, g_i the i-th component of the gravitational acceleration, and $\langle \tau_{ij} \rangle$ the viscous stress tensor of the mean flow.

For a Newtonian fluid, $\langle \tau_{ij} \rangle = 2\mu \langle \sigma_{ij} \rangle$ with μ being the molecular viscosity and $\langle \sigma_{ij} \rangle = \frac{1}{2}\left(\frac{\partial \langle u_i \rangle}{\partial x_j} + \frac{\partial \langle u_j \rangle}{\partial x_i} \right)$ the rate of strain tensor of the mean flow. In the momentum equation the influence of the turbulence fluctuations on the mean flow field is represented by the Reynolds stress tensor, $\rho \langle u_i' u_j' \rangle$.

The transport equation for the Reynolds stress tensor can be derived from the Navier-Stokes equations theoretically. Unfortunately, the resulting equation for the Reynolds stress tensor contains terms involving higher-order correlations among turbulence velocity components and turbulent pressure. Closure assumptions are necessary to relate the higher-order correlations of the turbulent flow field to the characteristics of the mean flow field, and so implementation of turbulent models are introduced.

2.4 TURBULENCE MODELS

More widely used model consists of two transport equations for the turbulent kinetic energy K and its dissipation ε, the so-called **K-ε model**. The K-ε model has been shown to provide reasonable approximations to many types of flows, although it sometimes requires modification of its dimensionless parameters.

Another, more recent turbulence model is based on **Renormalization-Group (RNG) model**. This approach applies statistical methods for a derivation of the averaged equations for turbulence quantities, such as turbulent kinetic energy and its dissipation rate. The RNG model uses equations similar to the equations for the K-ε model. However, equation constants that are found empirically in the standard K-ε model are derived explicitly in the RNG model.
Generally, the RNG model has wider applicability than the standard K-ε model. In particular, the RNG model is known to describe more accurately low intensity turbulence flows and flows having strong shear regions.

2.4.1 K-ε model

In the momentum equation the influence of the turbulent fluctuations on the mean flow field is represented by the Reynolds stress tensor, $\rho\left\langle u_i' u_j' \right\rangle$

$$\rho\left\langle u_i' u_j' \right\rangle = \frac{2}{3}\rho \cdot k\delta_{ij} - C_d \rho \frac{k^2}{\varepsilon}\left(\frac{\partial\left\langle u_i \right\rangle}{\partial x_j} + \frac{\partial\left\langle u_j \right\rangle}{\partial x_i} \right) - \rho \frac{k^3}{\varepsilon^2} \cdot$$

$$\cdot \left[\begin{array}{l} C_1\left(\frac{\partial\left\langle u_i \right\rangle}{\partial x_l}\frac{\partial\left\langle u_l \right\rangle}{\partial x_j} + \frac{\partial\left\langle u_j \right\rangle}{\partial x_l}\frac{\partial\left\langle u_l \right\rangle}{\partial x_i} - \frac{2}{3}\frac{\partial\left\langle u_l \right\rangle}{\partial x_k}\frac{\partial\left\langle u_k \right\rangle}{\partial x_l}\delta_{ij} \right) + \\ + C_2\left(\frac{\partial\left\langle u_i \right\rangle}{\partial x_k}\frac{\partial\left\langle u_j \right\rangle}{\partial x_k} - \frac{1}{3}\frac{\partial\left\langle u_l \right\rangle}{\partial x_k}\frac{\partial\left\langle u_l \right\rangle}{\partial x_k}\delta_{ij} \right) + \\ + C_3\left(\frac{\partial\left\langle u_k \right\rangle}{\partial x_i}\frac{\partial\left\langle u_k \right\rangle}{\partial x_j} - \frac{1}{3}\frac{\partial\left\langle u_l \right\rangle}{\partial x_k}\frac{\partial\left\langle u_l \right\rangle}{\partial x_k}\delta_{ij} \right) \end{array} \right]$$

where:

$k = \frac{1}{2}\left\langle u_i' u_i' \right\rangle = TKE$ Turbulent Kinetic Energy

$\varepsilon = \nu \left\langle \left(\frac{\partial u_i'}{\partial x_j} \right)^2 \right\rangle$ Turbulent Kinetic Energy Dissipation Rate

$\nu_t = \mu / \rho$ Turbulent Viscosity

The recommended values for these coefficients are (Rodi 1980):

$C_d = 0.09, \quad C_1 = 0.0054, \quad C_2 = -0.0171, \quad C_3 = 0.0027$

The governing equations for k and ε can be derived directly from the Navier-Stokes equations.
The Reynolds stress tensor only appears in the k-ε equation as the turbulence production term, $-\left\langle u_i' u_j' \right\rangle \partial \left\langle u_i \right\rangle / \partial x_j$

$$\frac{\partial k}{\partial t} + \left\langle u_j \right\rangle \frac{\partial k}{\partial x_j} = \frac{\partial}{\partial x_j}\left[\left(\frac{\nu_t}{\sigma_k} + \nu \right) \frac{\partial k}{\partial x_j} \right] - \left\langle u_i' u_j' \right\rangle \frac{\partial \left\langle u_i \right\rangle}{\partial x_j} - \varepsilon$$

$$\frac{\partial \varepsilon}{\partial t} + \left\langle u_j \right\rangle \frac{\partial \varepsilon}{\partial x_j} = \frac{\partial}{\partial x_j}\left[\left(\frac{\nu_t}{\sigma_\varepsilon} + \nu \right) \frac{\partial \varepsilon}{\partial x_j} \right] + C_{1\varepsilon} \frac{\varepsilon}{k} \nu_t \left(\frac{\partial \left\langle u_i \right\rangle}{\partial x_j} + \frac{\partial \left\langle u_j \right\rangle}{\partial x_i} \right) \frac{\partial \left\langle u_i \right\rangle}{\partial x_j} - C_{2\varepsilon} \frac{\varepsilon^2}{k}$$

in which empirical coefficients have been determined by performing many simple experiments; the recommended values for these coefficients are (Rodi 1980):

$C_{1\varepsilon} = 1.44, \quad C_{2\varepsilon} = 1.92, \quad \sigma_k = 1.0, \quad \sigma_\varepsilon = 1.3$

The Reynolds equations and the k-ε transport equations, with the appropriate boundary conditions have been used to predict successfully many complex turbulent flows. The empirical coefficients given up are surprisingly universal.

2.4.2 RNG model

The RNG model was developed using Re-Normalisation Group (RNG) methods by Yakhot et al. (1986) to renormalise the Navier-Stokes equations, to account for the effects of smaller scales of motion.
RNG theory, applied to turbulence modeling, is used to eliminate the highest wave number modes (i.e., the smallest turbulence scales) and replace their effect on the remaining flow by a small increase of effective viscosity. The resulting equations are rescaled (renormalized) to be "equivalent" to the original equations.
The iteration will continue until the rescaled equations are identical between the two successive iterations.
One of the major advantages of the RNG method is that by scale expansion, the important turbulence coefficients can be theoretically determined rather than being adjusted empirically.
The RNG approach results in the same k equation but a modified form of the ε equation:

$$\frac{\partial \varepsilon}{\partial t} + \langle u_j \rangle \frac{\partial \varepsilon}{\partial x_j} = \frac{\partial}{\partial x_j}\left[\left(\frac{\nu_t}{\sigma_\varepsilon} + \nu\right)\frac{\partial \varepsilon}{\partial x_j}\right] + C_{1\varepsilon}\frac{\varepsilon}{k} 2\nu_t S_{ij} \frac{\partial \langle u_i \rangle}{\partial x_j} - R - C_{2\varepsilon}\frac{\varepsilon^2}{k}$$

Where R is an ad hoc model not derived from RNG analysis and it plays an important role in the modeling of turbulent flows. Combining a few earlier studies, Orszag et al. (1996) suggested the following values of the turbulence transport coefficients:

$$C_d = 0.085, \quad C_{1\varepsilon} = 1.4, \quad C_{2\varepsilon} = 1.68, \quad \sigma_k = 0.72, \quad \sigma_\varepsilon = 0.72$$

2.4.3 Wall function

Before concluding this brief overview on the turbulence models, it's important emphasize that near the wall the dynamic of turbulence is significantly far from the hypothesis of homogenity and isotropy, and this implies significant changes in the turbulence patterns and in the evaluation of the computational resources required by various simulation techniques (DNS, LES and RANS).

So, for a long time, application of turbulence closure model is limited to region without the presence of a solid wall. Most practical flows however, are wall bounded.

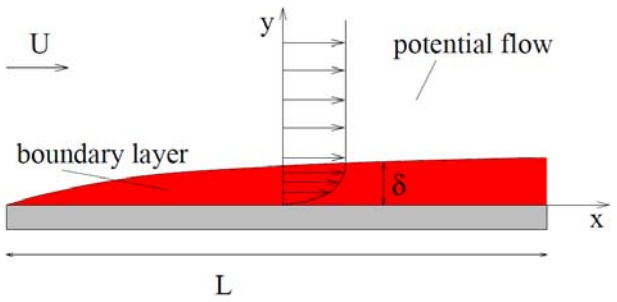

Figure 2.5 : Wall bounded flow

To compensate this lack of physical model, damping functions - f (y) - are used to change the turbulent viscosity. Wall function are important both from a physical point of view - because solid walls are the main source of vorticity and – both in engineering applications – because wall quantities (velocity gradients, pressure, etc.) are very important in several applications.
Over the years, many suggestions have been made to enable the use of turbulence closure models at low-Reynolds numbers and to describe the flow close to a solid wall. In fact, a first important effect of the wall is the decrease in the local Reynolds number.
Furthermore, application of such near-wall treatment will require large expenditure of computational resources since the near-wall viscous and buffer regions of the wall-bounded flows have to be resolved adequately and so it is required a very fine grid resolution to resolve the "steep gradients" near the wall. These dense grids will severely reduce the time-step due to the Courant-Friedricks-Levy (cfr 2.7.2) condition in order to attain stability and/or accuracy.
In addition, at the wall the velocity is zero. However, if the stress is computed directly using the finite-differencing and the grid resolution is not fine enough, severe errors result.
Generally, wall models are based on the "existence" of a logarithmic velocity profile in a turbulent boundary layer and the f(y) has unit value far from the walls and tends exponentially to zero near a solid surface.

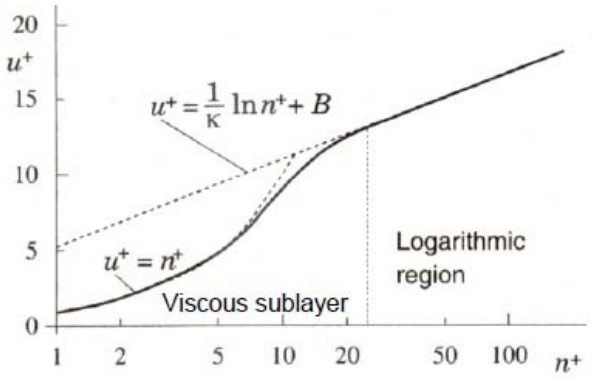

Figure 2.6: Logarithmic velocity profile in a turbulent boundary layer

2.5 FREE SURFACE DISPLACEMENT

A very important aspect of the applications is the presence of a free liquid surface. The reason for the "free" designation arises from the large difference in the densities of the gas and liquid (e.g., the ratio of density for water to air is 1000).
A low gas density means that its inertia can generally be ignored compared to that of the liquid. In this sense the liquid moves independently, or freely, with respect to the gas. The only influence of the gas is the pressure it exerts on the liquid surface.
In other words, the gas-liquid surface is not constrained, but free. Even then, free surfaces require the introduction of special methods to define their location, their movement, and their influence on a flow.

Regardless of the method employed, there are three essential features needed to properly model free surfaces:

1. a scheme is needed to describe the shape and location of a surface,
2. an algorithm is required to evolve the shape and location with time, and
3. free-surface boundary conditions must be applied at the surface.

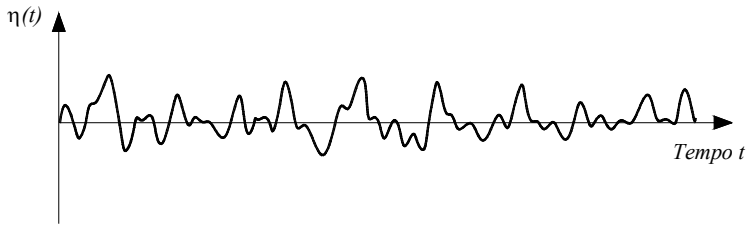

Figure 2.7: Free surface elevation as function of time

Many methods for the treatment of the free surface are described in the literature; the most popular one is the Volume-of-Fluid method, which is adopted in the current method.

2.5.1 Volume-of-Fluid (VOF) Method

To describe the complicated contact surface between two fluids (air and water), the VOF method is used. The VOF method introduces a volume of fluid function F to define the water region. The physical meaning of the F function is the fractional volume of a cell occupied by water. In particular, a unit value of F corresponds to a cell full of water, while a zero value indicates that the cell contains no water. Cells with F value between zero and unity must then contain the free surface (cfr. Figure 2.8). The fractional function F can be evaluated as follows:

$$F = \frac{V_w}{V_c}$$

where V_w is the volume of water inside a cell and V_c is volume of the cell. The algorithm for tracking the interface consists of two steps.
In the first step, the interface is approximated by a linear line segment at each cell, which has the value of fractional function between zero and unity.
In the second step, the interface is tracked by solving the evolution of the fractional function in time.

The two-dimensional transport equation for the fractional function is given by:

$$\frac{\partial F}{\partial t}+\frac{\partial uF}{\partial x}+\frac{\partial wF}{\partial z}=0$$

According to the definition of the VOF function, the density and viscosity can be expressed in term of the fractional function F:

$$\rho=(1-F)\rho_a+F\rho_w$$
$$\nu=(1-F)\nu_a+F\nu_w$$

where ρ_a and ν_a is the density and viscosity of air; ρ_w and ν_w is the density and viscosity of water.

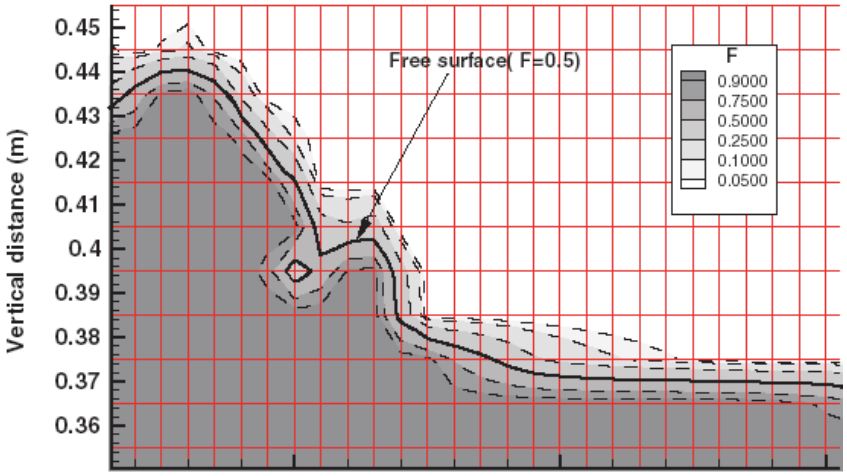

Figure 2.8: Typical values of the VOF function near free surface

The VOF method is extremely suitable in fixed grid simulation methods, where the free surface should be able to have an arbitrary complex topology. For example, in wave simulations the waves are sometimes overturning, such that the interface intersects itself and merges. The VOF method automatically takes this into account.

If we know the amount of fluid in each cell it is possible to locate surfaces, as well as determine surface slopes and surface curvatures. Surfaces are easy to locate because they lie in cells partially filled with fluid or between cells full of fluid and cells that have no fluid.
Slopes and curvatures are computed by using the fluid volume fractions in neighbouring cells.
It is easy to accurately model the solution in one dimension such that the F distribution retains its zero or one values. Imagine fluid is filling a column of cells from bottom to top. At some instant the fluid interface is in the middle region of a cell whose neighbour below is filled and whose neighbour above is empty. The interface must be located above the bottom of the cell by an amount equal to the fluid fraction in the cell. Then the computation of how much fluid to move into the empty cell above can be modified to first allow the empty region of the surface-containing cell to fill before transmitting fluid on to the next cell.

2.6 BOUNDARY CONDITIONS

To continue the mathematical description of the problem, boundary conditions are required for all sides of the computational domain.
For time-dependent problems, initial conditions would also have to be provided, which means that the values of all dependent variables would be given at some time (usually taken at t=0).
The numerical wave channel is considered impermeable at the left and right wall and at the bottom, while it is considered open at the top.
At the **impermeable boundary** the following velocity conditions are adopted.

$$u_n = 0$$

$$\frac{\partial u_s}{\partial n} = 0$$

where n is the coordinate in the normal direction to the impermeable surface, u_n the normal velocity component and u_s the velocity component along the surface. The pressure gradient for the left and right boundaries is set zero while for the top and bottom boundaries it is the product of density and gravitational acceleration (hydrostatic pressure gradient).

On the **interface of air and water**, kinematic boundary condition is satisfied by the equation of VOF function; zero pressure is considered at the top of the solution domain.
At the **inflow boundary**, a wave generator source is adopted (cfr. 3.3).
For **outflow boundary** conditions, in wave propagation problems, special boundary treatments have been devised that try to determine the speed and direction of waves approaching the boundary and then set boundary conditions in such a way as to allow their continuation through the boundary with a minimum of reflection. For wave propagation problems, it is natural to seek a boundary condition that will allow outgoing waves to smoothly leave the computational mesh with minimum reflection.
This problem is analogous to wave absorption in experimental wave tanks, where one wants to eliminate the reflection of waves from the downstream end of the tank. In these tanks a variety of techniques are used, but nearly all of them employ some sort of energy dissipation (e.g., porous beaches). Regardless of the method employed, the length of absorption must be at least as long as the longest waves to be trapped.

2.7 NUMERICAL IMPLEMENTATION

2.7.1 Grid based systems

Gridding is the process of subdividing a region to be modeled into a set of small control volumes. Associated with each control volume are one or more values of the dependent flow variables (e.g., velocity, pressure, temperature, etc.). Usually these represent some type of locally averaged values. Numerical algorithms representing approximations to the conservation laws of mass, momentum, and energy are then used to compute these variables in each control volume.
In summary, the best choice for a grid system depends on several factors: convenience in generation, memory requirements, numerical accuracy, flexibility to conform to complex geometries, and flexibility for localized regions of high or low resolution.
Some computational schemes use grids that deform to follow the motion of a fluid (Lagrangian grids) while others use fixed grids (Eulerian grids).

Sometimes a combination is used so that moving grids don't become too distorted (Arbitrary-Lagrangian-Eulerian grids).
Grids may be structured or unstructured. A structured grid means that the volume elements are well ordered, and a simple scheme (e.g., I,J,K indices) can be used to label elements and identify neighbours. In unstructured grids, volume elements can be joined in any manner, and special lists must be kept to identify neighbouring elements.
Structured grids come in several varieties, depending on the shape of their elements; the simplest grid is generated from a rectangular box by subdividing it into a set of rectangular elements whose faces are parallel to the faces of the box. Most often the elements are ordered by counting in the x then y and finally the z-direction, so that grid element (I, J, K) would be the i-th element in the x-direction, etc.
Grids composed of regular brick elements have the simplest structure since it is only necessary to define three one-dimensional arrays for the x, y, and z values of the surfaces defining the element surfaces. If I, J, and K are the maximum indices in the x, y, and z directions, then the total number of values needed to define the grid is I+J+K. Rectangular grids with slowly varying element sizes also exhibit a regularity that helps to maintain numerical accuracy.

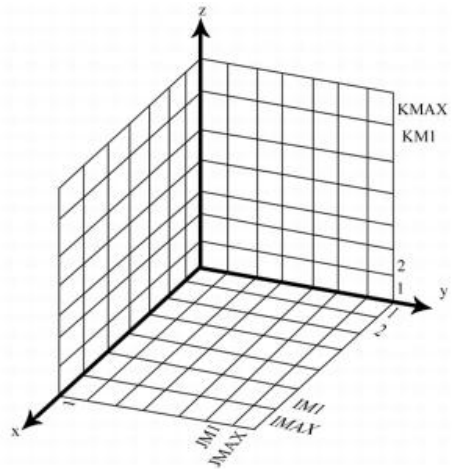

Figure 2.9: Mesh arrangement and labeling convention

2.7.2 Stability condition

In the computation of time domain, the stability of the calculation which is related with the convergence of the numerical solution is assured by applying stability criteria.

Time stepping in computational fluid dynamics is generally non uniform and adjusted such that fluid does not cross more than one computational cell over one time step, Δt, and is limited by the Courant-Friedrichs-Levy condition $\Delta t \leq \min\left(\Delta x/u,\ \Delta y/v,\ \Delta z/w\right)$ and by a diffusive limit condition.

2.7.3 Numerical Viscosities

Numerical viscosity, which is an unwanted consequence of certain types of numerical approximations, arises from discrete approximations to the momentum advection terms in Eulerian equations.
Research into numerical approximation schemes that minimize numerical viscosity effects is a continuing activity of a large part of the CFD community. The difficulty in developing such schemes is that some smoothing must always be incorporated into a numerical solution to keep it computationally stable and to smooth out errors. Dispersion errors are those errors that arise because components of a solution having different grid resolution requirements may propagate through the grid with slightly different speeds. Whenever this occurs, unphysical oscillations develop in the solution where these components reinforce or cancel one another.

3 NUMERICAL METHODOLOGY OF RANS/VOF MODELS

3.1 GENERAL DESCRIPTION OF RANS/VOF MODELS

The process and models outlined in the previous paragraphs have been implemented, in the last few years in a number of numerical codes which are generally employed by the CFD community in the field of marine hydraulic applications

Numerical Navier Stokes models, integrated with turbulence modeling and with volume of fluid surface tracing algorithms (RANS/VOF), are now able to provide a detailed picture of free-surface elevation, pressure and velocity field within the surf zone. They thus allows a 2D direct computation of relevant quantities in near-shore hydrodynamics (i.e., energy flux, momentum flux), and extension to 3D may well be near to become operational.

RANS/VOF methods were first developed by Lin and Liu's (1998) and have now evolved into a fully reliable technique (see for instance Christensen 2006). Also, innovative Lagrangian SPH methods are quickly evolving, and it is most likely that they will soon be able to compete with Eulerian methods (Dalrymple et al 2006; Shao et al 2006), even though at present there is not enough available experience to support their application to real wave action problems.
By far the most commonly RANS/VOF software systems for this kind of calculation are COrnell BReaking waves And Structures, COBRAS-originally developed by Lin (1998) at Cornell University and FLOW-3D by Flow Science (Bradford, 2000; Chopakatla et al, 2008; Dentale et al 2008).

The work discussed in this thesis was carried out by making use of Flow-3D (produce by Flow Science), with various grid sizes and time steps; K–ε turbulence model was used for most of the computations, while RNG was occasionally employed to verify the consistence of results.
FLOW-3D utilizes a true volume of fluid (TrueVOF) method for computing free surface motion (Nichols et al., 1980; Hirt and Nichols, 1981) and the fractional area/volume obstacle representation (FAVOR) technique to model complex geometric regions (Hirt and Sicilian, 1985). The TrueVOF method tracks the sharp interface accurately and does not compute the dynamics in the void or air regions. The portion of volume or area occupied by the obstacle in each cell is defined at the beginning of the analysis. The fluid fraction in each cell is also calculated. The continuity, momentum or transport equation of fluid fraction is formulated using the FAVOR function. A finite difference approximation is used for discretization of each equation.
Fluid velocities and pressures are located at staggered mesh locations as shown for a typical cell in the figure below: u velocities and fractional areas Ax at the centers of cell-faces normal to the x-direction, v velocities and fractional areas Ay at the centers of cell-faces normal to the y-direction, and w-velocities and fractional areas Az at the centers of cell-faces normal to the z-direction. Pressures (p), fluid fractions (F), fractional volumes (V), densities (ϱ), internal energy (I), turbulence quantities for energy (q), dissipation (D), and viscosity (μ) are at cell centers.

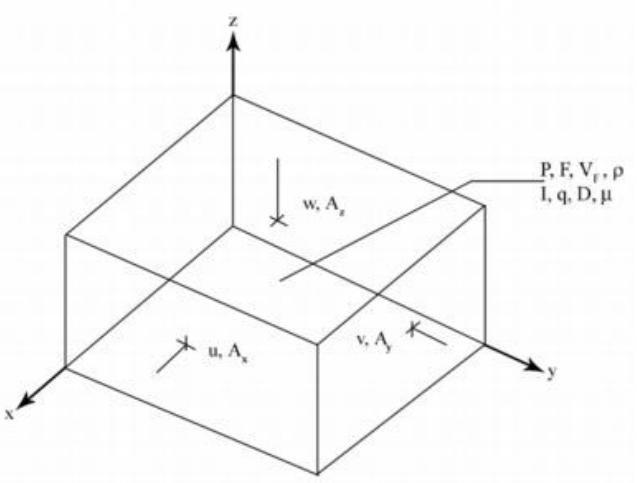

Figure 3.1: Location of variables in a mesh cell

The basic algorithm for advancing a solution in a one time increment consists of the following three steps (Flow Science, 2008):

1. Compute the velocities in each cell using the initial conditions or previous time step values for all advective pressure, and other accelerations based on the explicit approximations of the momentum (Navier–Stokes) equations.
2. Adjust the pressure in each cell to satisfy the continuity equation.
3. Update the fluid free surface or interface to give the new fluid configuration based on the volume of fluid value in each cell. A mixture of explicit and implicit solution schemes can be used to solve for the partial differential equations. The selection depends on the complexity of the fluid flow problem in question.

3.2 PROCEDURE OF SIMULATION

The basic procedural steps are shown below:

1. create or import geometry files;
2. create a computational mesh;
3. specify the boundary conditions;
4. specify fluid and void initial conditions;
5. select output options (frequency of plot output or animation output);
6. adjust parameters associated with the numerical methods (time-step controls, explicit/implicit solver options, etc…);
7. calculate a solution.

If necessary, refine the grid or consider revisions to the numerical or physical model.

3.3 WAVE GENERATION

Wave generation is an essential aspect of wave laboratory experiments as well as in numerical simulations.

In **hydraulic laboratories**, different wave makers are available. Most wave makers consist of a hydraulic piston which drives a wave flap The flap generates the wave by moving forwards and backwards.
Another possibility is to connect the have the flap rotate on a hinge at the bottom of the flume (Figure 3.2).
In shallow water, the piston wave paddle is more effective than the flap as the horizontal paddle velocity are nearly constant over the water column, very much like the velocities of the wave particles. In deep water, the reverse is true, as both the wave and the paddle motions are confined near the surface (Dean and Dalrymple 1984).

Figure 3.2: Different types of wave generators

In **numerical simulation** there are two different possibilities to model the wave generation. The first option is to generate the waves on by prescribing the free surface elevation, η , and the two components of the water particle velocity. Alternatively, the waves can be generated by using a solid boundary that can move horizontally and/or rotate about different axes., thus mimicking the behaviour of a physical wave tank paddle.

After the wave is generated at the inflow boundary, it propagates through the computational domain. The propagation of waves needs to be carefully taken into account, since the steepness and height of the waves determine the loads on the structures in the waves.

The influence of the grid size and of the time step must be investigated as well as the influence of the boundary conditions.
Further, attention has to be paid to the dissipation due to effects of the numerical viscosity, always present in the discretization of the in the Navier-Stokes convective term.

3.3.1 Generation of waves using wave description theory

A wave description theory is used to generate the waves at the inflow boundary of the domain. Note that at the inflow boundary positive and negative velocities can occur, so fluid can flow in and out. The wave is generated by prescribing velocities at the inflow boundary. Different kind of wave descriptions can be used to determine the velocities at the inflow boundary; the easiest is a linear wave description (Airy wave) but this means that only waves with a very small amplitude can be generated using linear theory accurately. The Airy theory assumes that the fluid is inviscid and that there are no currents in the flow.

As shown in the figure below, the linear wave is assumed to come from a flat bottom reservoir into the computational domain. A linear wave is characterized by the wave amplitude A, wavelength L, wave frequency ω and wave number $k=2\pi/L$.

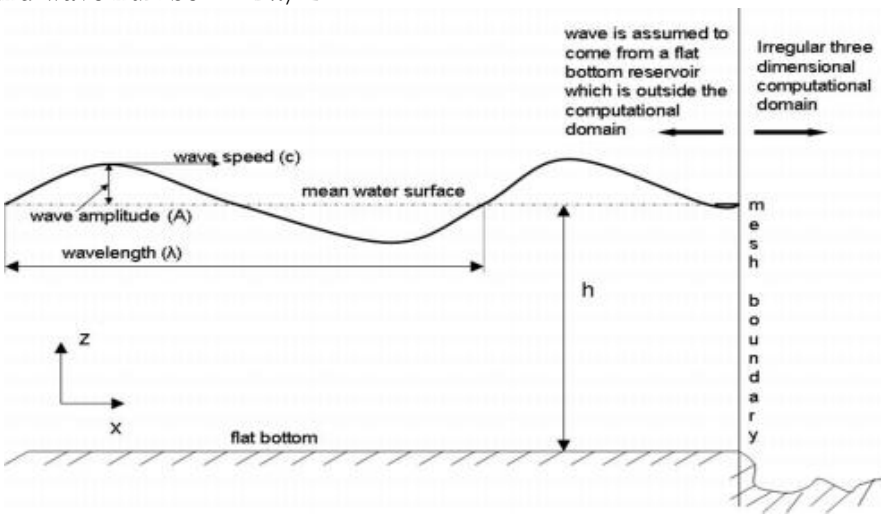

Figure 3.3: Schematic diagram showing a linear wave coming from a flat bottom reservoir on the right into the computational domain through the mesh boundary.

The free surface evolution in the wave can be described by it coordinate in the vertical direction:

$$z = \eta(x,t)$$

with:

$$\eta(z,t) = A\cos(kx - \varpi t + \varphi)$$

where φ is the phase shift angle.

The linear wave theory is based on the following assumptions:

- fluid is incompressible, inviscid, irrotational , two-dimensional flow;

- wave is generated in quiescent body of water (no currents);

- Stokes wave approximation: the amplitude of wave (A) is smaller than the depth of water (d) and wavelength (L).

With the above assumptions, the wave problem can be reduced to a Laplace equation; the solution of Laplace equation is given by:

$$\phi(x,y,t) = \frac{A \cdot \omega \cdot \cosh(k[z+d]) \cdot \sin(kx - \omega t + \varphi)}{k \cdot \sinh(kd)}$$

where Φ is the potential function.

The fluid velocity component can be obtained as:

$$u(x,y,t) = \frac{A \cdot \omega \cdot \cosh(k[z+d]) \cdot \cos(kx - \omega t + \varphi)}{\sinh(kd)}$$

$$w(x,y,t) = \frac{A \cdot \omega \cdot \sinh(k[z+d]) \cdot \sin(kx - \omega t + \varphi)}{\sinh(kd)}$$

The wave speed c = ω/k is expressed as:

$$c^2 = \frac{gL}{2\pi}\tanh\frac{2\pi d}{L}$$

where d is the average depth of the fluid in the wave.

This relationship implies that the wave frequency and wave amplitude are not independent but are related as:

$$\omega^2 = \frac{2\pi g}{L}\tanh\frac{2\pi d}{L}$$

The user can either specify wave frequency or wave amplitude and the other quantity will be calculated by the code.

The linear wave theory assumes a flat bottom reservoir and this assumption is required to generate the wave at the mesh boundary. Once the wave enters the computational domain, the bottom surface no longer needs to be flat, in which case the wave may deviate from the analytical solution given by the equations above.

3.3.2 Generation of waves using a wave maker

To generate the desired incident waves, the lateral boundary condition at the wave-maker must be determined. The height of the wave created by the paddle motion is related to the stroke of the paddle, which will be denoted by the horizontal displacement of the paddle at the still water line. For the generation of small-amplitude waves with a surface elevation $\eta = A\cos(kx - \varpi t)$, where A=wave amplitude; k=wave number; and ω=circular frequency, the displacement of the wave-maker is determined from the linear wave-maker theory (Dean and Dalrymple 1984) as:

$$\xi(t) = -\xi_0 \cos \omega t$$

$$\xi_0 = \frac{a \cdot n}{\tanh(kh_0)}, \qquad n = \frac{1}{2}\left(1 + \frac{2kh_0}{\sinh(2kh_0)}\right)$$

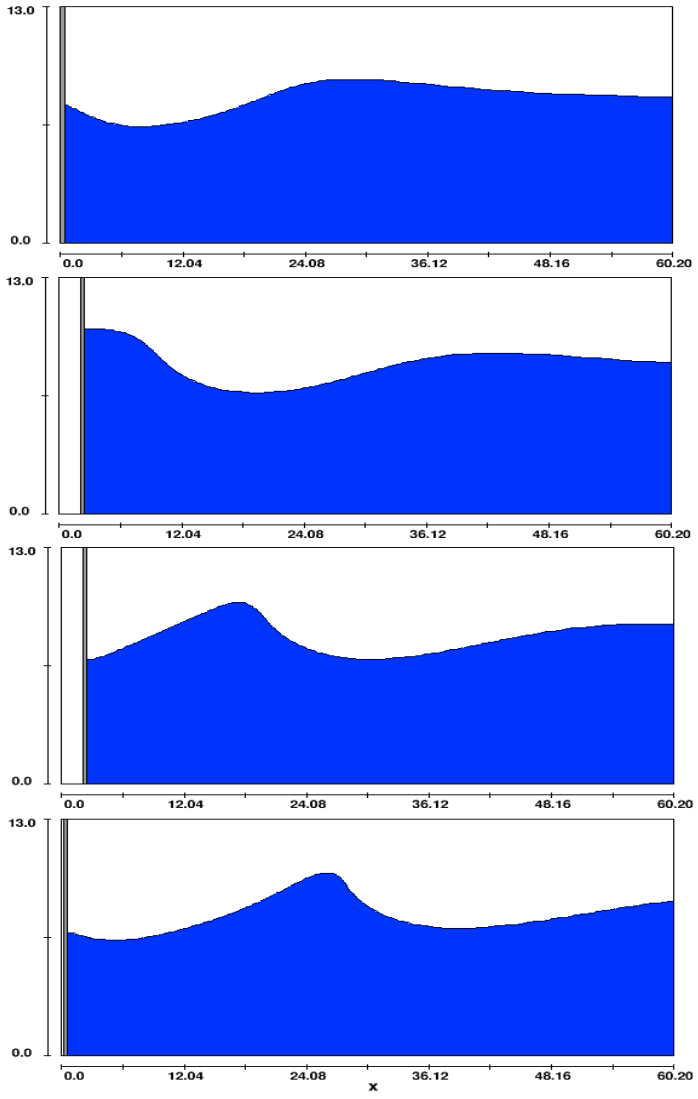

Figure 3.4: Wave generated by piston motion

4 SIMULATION OF REGULAR WAVES ON BEACH

In this section, the numerical results, simulating the evolution of a sinusoidal wave train breaking on a sloping beach, are presented. Wave breaking on a gently sloping beach, in fact, is an obvious starting point for any testing of a breaking model.

4.1 VALIDATION OF THE NUMERICAL MODEL

First, laboratory data were used to validate the numerical model.
In fact, no Navier Stokes/VOF numerical integration solution of breaking waves can be considered reliable unless a proper calibration is first carried out. A large number of tests thus were run by making use of a conventional numerical set up as in Figure 4.1 (modified as necessary for the slope m) and comparing results with of published data.

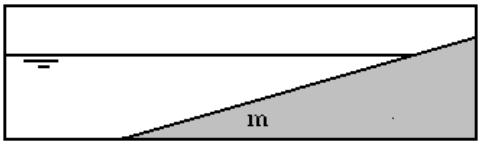

Figure 4.1: General numerical set-up

The comparison are done between the experimental (Ting and Kirby, 1995-1996; Mossa and De Serio, 2006) and the simulated (FLOW-3D) wave heights in various probes located (dots in the enclosed scheme) along the submerged slope, both in the constant depth zone (regular wave) and in the breaking zone (spilling and plunging wave – Figure 4.2).

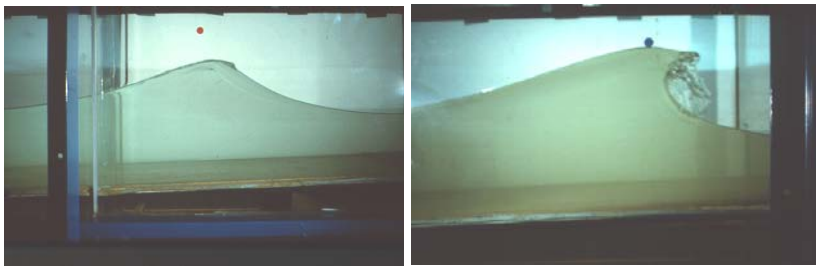

Figure 4.2: Experimental images from Ting & Kirby (1996): a) spilling; b) plunging

Next graph summarizes the general results of the validation.

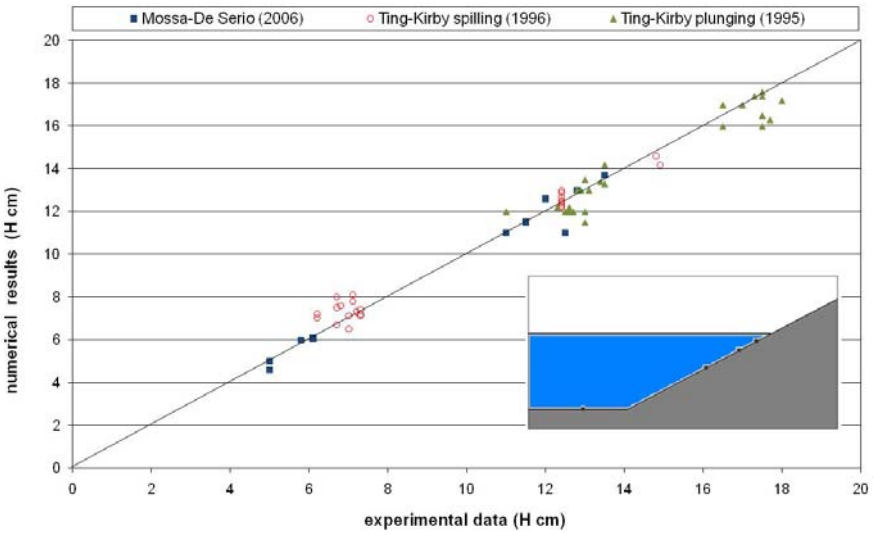

Figure 4.3: Correlation between numerical and experimental wave heights at different probes

A more recent set of results recently published by Mossa and De Padova (2008a, 2008b) allows a more accurate control of the calibration, but also raises some interesting consideration on the role of viscosity – and therefore of the Reynolds number.

Figure 4.4 shows an excellent agreement between Mossa and De Padova's experimental and numerical (SPH) results – which indeed supports the validity of the procedures being applied - both Eulerian NS/VOF and SPH.

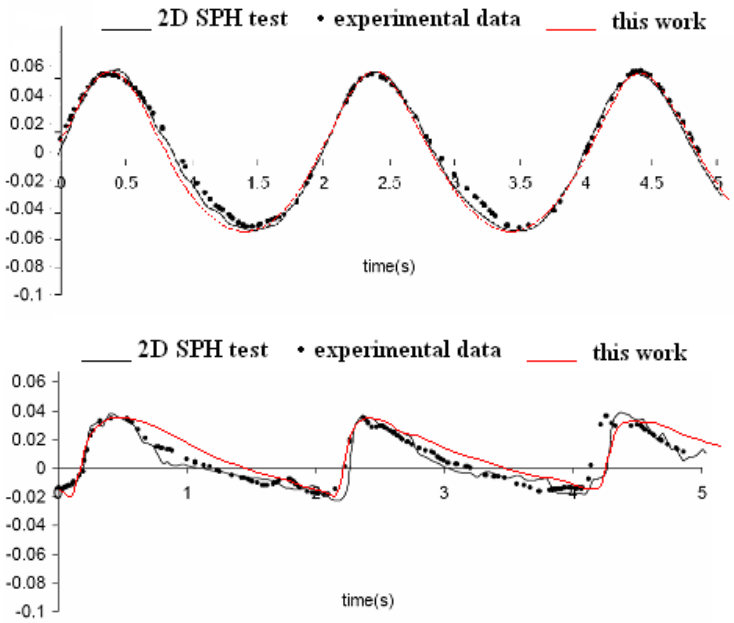

Figure 4.4: Comparison between instantaneous water height η, from experimental data, FLOW-3D numerical results and 2D SPH (from De Padova 2008a)

4.2 NUMERICAL SETUP

In the first simulation, a beach with constant slope of s=1/20 is connected to a region with constant depth dc=8 m; the computational domain is 370 m long with the left slope starting at 70 m away from the wave-making boundary.

The coordinate system is chosen so that x=0 is located at the left boundary position, where the still water depth is constant, and z=0 corresponds to the bottom.

As stated in the previous chapters, there are two kinds of boundaries, namely inflow boundary and domain boundary. The inflow boundary represents the wave generator while the domain boundary represents variables at fictitious cells adjacent to real cells.
At the inflow boundary (Zmin), a piston type wave maker is simulated to generate incident linear waves, setting time-dependent conditions for velocities and fluid height, based on the analytical solution for sinusoidal waves (Airy theory).
At the domain boundary, tree types of boundaries are incorporated: the lower and upper floors (Zmin and Zmax) were regarded as solid walls (condition "Wall") while boundaries side (Ymin and Ymax) are set as symmetry planes (condition "Simmetry"). For Xmax was set a condition that allowed fluid to freely exit the computational domain with a minimum of reflection; this condition is known like "Outflow". For wave propagation problems, in fact, it is natural to seek a boundary condition that will allow outgoing waves to smoothly leave the computational mesh with minimum reflection. This problem is analogous to wave absorption in experimental wave tanks, where one wants to eliminate the reflection of waves from the downstream end of the tank.
Fluid properties were set by loading through a Fluids Database those of water at 20° on CGS.
Turbulence was simulated using a K–ε model.

The incident sinusoidal wave has a wave height H_0=2.0m in the constant-water-depth region and wave period T=4.8s. The simulation was run for 60s, which allowed 12 complete waves into the domain; the simulation time was chosen long enough to allow the waves to reflect off the beach and establish a return flow. Others geometrical and numerical parameters are summarized in Table 4.1.

The free-surface displacement, velocities and turbulent kinetic energies were measured at tree vertical probes, one (P1) in the constant depth zone, another (P2) at the beginning of the sloping beach and the last (P3) well into the surf zone (see Figure 4.5).

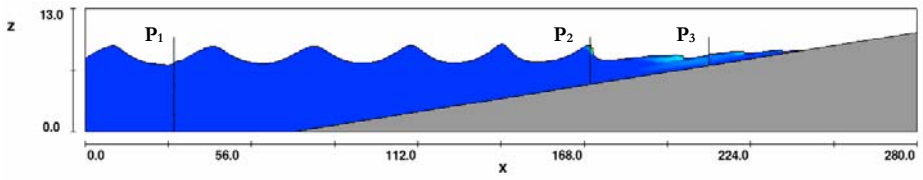

Figure 4.5: Numerical set up

Table 4.1: Geometrical and numerical parameters

slope	0.05
Ho (m)	2.00
To (s)	4.85
Lo (m)	33.29
Irribarren parameter	0.20
depth (m)	8.00
simulation time (s)	60.00
dt output (s)	0.40

4.3 VOF AND TRUEVOF METHODS

In most classical RANS/VOF simulations the total volume of fluid within the computational domain is found to increase with time. Such an accumulation dosen not only derive from the Stokes drift (cfr. Paragraph 5.2), which decreases with wave, but, mostly from a numerical problem in the free-surface tracking.
Accuracy in the free surface tracking is actually one of the cornerstones of the methods and specially so even more when the Piecewise Linear Interface Calculation (PLIC) method is used.
The standard VOF method, in fact, makes use of the previous time step values of the F volume of fluid function to compute fluxes in the three coordinate directions. This results in overfilling or over-emptying the computational cells when volume fluxes are significant in all three directions, specially so for time.

A new approach, called TruVOF, alleviates these deficiencies of the old algorithm; the fluid interface is reconstructed in 3D, using a piecewise linear representation, in each volume (or cell) containing the interface. The fluid volume bounded by the interface and cell faces is then moved according to the local velocity vector in a Lagrangian manner. Finally, the advected volume is overlaid back onto the Eulerian grid to obtain the new values of the fraction-of-fluid function.

The new VOF advection method (Figure 4.6) is thus based on three steps:

1. Approximate fluid interface in a cell with a planar surface;
2. Move the fluid volume according to the local velocity field;
3. Compute new fluid fraction values in the computational cells using an overlay procedure.

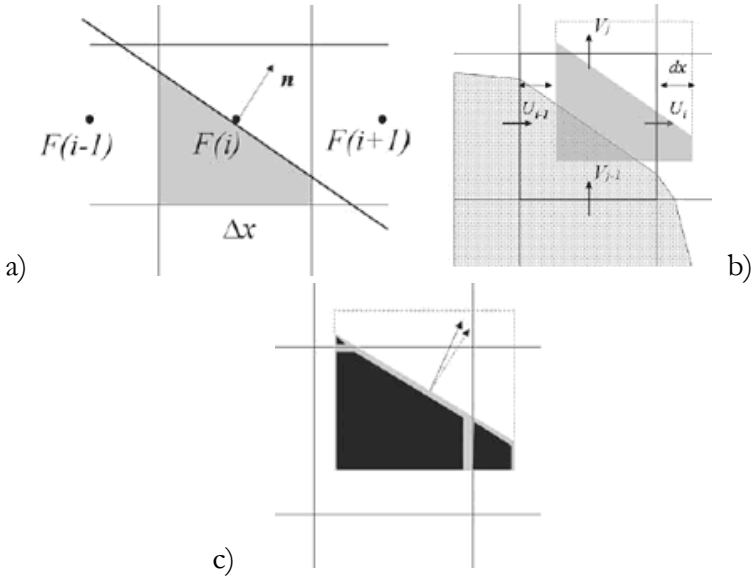

Figure 4.6: Three steps of the Lagrangian interface tracking method: a) piecewise linear interface reconstruction with the normal n; b) moving the control volume; c) overlaying the advected volume onto the grid.

Its main advantage over the standard method is an increased accuracy in moving fluid interfaces in arbitrary directions within the rectangular grid.

In Fig. 4.7 and 4.8, the volume of fluid and the water surface as function of time are reported, and is clearly the improvement resulting by the use of the TruVoF method.

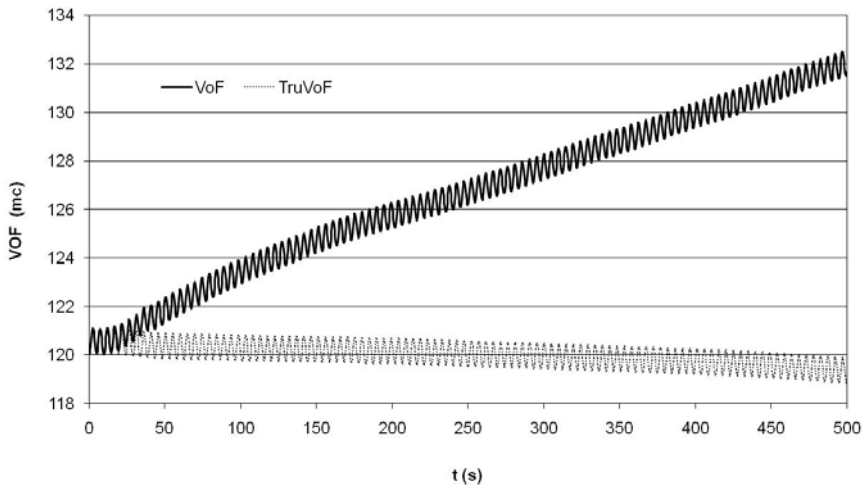

Figure 4.7: Volume of Fluid as function of time

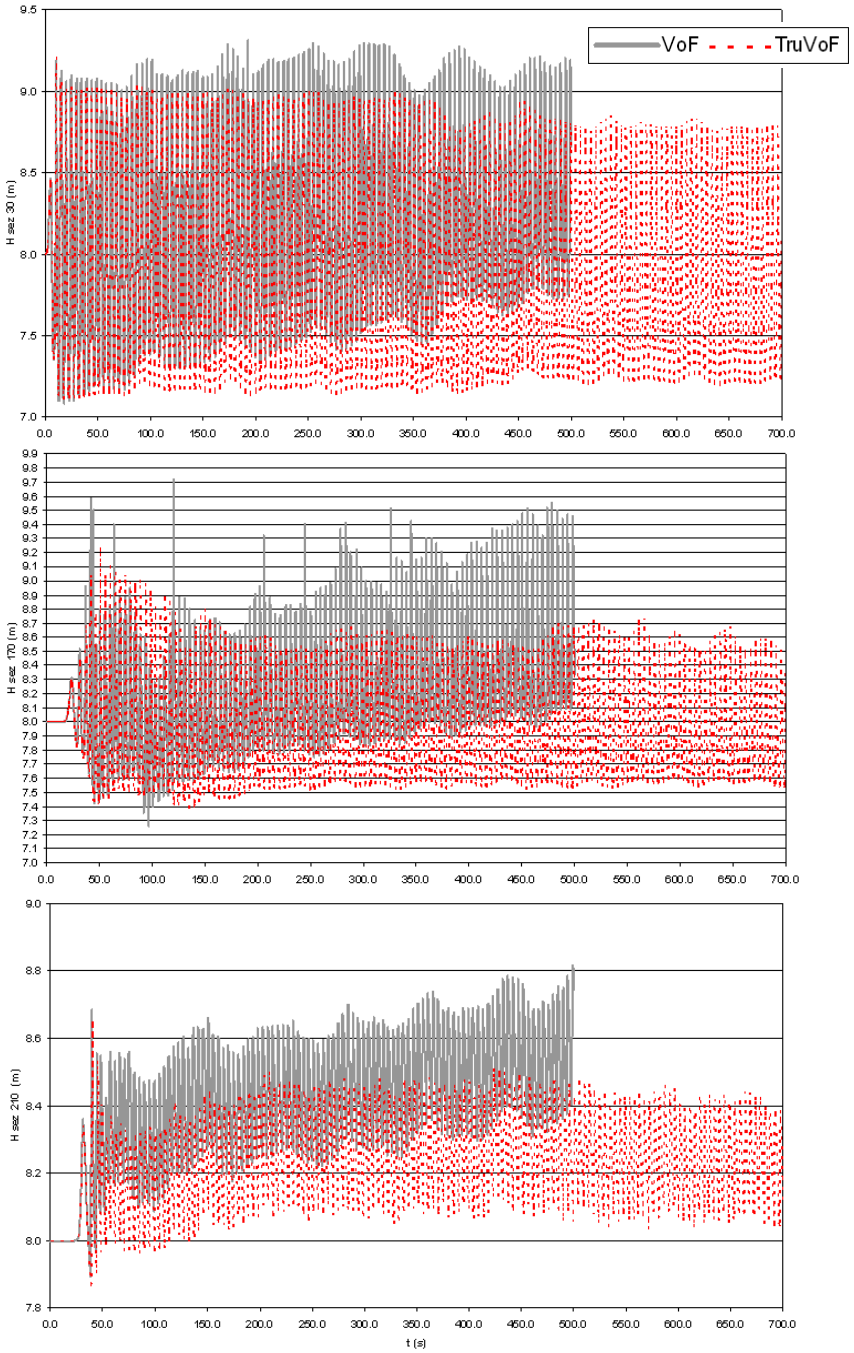

Figure 4.8: Surface Height as function of time in the probes P1, P2 and P3

4.4 COMPARISON BETWEEN WAVE MAKERS

If the motion of the piston-type wave-maker is set to be sinusoidal, the generated finite-amplitude waves will not have a permanent form: these waves will decompose into a primary and one or more secondary waves. The symptoms of the unstable wave train are that due to the superposition of the waves with lower side band frequencies.

For a sinusoidally moving wave maker, the theory predicts secondary waves to occur as a result of the generation of a second harmonic free wave (Ciardulli, 2009). The primary and secondary waves travel at different speeds and the resulting surface profile may exhibit, more or less pronounced, the presence of secondary waves, depending on the distance from the wave maker. For waves of small amplitude, these secondary waves will be extremely small and may in most cases be neglected. It should be noted that, in numerical like in experimental conditions, this second harmonic motion (or higher harmonics) is amplified more with an external than an internal piston type wave-maker, such an extent that it no longer can be neglected (cfr. Fig.4.9).

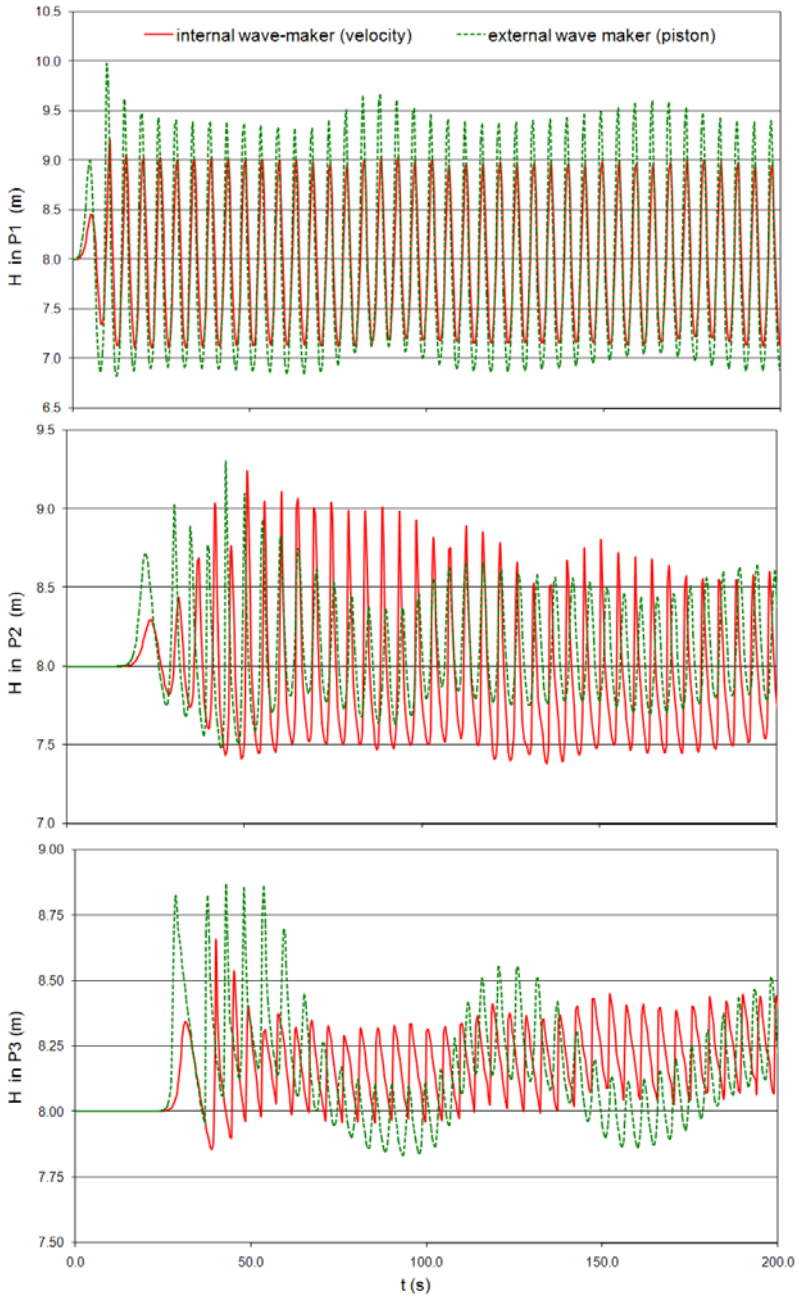

Figure 4.9: Wave height in the tree probes by internal and external wave makers

4.5 CONVERGENCE ANALYSIS ON COMPUTATIONAL DISCRETIZATION

In this section, attention will be paid to the size of cells and the inflow boundary condition time step, that are needed for an accurate description of the wave. In the wave simulations, some numerical parameters have been varied: spatial discretization (number of cells for wavelength - number of cells in the wave height) and temporal discretization (number of time steps for period). The results have been presented as diagrams of surface elevation *srfht*, horizontal velocity *Vx*, turbulent kinetic energy *TKE* and dynamic viscosity *mu*, on a simulation time of 12 periods.

4.5.1 Spatial discretization

Grid resolution is an important numerical parameter that involves a tradeoff between accuracy and computational effort. Grid resolution can critically affect the results. Stability of the model from a coarser to finer mesh is examined in the following figures.

In the numerical simulations, tree different uniform grid systems with a smaller cell size were used to represent the computational region, in order to perform a convergence analysis. The time step is automatically adjusted during the computation to satisfy the stability constraints. The meshes are summarized in Table 4.2 and represented in Figure 4.10.

Table 4.2: Different grid size

	Δx	Δz	n. cells x	n. cells z	tot cells
Coarse grid	0.20	0.20	1850	80	148000
Medium grid	0.10	0.10	3700	160	592000
Fine grid	0.05	0.05	7400	320	2368000

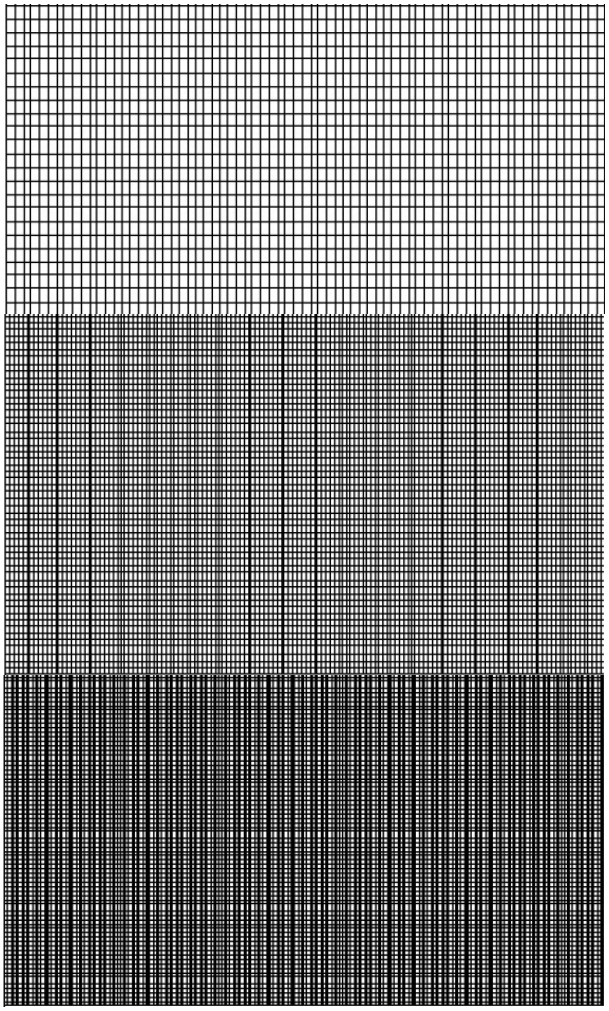

Figure 4.10: Sketch of different grid size

Figure 4.11 shows the influence of different mesh sizes on the wave height, in the selected probes.
It is seen that, the finer mesh sizes give the better results and the simulated wave troughs are less sensitive with the mesh size than the wave crests.

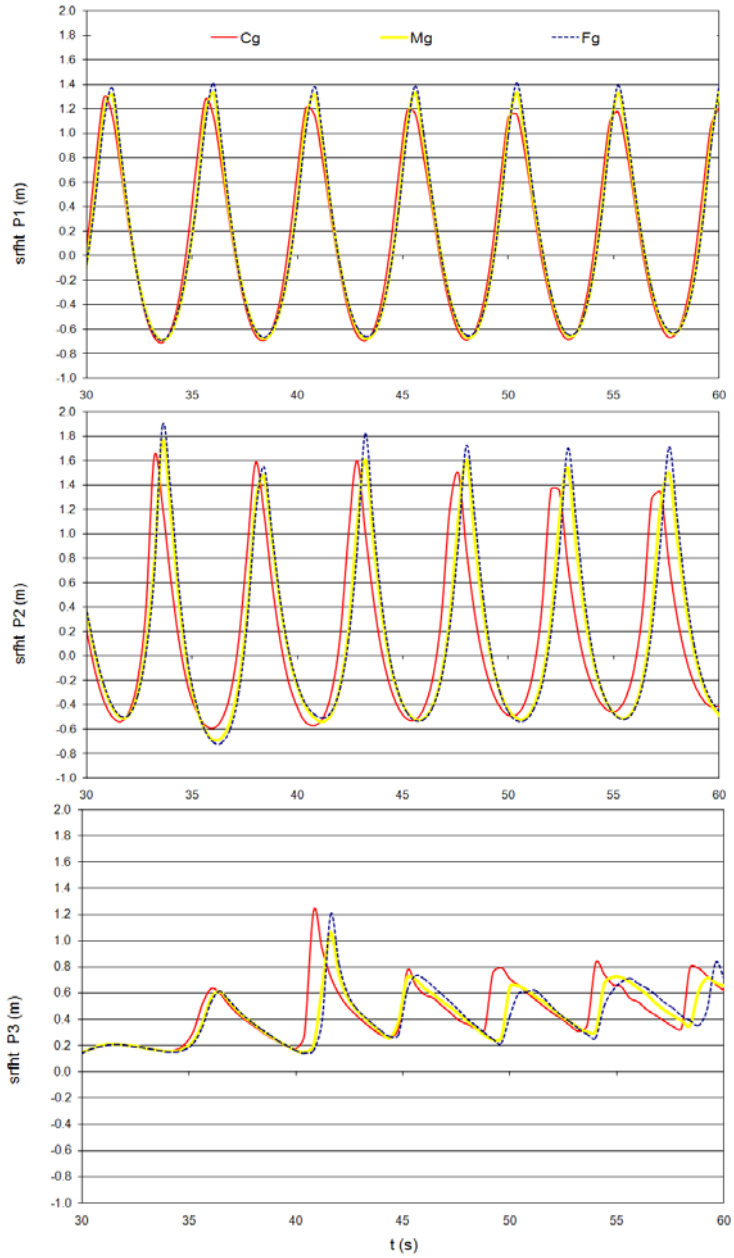

Figure 4.11: Comparison between wave height at different grid size: / coarser grid; / medium grid; / finer grid

There seems to be a good coincidence between the finer and the medium grid; based on tradeoff between accuracy and computational effort, case Mg is optimal so square cells of 0.10 m sides can be accepted.

The wave height differences with different grids obviously depend on the sampling and the numerical viscosity.
In fact, using of different grids involves a different number of sampling points for a single wave. In this case, the wave length is about 33 meters, and so, with the three different Δx, we have about 165, 330, 660 points for wave.
If the points are too few - considering also that the software provides the averaged value on the cell size (numerical approximation) – results might be underestimated. For example, for high Δx values, some parameters such as the peaks of η, could be killed considering . Another error is of course due to numerical viscosity, that obviously it weighs more, as the grid computing space becomes larger.

For the comparison of horizontal velocity (Vx), turbulent kinetic energy (TKE) and dynamic viscosity (mu), the vertical profiles at the three probes for the coarse and medium grids, during a whole wave period, have been reported below.

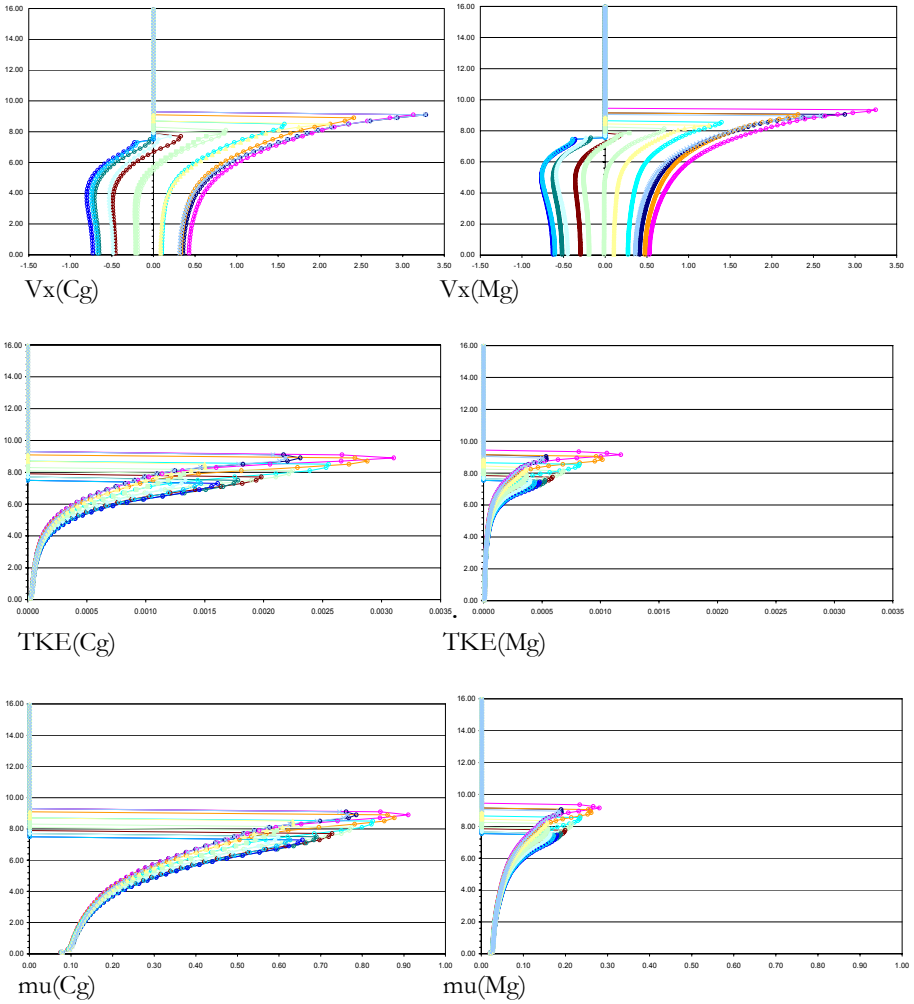

Figure 4.12: Vertical profile of horizontal velocity (Vx), turbulent kinetic energy (TKE) and dynamic viscosity (Mu) at different grid sizes (coarse grid on the left and medium grid on the right) in the probe P1

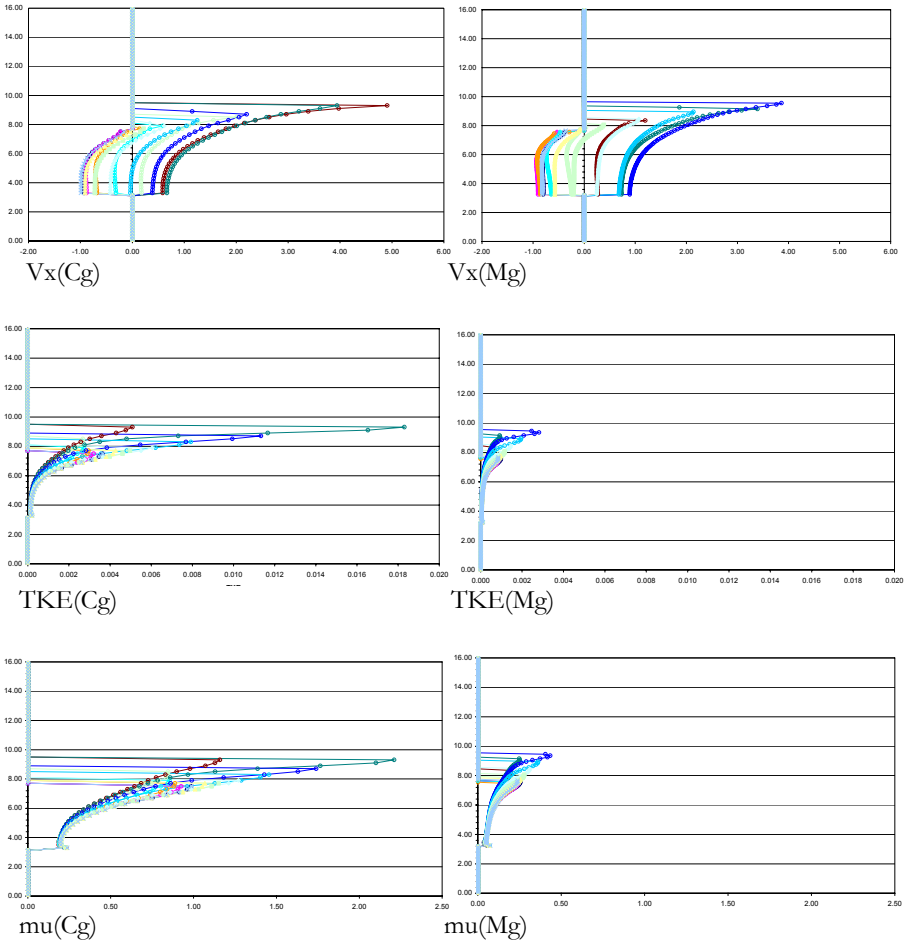

Figure 4.13: Vertical profile of horizontal velocity (Vx), turbulent kinetic energy (TKE) and dynamic viscosity (Mu) at different grid sizes (coarse grid on the left and medium grid on the right) in the probe P2

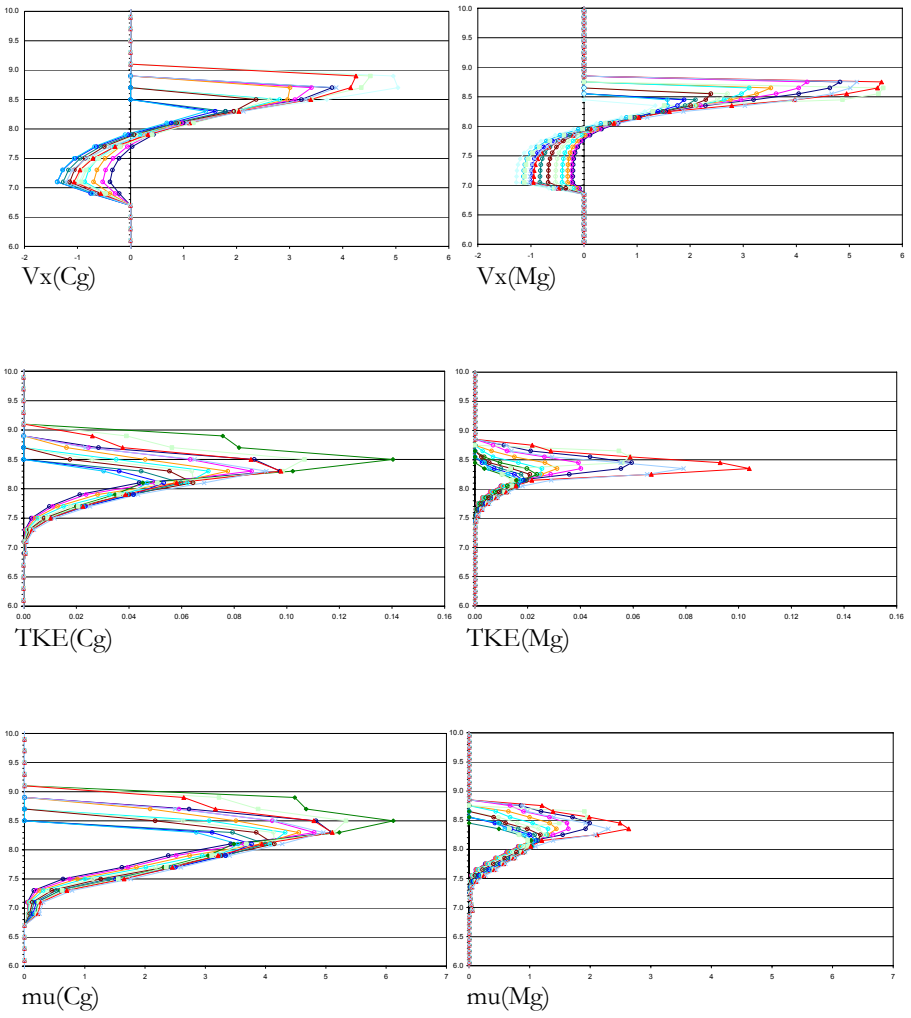

Figure 4.14: Vertical profile of horizontal velocity (Vx), turbulent kinetic energy (TKE) and dynamic viscosity (Mu) at different grid sizes (coarse grid on the left and medium grid on the right) in the probe P3

From Figures 4.12 to 4.14 derives that the values of TKE for the simulation with Cg grid are always higher than those with Mg grid.
This behaviour is due to the numerical and turbulent viscosity as estimated by the turbulence model, in this case K-ε. In fact, the numerical model determines the rate of turbulent dissipation (ε) as inversely proportional to TLEN (length scales of the eddies), that is defined as percentage of the minimum cell size:

$$\varepsilon = C_d \sqrt{\frac{3}{2}} \frac{TKE^{\frac{3}{2}}}{TLEN}$$

When the turbulence option is used, the viscosity is a sum of the molecular and turbulent values and we can defined the turbulent kinematic viscosity, ν_t, as:

$$\nu_t = TLEN \sqrt{\frac{2TKE}{3}}$$

In conclusion, small computational cells sizes return small TLEN, increasing ε and reducing TKE and νt ; accordingly, the values of free surface elevation and horizontal velocity get higher.
Other details for the convergence analysis on turbulence models are presented in the section 4.6.

4.5.2 Temporal discretization

To get a better result, also model sensitivity on the inflow boundary condition (input velocity and fluid height) time step was monitored.
It is indeed important to choose an appropriate sampling time for the inflow input to avoid excessive approximations on the boundary conditions in the simulation.

In the convergence analysis, the following sample for wave are used and the differences are shown in Figure 4.15. Time sampling for wave period has to be at least 8 points.

4 points (Δt = 1.0 s);
8 points (Δt = 0.6 s);
16 points (Δt = 0.3 s);
48 points (Δt = 0.1 s).

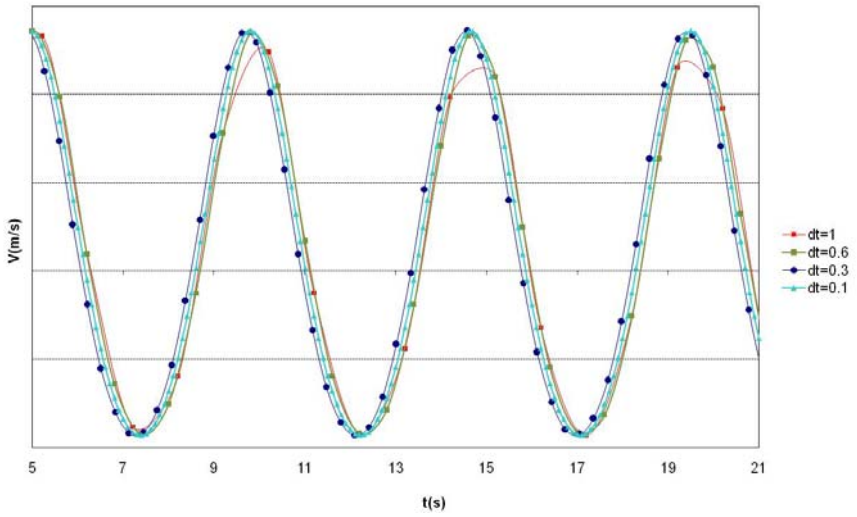

Figure 4.15: Input velocity with different temporal increment

4.6 CONVERGENCE ANALYSIS ON TURBULENCE MODELS

The principal goal of any turbulence model is to provide a mechanism for estimating the influence of turbulent fluctuations on mean flow quantities. This influence is usually expressed by additional diffusion terms in the equations for mean mass, momentum, and energy.
Wherever the coefficient of dynamic viscosity appears, and we assume that it is a sum of the molecular and "turbulent" viscosities, $\mu = \rho(\nu_T + \nu)$.

Strictly speaking, this is not always correct, but it is a good approximation for high levels of turbulence (i.e., when the turbulent viscosity is much larger than the molecular value).

At low levels of turbulence, the turbulence models are not correct without additional modifications. In what that follows we shall assume the turbulence models will only be used when turbulence in the physical problem is important (i.e., in the high intensity limit).
The turbulent, or "eddy" viscosity associated with turbulence is computed from a conceptual model of turbulent eddies transporting momentum (and other quantities) as they move about. This transport is characterized by the velocity and length scales of the eddies.
Defining TLEN as the characteristic length scale of the energy containing eddies and using the square root of the turbulence kinetic energy TKE, to characterize the velocity scale, we define the turbulent kinematic viscosity, ν_T, as:

$$\nu_T = TLEN\sqrt{\frac{2TKE}{3}}$$

In the two-equation model of turbulence the constant length scale parameter is replaced by the turbulence energy dissipation function ε, and the viscosity is then expressed as:

$$\nu_T = C_d \frac{TKE^2}{\varepsilon}$$

where C_d is a user-definable constant (a typical value in the standard k-ε model is C_d=0.09, and C_d=0.085 in the RNG model). Combining the above two expressions we see that ε, TKE and TLEN are related according to:

$$\varepsilon = C_d\sqrt{\frac{3}{2}}\frac{TKE^{3/2}}{TLEN}$$

4.6.1 Characteristic length scale

It is, therefore, important to understand the effect of TLEN on the simulations. In the following figure a comparison, between three different TLEN limits, is carried on.

TLEN is used by the K-ε and RNG turbulence models to limit the turbulent dissipation so that the turbulent viscosity does not become excessively large.
If TLEN is too large, the turbulence energy dissipation function will be under-predicted, the turbulent viscosity will be over-predicted and the turbulent kinetic energy will be higher.
If TLEN is too small, the dissipation will be over-predicted and turbulence will be excessively damped out.

The default value of TLEN is computed as 10% of the smallest domain dimension, excluding any mesh direction which has only 1 cell.
For example, if the simulation contains 3 mesh blocks and the smallest dimension of all mesh blocks is 1 meter, the default value of TLEN would be 0.1.

In the figure below the wave height comparison with different TLEN (10% and 20% of the smallest grid size) is carried on; some, but irrelevant differences are visible only in the probes P3, where the wave is broken and the turbulence plays some effects. For the probes P3, also the horizontal velocity, turbulent kinetic energy and dynamic viscosity vertical profiles are reported.

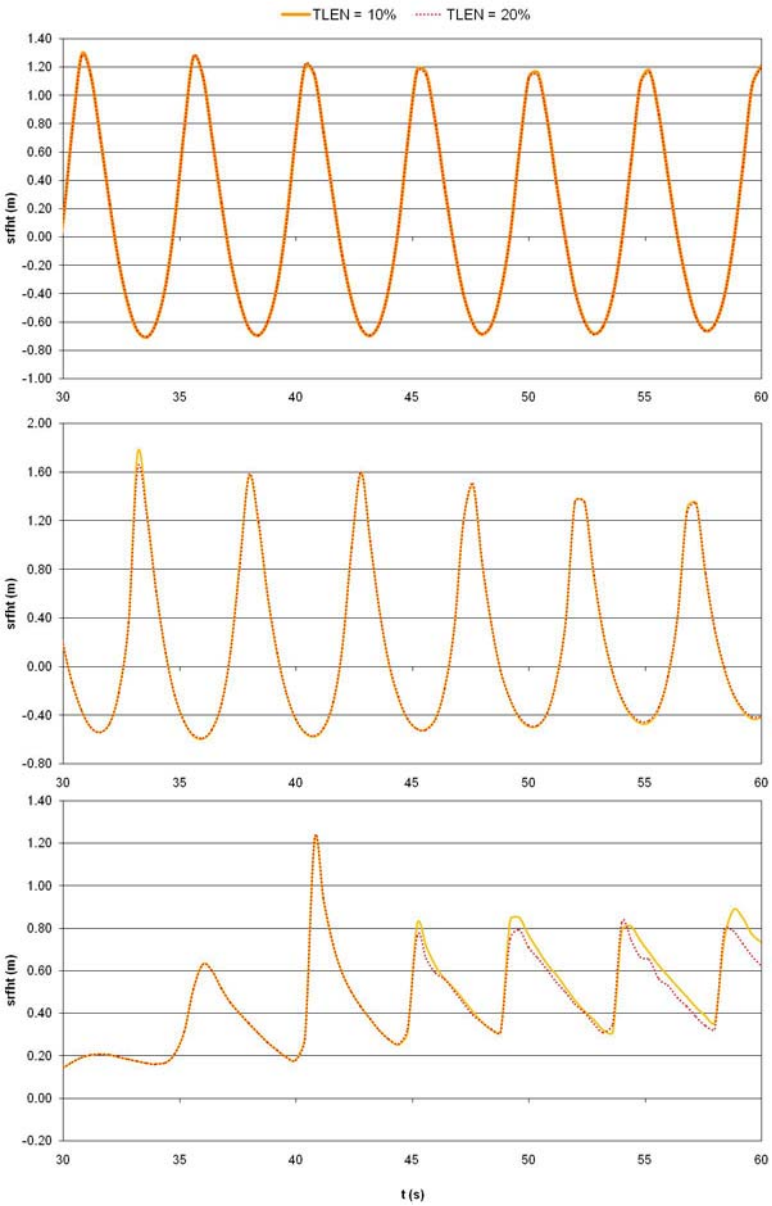

Figure 4.16: Influence of different TLEN on wave height in probes P1, P2, P3

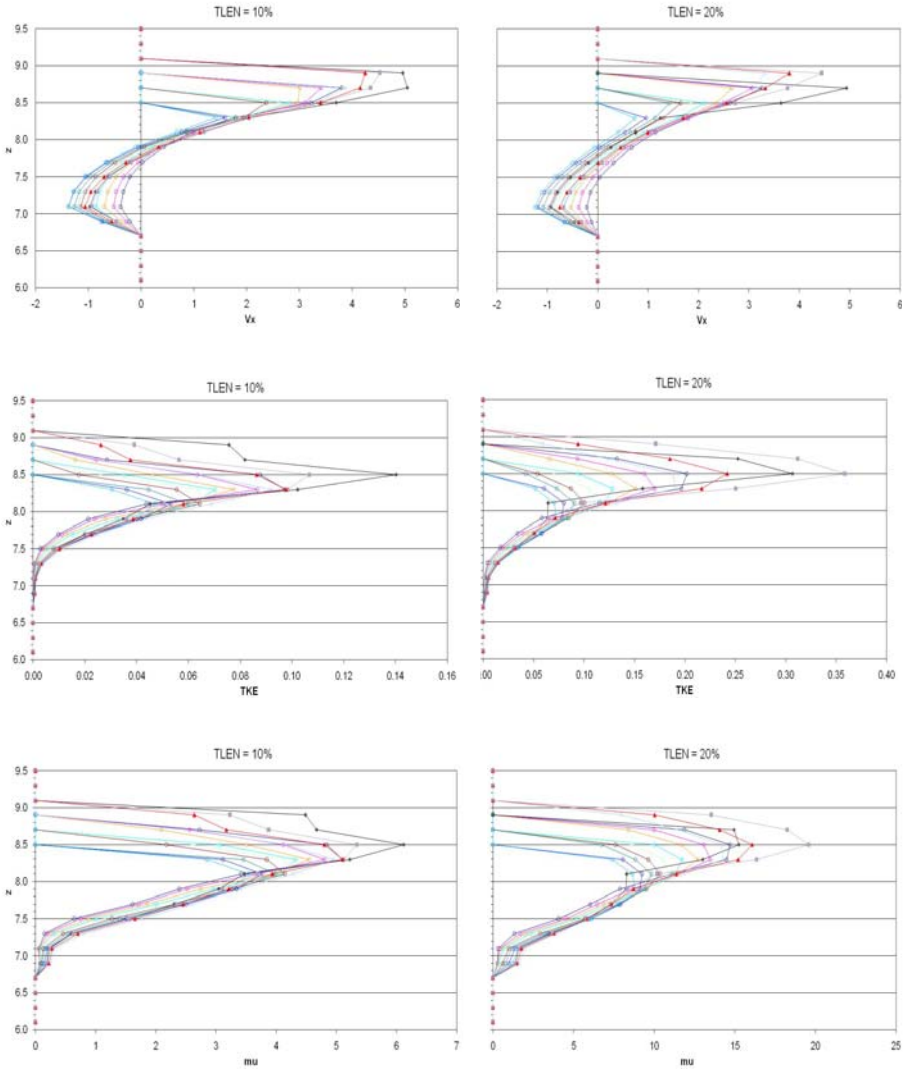

Figure 4.17: Influence of different TLEN on horizontal velocity, turbulent kinetic energy and dynamic viscosity vertical profiles in probe P3

4.6.2 Turbulence Models

Tests are also done to understand the influence of turbulence models on the wave simulations. The same test (Figure 4.5) is elaborated with K-ε model, RNG model, no-TURB (newtonian viscosity + laminar turbulence options) and no-VISC (inviscid fluid + laminar turbulence options). Visible effects are recorded only in the probe P3, where the wave is broken and so viscosity and turbulence play an important role, as reported in Figure 4.18 and 4.19.

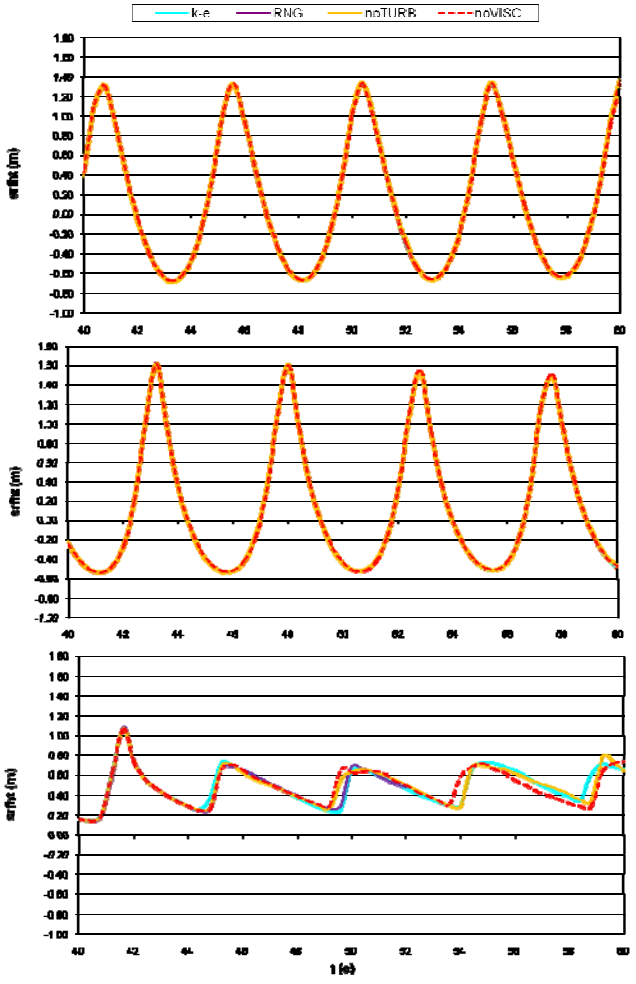

Figure 4.18: Influence of turbulence models on the wave height in P1, P2 and P3

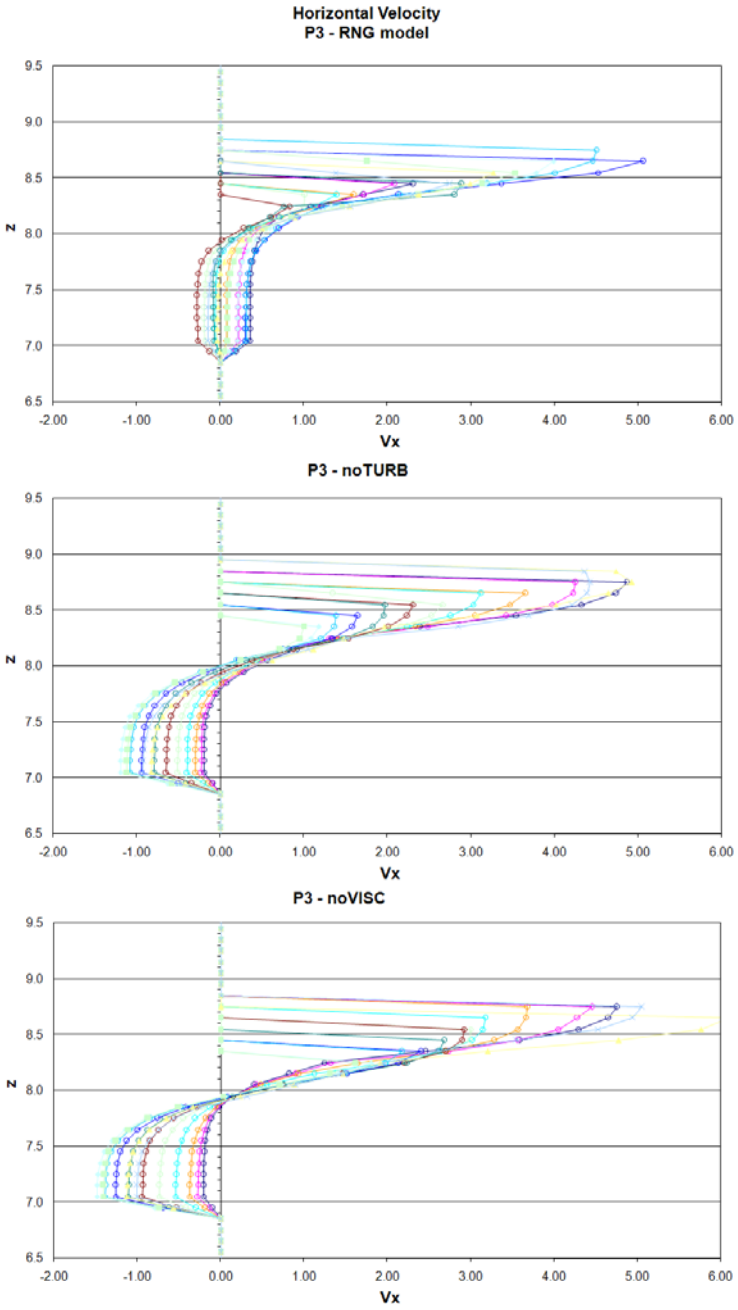

Figure 4.19: Influence of turbulence models on the horizontal velocity in P3 (broken wave)

5 WAVE PROPAGATION ANALYSIS

5.1 SPILLING ON LONG SLOPING BEACH

To test the software potential and the benefits arising from the use of Parallel Computing, simulations were conducted on a very large spatial-temporal domain.
A 64-bit processors cluster, owned and run by C.U.G.RI, was employed. The cluster is made up by a Quad processors server and a number of dual processors computers (Xeon 3 Ghz, 2 Gb RAM, 80 Gb HD).

The set-up, represented in Figure 5.1 and summarized in Table 5.1, is made up of a long horizontal constant depth stretch, followed by a sloping beach; this profile, beside, respecting the practical rule of having a 2-3 wavelengths long constant depth stretch before the start of the slope, is also useful to investigate the wave-maker influence .

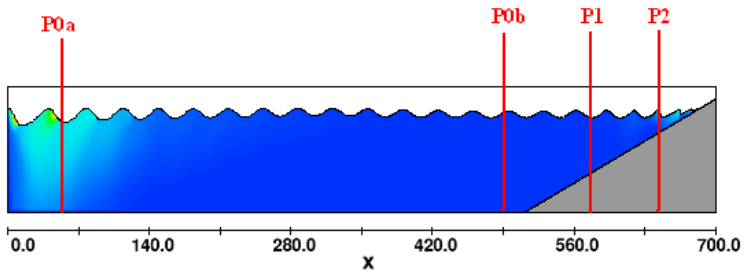

Figure 5.1: Numerical set-up of long sloping beach

In this simulation a variable grid is adopted, as summarized in Table 5.2; the whole domain is discretized into a 1870*80 grid system with a non-uniform grid in the x-direction and z-direction. The minimum grid x_{min} = 0.125 and z_{min} = 0.1 m, distributed near the beach and the free surface. The time step is automatically adjusted during the computation to satisfy the stability constraints.

Table 5.1: Geometrical and numerical parameters

slope	0.05
Ho (m)	2.00
To (s)	4.85
Lo (m)	33.29
Irribarren parameter	0.20
depth (m)	8.00
simulation time (s)	155.00
dt output (s)	0.40

Table 5.2: Numerical variable grid

Nx tot	1870				
px1	0	1			
px2	400	400	0.5		
px3	510		220	0.2	
px4	600			450	0.125
px5	700				800

Nz tot	80		
px1	0	0.2	
px2	5	25	0.1
px3	10.5		55

Moreover, the same simulation, with an uniform grid (dx=dz=0.2m) was running and Figure 5.2 shows the comparisons at the four different probes depicted in Figure 5.1.
The agreement between the numerical results, obtained from the variable and uniform grid system in terms of free-surface displacement, isn't good and the differences are caused by the computing error brought in by the use of larger cell size at the left side of the geometrical domain.

In order to verify the quality of the constant grid system, different but constant size square cells (0.15 m size) were used in another simulation. The comparison is represented in Figure 5.3 and, apart from the initial transitory phase, it shows a good resemblance.

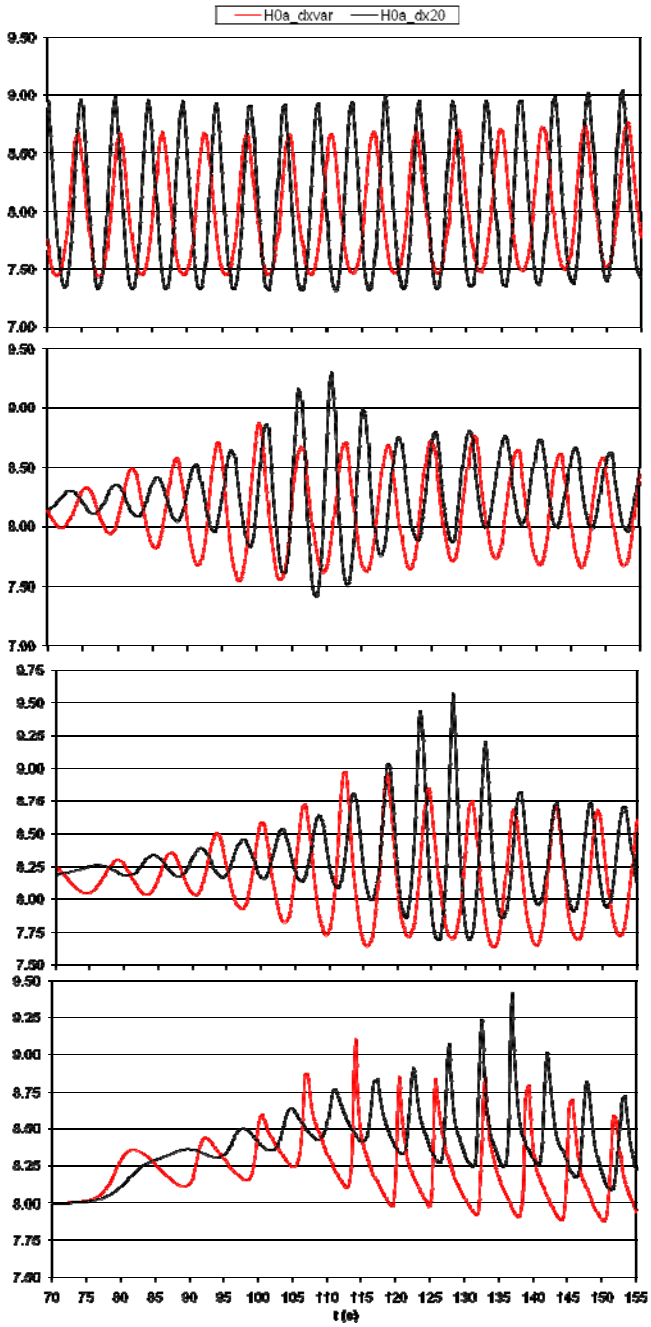

Figure 5.2: Comparison between wave height in different probes: / variable grid size; / constant grid size

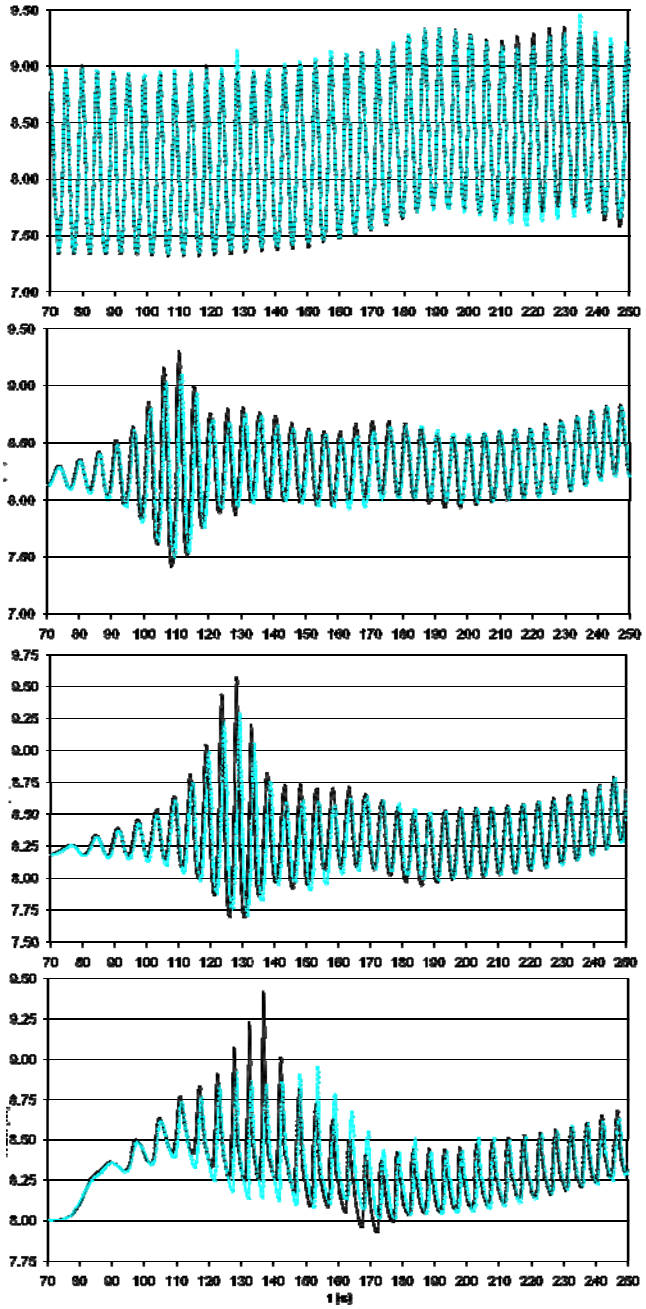

Figure 5.3: Comparison between wave height in different probes with a constant grid size: / 20cm; / 15cm.

When waves are simulated, the influence of the artificial dissipation on the wave propagation must be investigated.
From the results in the Figure 5.4, where the water surface elevation is shown as function of distance to the inflow boundary, it can be seen that the influence is definitely not very large over a short distance (a), because no real damping is visible in the simulation with 70m of constant depth before the sloping beach, while the effect is well evident in the long sloping beach (b).

Clearly, the artificial viscosity is not the only reason for dissipation of energy in the wave simulations; boundary conditions and the displacement of the free surface - that sometimes is made to be dissipative in order to get a stable solution - also play a role.

Summarising, for wave simulation in a very long geometrical domain, where many wavelengths are simulated, a clear damping is visible.
This dissipation of energy is largely due to the artificial viscosity that is added when using an upwind discretisation as well as from the treatment of the boundaries and the free surface.
The loss of energy is only a few percent in a small domain when not that many wavelengths are simulated.

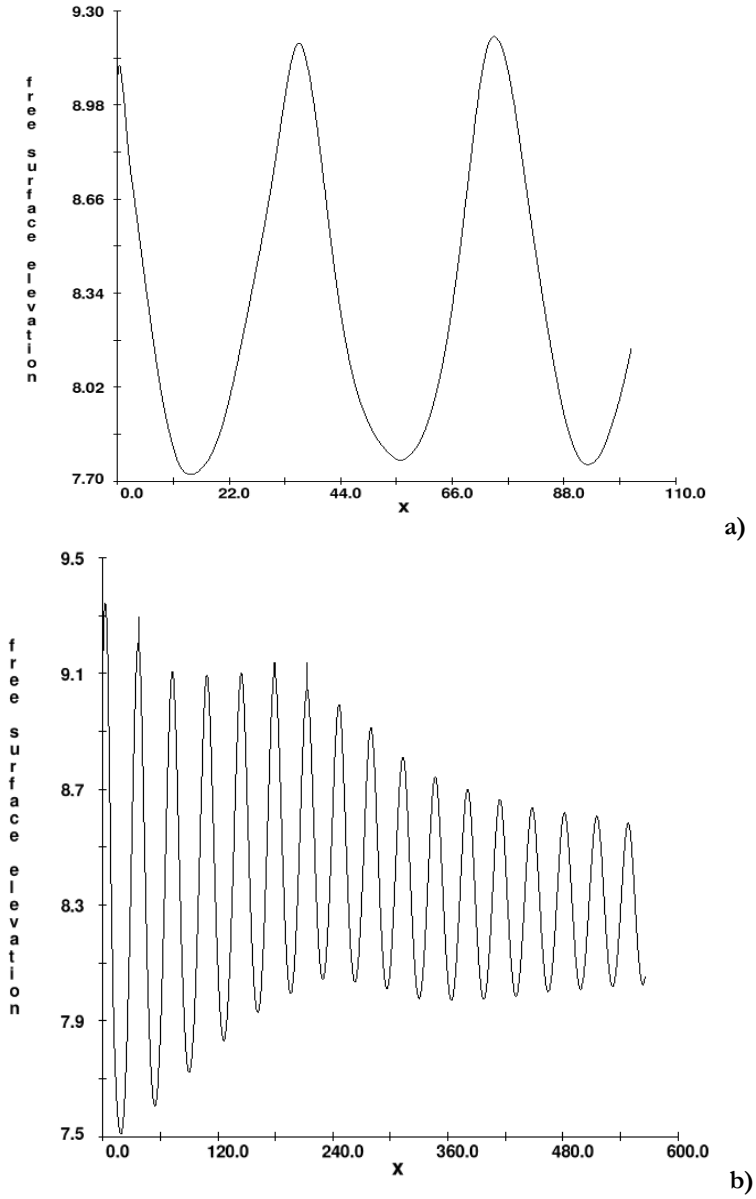

Figure 5.4: Wave elevation in the constant depth zone as function of place: a) short sloping beach; b) long sloping beach.

5.2 STOKES DRIFT

In the simulations, the waves enter through the inflow boundary and arrive to the sloping beach; when applying this to a finite amplitude wave, some problems arise, due to the fact that the net amount of water flowing into the domain at the inflow boundary is positive over one period and not zero, i.e. the so-called Stokes drift.

This is visible in Figure 5.5, where volume flow rate, for input waves with height of 2 and 3 m, is shown at the left boundary.
The integral over one period is not exactly zero but slightly positive; in particular the average left boundary volume flow rate is 15.8 l/s for H=3m and 2.7 l/s for H=2m.

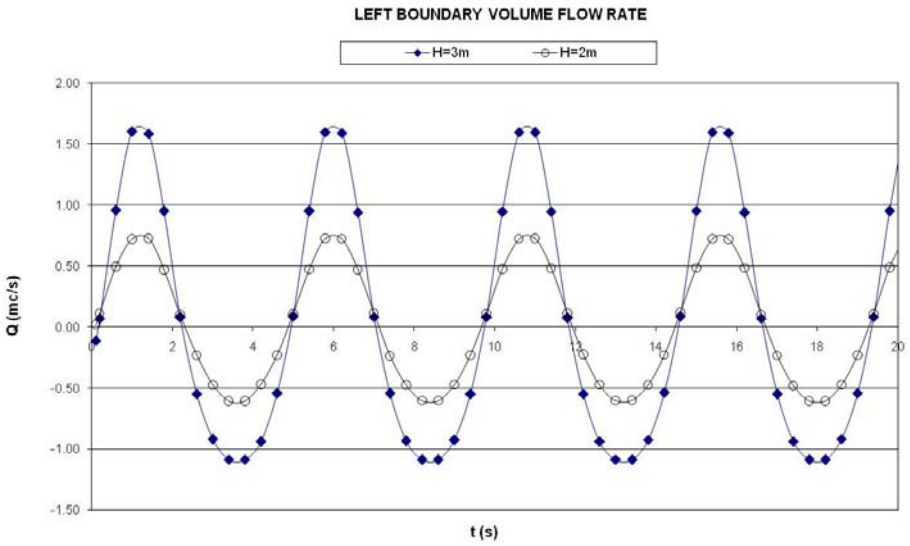

Figure 5.5: Left boundary volume flow rate

5.3 REFLECTION AND SEICHING

In numerical model, like in physical ones, wave absorption generally is divided into active systems and passive systems. An active system provides an active response to the waves; a passive system damps (mostly by energy dissipation) the wave motion.

Troch and De Rouch (1999), for example, developed methods for reducing the trapping of reflected waves in the domain with an active wave generating–absorbing boundary condition for RANS/VOF systems. A passive absorbing boundary condition is, instead, a sponge layer that can be on the side of the domain to properly dissipate the outward-going waves (Larsen and Dancy, 1983).

In laboratory and numerical experiments involving wave reflection from sloping beaches or structures, one of the most fundamental and important task is to determine the characteristics of incident waves, because various experimental results are interpreted in terms of the incident wave parameters.

There are several ways to determine the incident waves in a wave flume. The easiest way is to divide the test section of the flume into two along the flume. The beach or structure is installed in one of them, and the other is left empty, just having a wave absorber at the down-wave side. The waves measured in the latter section are then considered as the incident waves.
Another way is to simultaneously measure the waves at several locations along the flume in front of the beach or structure and separate the incident and reflected waves from the wave records (Goda and Suzuki, 1976; Mansard and Funke, 1980).
The method of Mansard-Funke uses three wave gauges and is less sensitive than the method of Goda-Suzuki because there is no limitation in its application range of frequency (or wavelength). The aforementioned methods was used to separate incident and reflected waves with the aid of the software WaveLab 3.02 (Hydraulic and Coastal Engineering-Aalborg University), and results are shown in the Figure 5.6.

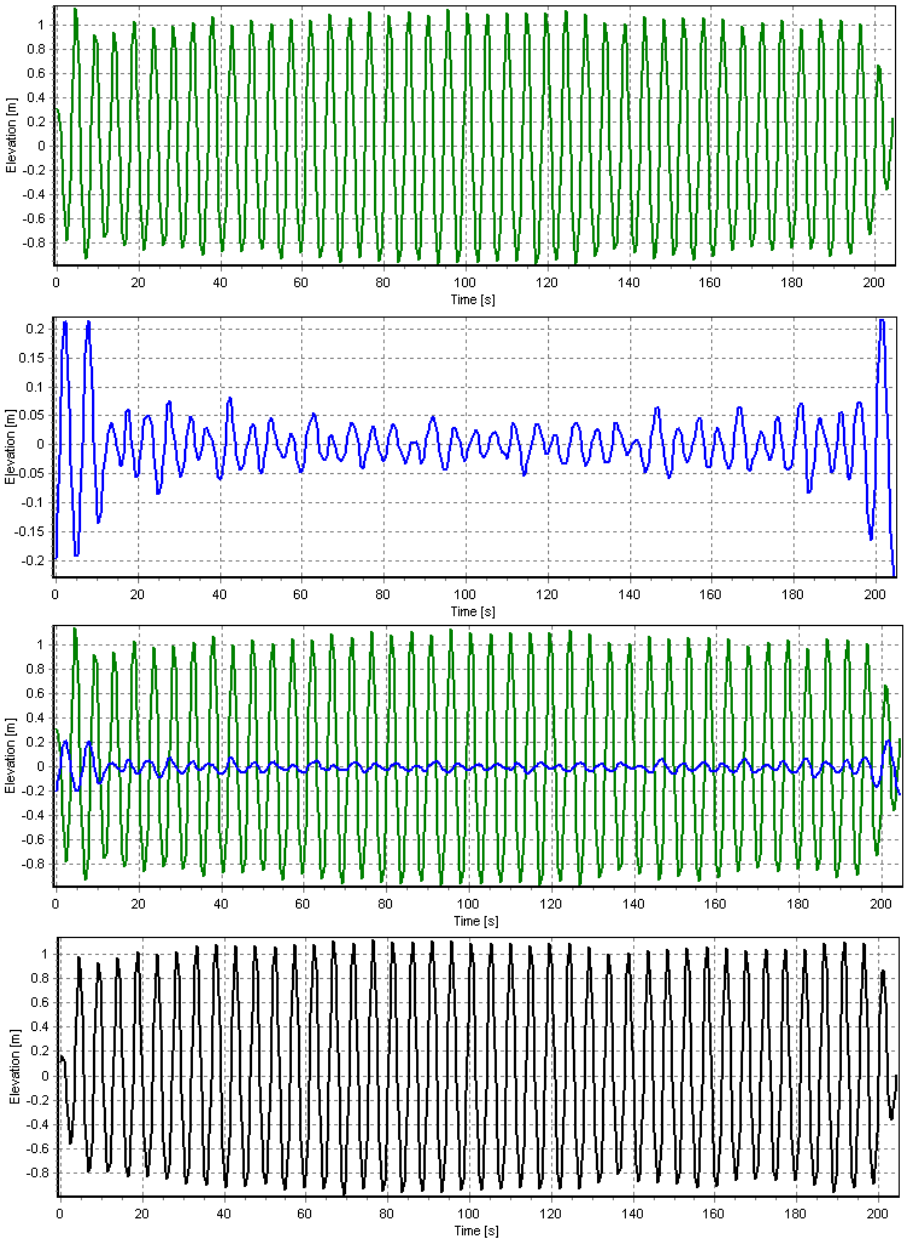

Figure 5.6: / Incident, / Reflected and / Total wave

In our simulations, a fluctuation of the water volume around the initial amount of water can be observed (Figure 5.7). The fluctuation is probably due to reflection, since the period of the fluctuation is about 90s (18 wave periods) in the short sloping beach (scheme Figure 4.5).

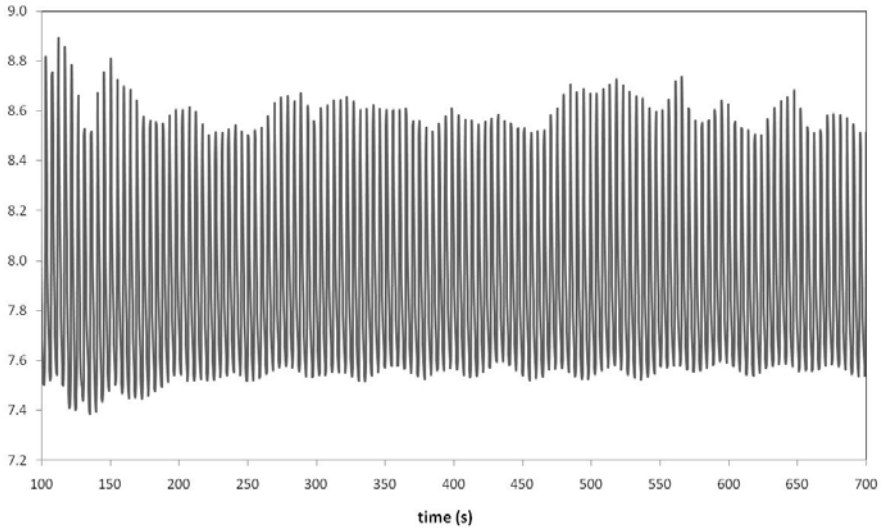

Figure 5.7: Wave elevation as function of time in the probe 170 for the short sloping beach

The model generated long waves are trapped artificially within the domain; these resonant oscillations, induced in an enclosed basin under the influence of a disturbing force, are called seiching.
A seiche is a standing wave in an enclosed or partially enclosed body of water. Seiches and seiche-related phenomena have been observed on lakes, reservoirs, swimming pools, laboratory tank, bays and seas. The key requirement for formation of a seiche is that the body of water be at least partially bounded, allowing natural phenomena to form a standing wave. Vertical harmonic motion results, producing an impulse that travels the length of the basin at a velocity that depends on the depth of the water; the impulse is reflected back from the end of the basin, generating interference. These seiches appear to have reached finite amplitude (i.e., they do not appear to be growing in time).
The frequency of the oscillation is determined by the size of the basin, its depth and contours, and the water temperature.

The longest natural period for a seiche in an enclosed rectangular body of water is usually represented by the Merian formula:

$$T = \frac{1}{n}\frac{2L}{\sqrt{gh}}$$

where L is the horizontal dimension of the basin measured in the direction of wave motion, h the average depth of the body of water, n is the number of nodes and g the acceleration of gravity.

Although incident wave energy is destroyed by wave breaking in the surf zone, low frequency energy is not, and remains high throughout the domain; these strong seiches appear to impact the incident wave transformation to a high degree, so the lack of regularity on the numerical results is just due to the reflection.

5.4 BREAKING: TYPES AND CRITERIA

When a wave train propagates from deep water into shallow water region, the wave profile becomes steeper and eventually breaks at a certain depth. Wave breaking is the most interesting phenomenon of the wave transformation in the nearshore region. The breaking wave not only produces a large force on maritime structures, but also induces the nearshore current circulation that affects shoreline change. Therefore, the prediction of wave shoaling and breaking is essential for the nearshore hydrodynamics, as well as for the design of coastal structures. Many theories and empirical formulas for the calculation of wave shoaling and the prediction of breaking have been proposed in the literature.
In previous models, wave transformation across the surf zone was determined by specifying the wave breaking distribution or criteria ahead of time. These distributions and criteria have been based largely on observation from the field, and in general have performed very well in determining the wave height transformation for both barred and non-barred bathymetric profiles (Thornton and Guza, 1983; Lippmann, et al., 1996; and others).

One limitation of the early transformation models is the a priori specification of the breaking patterns. Although they work well for wave height prediction, they do not well represent the observed spatial distribution of the wave breaking patterns. The inclusion of wave rollers in the time and depth-averaged long-shore momentum balance can lead to improved fit to the spatial distribution of observed breaking pattern, but requires iterative fit of two free parameters (Lippmann, et al., 1995).
In RANS-VOF numerical simulations, wave breaking is calculated as a part of the whole fluid dynamic procedure, so it does not require an a-priori specification of any special parameter (turbulence parameters are obtained from the literature as accepted values based on theoretical or laboratory observation). The model simulations are thus able to well reproduce both the observed wave height transformation, the mean undertow and wave breaking distributions. This suggests that CFD models can be used as a numerical laboratory at prototype field scales in order to study in detail the wave transformation and breaking process.

Having chosen the geometrical scheme in Figure 4.5 and grid Mg as the optimal discretization, some considerations can be made.

Observing Figure 5.8, it's possible to note that:
- in the first zone, the wave generated is sinusoidal;
- in the second zone, wave isn't yet broken, but it shows the shoaling effects;
- in the third zone, the wave is broken, and the mean sea level increases due to the set-up phenomenon.

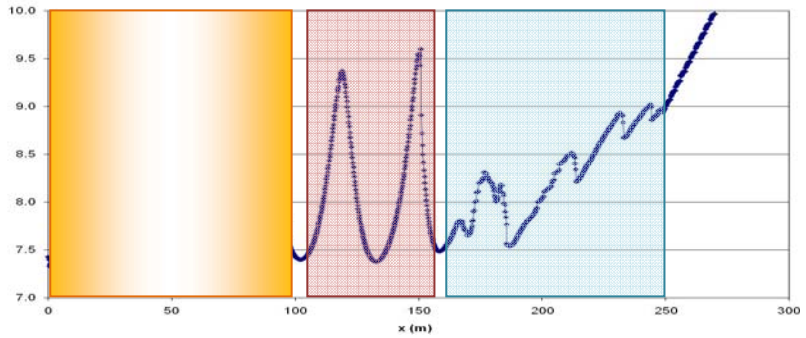

Figure 5.8: Surface height at t=96.60s

Breaker types refer to the form of the wave at breaking point. Wave breaking may be classified in four types (Galvin, 1968), as: spilling, plunging, collapsing, and surging.
In spilling breakers, the wave crest becomes unstable and cascades down the shoreward face of the wave producing a foamy water surface.
In plunging breakers, the crest curls over the shoreward face of the wave and falls into the base of the wave, resulting in a high splash.
In collapsing breakers the crest remains unbroken while the lower part of the shoreward face steepens and then falls, producing an irregular turbulent water surface. In surging breakers, the crest remains unbroken and the front face of the wave advances up the beach, with minor turbulence. Often, it appears to be a smooth gradation between all these types of waves. Breaker type may be correlated to the surf similarity parameter ξ, defined as (Galvin 1968, Battjes 1974):

$$\xi = \frac{\tan\theta}{\sqrt{\frac{H}{L_o}}} = \frac{\tan\theta}{\sqrt{\frac{2\pi H}{gT^2}}}$$

On a uniformly sloping beach, breaker type is estimated by:

Table 5.3: Breaking type limits

Breaking type	**ξ**
spilling	<0.4
plunging	0.4-3.3
surging/collapsing	>3.3

As expressed in the table, spilling breakers tend to occur for high-steepness waves on gently sloping beaches.
Plunging breakers occur on steeper beaches with intermediately steep waves, and surfing and collapsing breakers occur for low steepness waves on steep beaches. Extremely low steepness waves may not break, but instead reflect from the beach, forming a standing wave.

A case of plunging wave is, also, simulated on the same sloping beach, modifying the wave steepness.

Table 5.4: Wave parameters

	spilling	plunging
m	1/35	1/35
H	0.125	0.125
T	2	5
ξ	0.2	0.5

The different breaking type is clear on Figure 5.19.

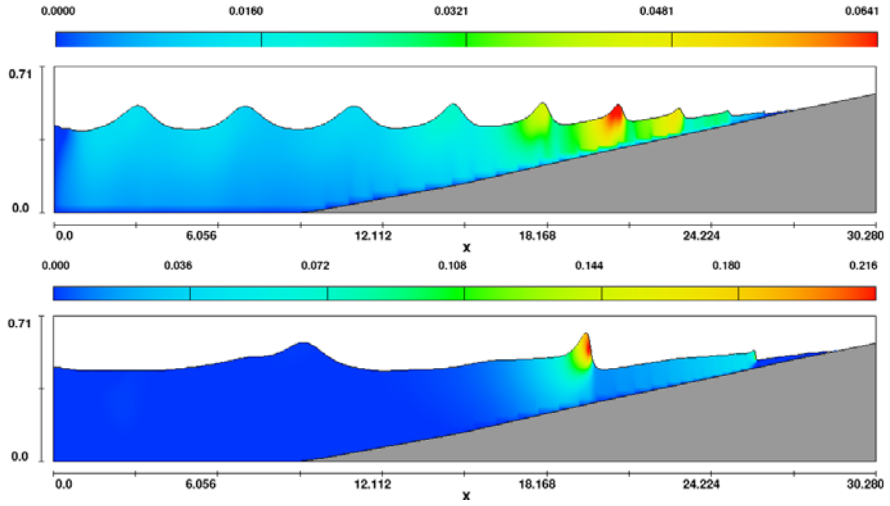

Figure 5.9: Surface height for different breaking wave: a) spilling; b) plunging

Further, a more complex geometry is adopted: a natural, mild-sloped, fine-grained, long-shore uniform beach (Scripps Beach, California) selected by the SwashX experiment data set (Raubenheimer, 2002).
As well in this case, Figure 5.10, the surface height is correspondent to the field data.

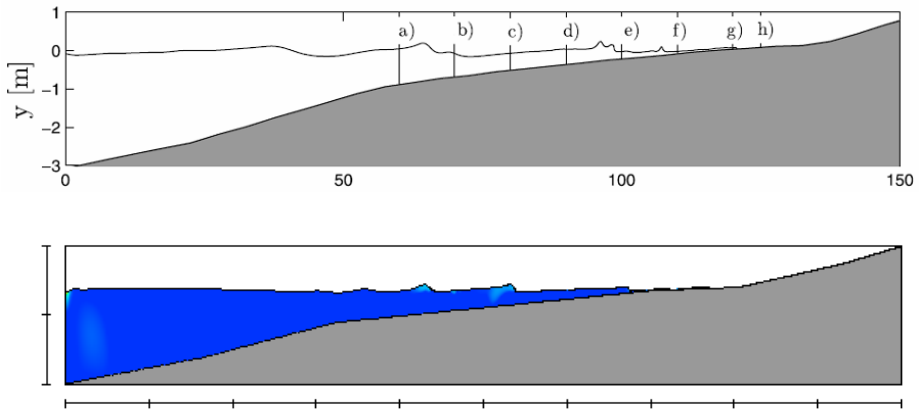

Figure 5.10: Surface height for a natural beach. a) field data; b) numerical results

For the spilling on sloping beach, the classical breaking criteria are numerically verified.
In the Figure 5.11, the geometrical criterion, expressed by the ratio of breaking wave height to the water depth, is represented:

$$\gamma_b = \left(\frac{H}{d}\right)_b = 0.78$$

in which the subscript *b* denotes the value at breaking.

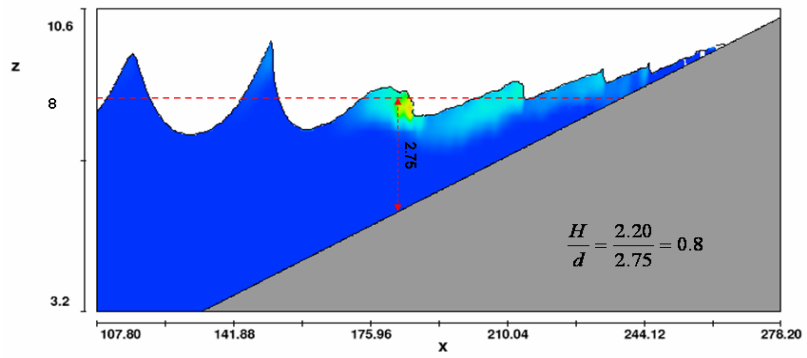

Figure 5.11: Verification of the classical breaking criterion

Obviously the water depth (d), in the formula, is the sum of the depth in steady water plus the setup.
Also the kinematic breaking criterion is verified: the wave breaking occurs when the velocity of water particle at the wave crest is greater than the local wave celerity. In fact, in the Figure 5.12, the particle velocity is 5.5 m/s, while the wave celerity, in Airy theory, is:

$$C = \frac{gT}{2\pi}\tanh\left(2\pi\frac{d}{L}\right) = 4.6 m/s$$

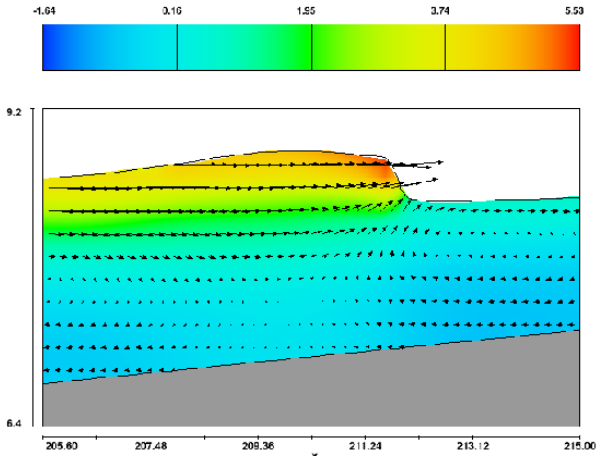

Figure 5.12: Horizontal velocity at breaking point

Another comment concerns the values of TKE that are growing closer to the breaking zone, where the influence of turbulence is significant.
The generation and localization of turbulence in the surf zone is illustrated in Figure 5.13, both for spilling and plunging breakers, as reproduced in the laboratory tests by Ting and Kirby (Ting and Kirby, 1995-1996).
Figure 5.14 (a) shows, a spilling wave that is starting to break and just after breaking where high levels of turbulence were generated in the crest and back side of the wave; instead the previous breaking wave to the right side continues the transformation into a turbulent bore.
From Figure 5.14 (b) it is seen that, for the plunging breaking wave, the high shear rates at the wave front have generated most significant, but shorter in time, levels of TKE at the lower front face of the wave, where the jet is located.

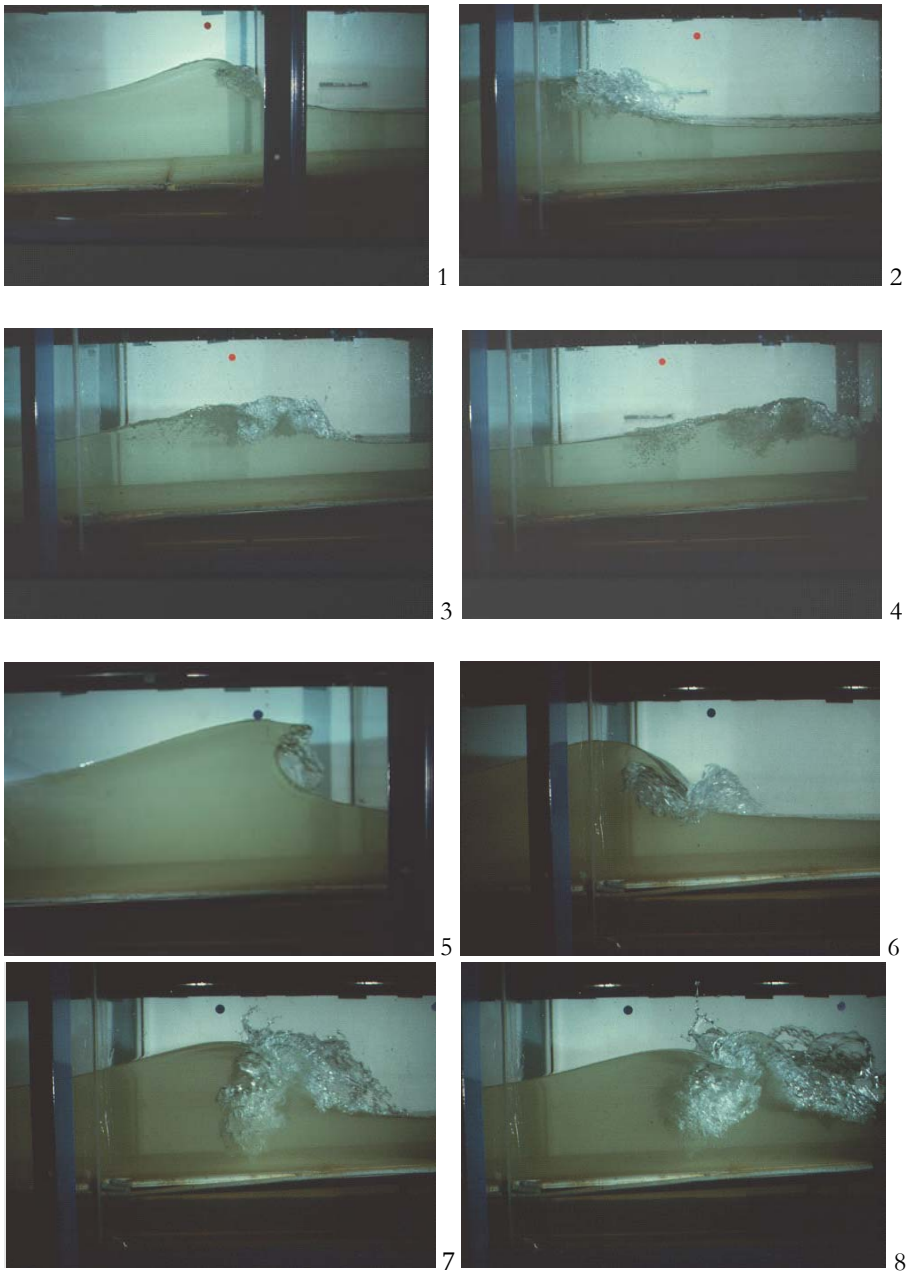

Figure 5.13: Turbulence generation and localization at different time:
1-2-3-4) spilling; 5-6-7-8) plunging
(photos by Ting and Kirby laboratory experiments)

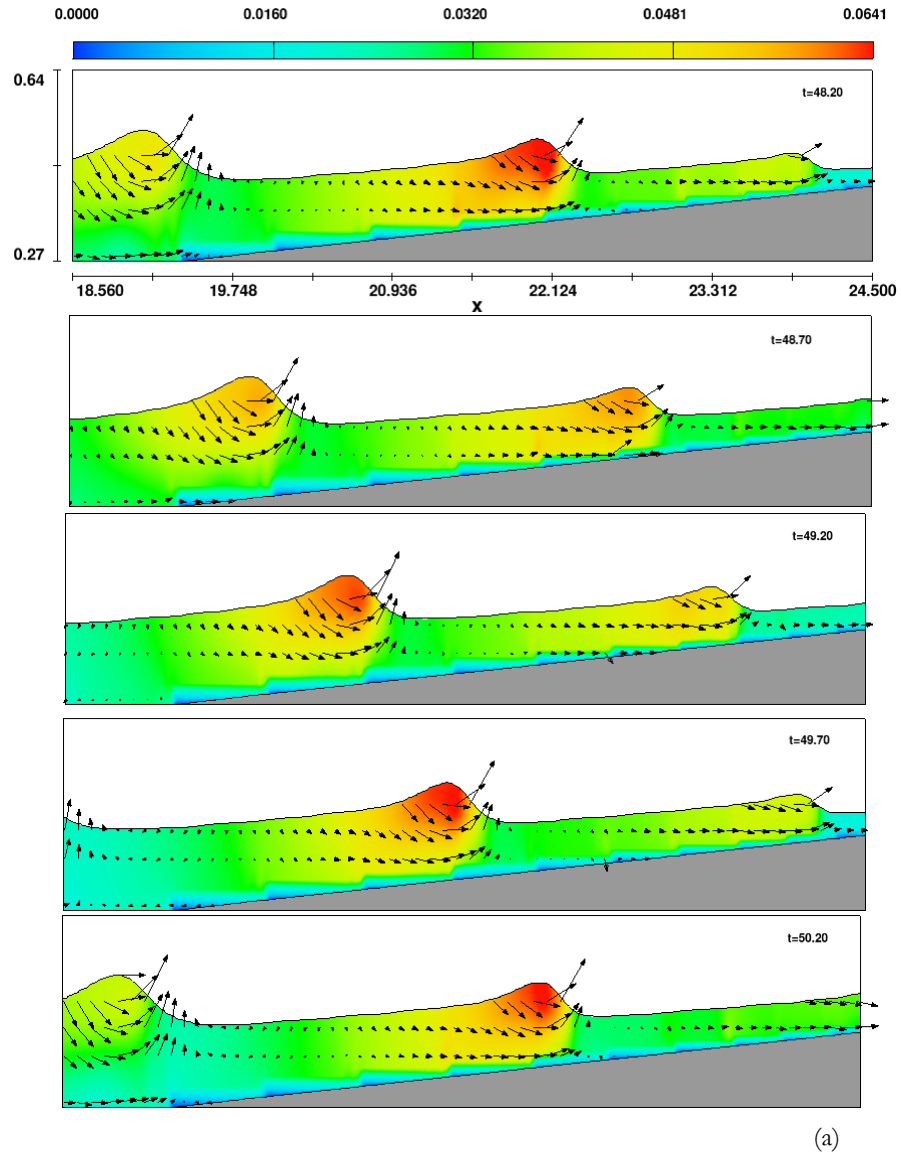

Figure 5.14 (a): Turbulent Kinetic Energy amount and localization at different time and for different breaking types: a) spilling; b) plunging

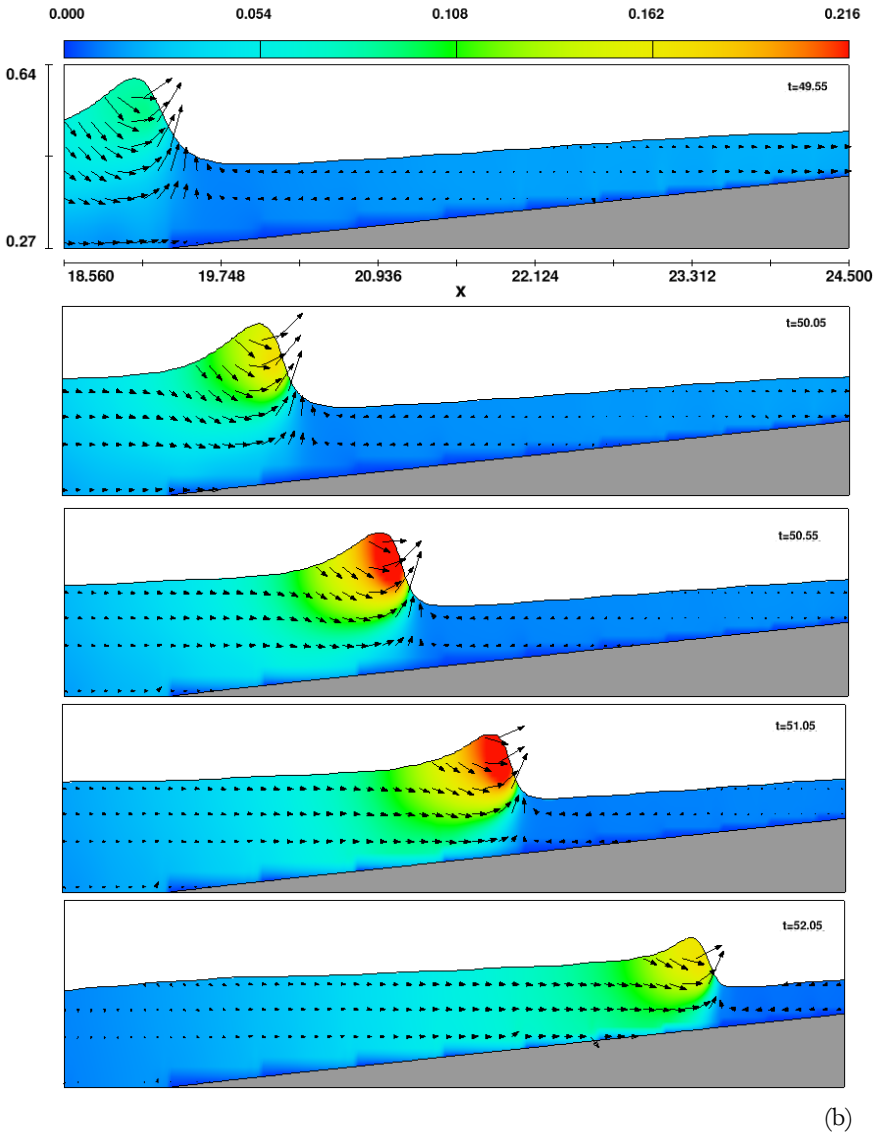

(b)

Figure 5.15 (b): Turbulent Kinetic Energy amount and localization at different time and for different breaking types: a) spilling; b) plunging

5.5 EVALUATION OF RUN-UP LENGTH

When waves break on a beach, they produce a set-up, i.e. a rise in the mean water level above the still-water elevation of the sea; the maximum vertical extent of wave up-rush on a beach or structure above the still water level (SWL) is the wave run-up (Sorensen, 1997). This definition is illustrated in the figure below.

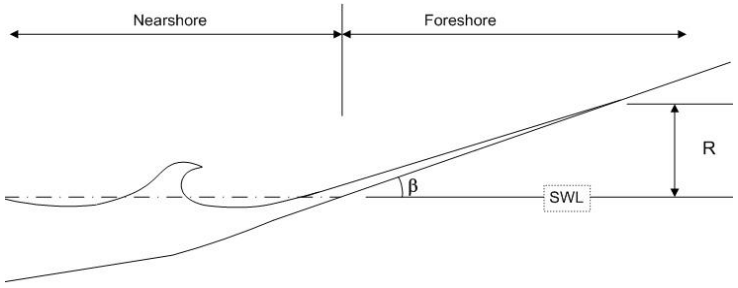

Figure 5.16: Definition of wave runup

When the incoming waves are regular, with a fixed height and period, they will all run up to same height on the beach. In this case it makes sense to talk about the run-up height R. Experiments have shown that, when the waves are breaking, the run-up height measured from the still water level is proportional to the wave height and to the surf similarity parameter:

$$R = H\xi = H \tan\vartheta_F \sqrt{L_0 / H} = \tan\vartheta_F \sqrt{HL_0} = \tan\vartheta_F \sqrt{H \frac{gT^2}{2\pi}}$$

In connection with this formula, we note, that the run-up height depends more on the wave period than on the height: this explains why very long waves, like tsunamis, can cause very severe run-up damage, even though their height in deep water is often very low.

The previous equation, which is often called Hunt's formula, is only valid for breaking waves with $\xi \leq 2$ corresponding to $R \leq 2H$, but this does cover the range of wind waves on natural beaches.

For irregular wave trains, Run-up is a random functions; statistical run-up parameters must be considered, such as for instance: mean wave run-up R_m, two percent wave run-up $R_{2\%}$, significant wave run-up $R_{1/3}=R_s$

Mean run-up is simply the average run-up (R_m) of all waves observed. The two percent wave run-up ($R_{2\%}$) is the run-up that only two percent of the wave run-up values observed will reach or exceed. The significant wave run-up (R_s) is the run-up reached or exceeded by the one-third highest wave.

For the scheme used in this work, the wave run-up is calculated with the formulas reported in table Table 5.5; the results are resumed in Table 5.6 and Fig. 5.16

Table 5.5: Applied Run-up formulas

Method	Slopes	Waves	Setting	Equations
1)Hunt	Smooth, impermeable, continuous	Regular	Laboratory	$R = \tan\beta_F \sqrt{H \frac{gT^2}{2\pi}}$
2)Holmann & Sallenger	moderately steep beach	Irregular	Field	$R_s^T = 0.307 \cdot g^{0.5} \cdot \tan\beta \cdot H_{s0}^{0.5} \cdot T$
3)Mase	Smooth, impermeable, continuous, gentle slope	Irregular	Laboratory	$R_s^T = 0.725 \cdot g^{0.35} \cdot (\tan\beta)^{0.7} \cdot$ $\cdot H_{s0}^{0.65} \cdot T^{0.7}$
4) Nielsen	Natural sand beaches	Irregular	Field	$R_s^T = 0.02257 \cdot g^{0.5} \cdot H_{s0}^{0.5} \cdot T + 0.17 \cdot H_{s0}$ $\rightarrow per \quad \tan\beta < 0.1$ $R_s^T = 0.447 \cdot g^{0.5} \cdot (\tan\beta) \cdot H_{s0}^{0.5} \cdot T$ $\rightarrow per \quad \tan\beta > 0.1$

Table 5.6: Values for run-up calculation

H	2
T	4.8
$\tan\vartheta$	0.05
ξ	0.07746
Runup (1)	0.42
Runup (2)	0.33
Runup (3)	0.93
Runup (4)	0.82

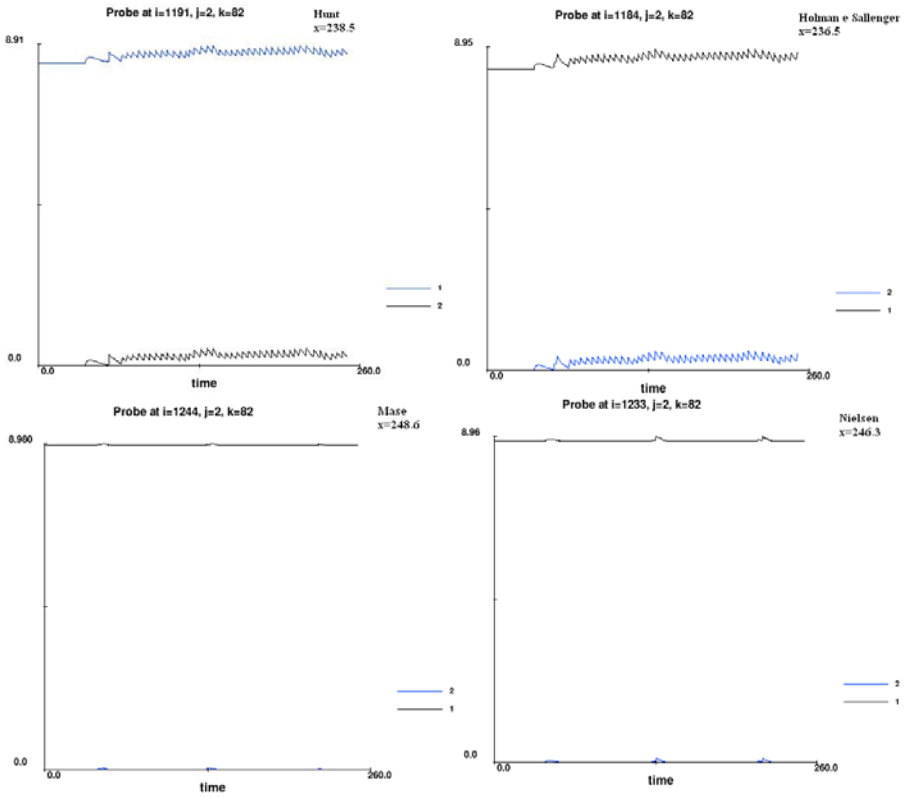

Figure 5.17: Numerical results: (1) free surface elevation above bottom; (2) free surface elevation above still water level

6 THE SCALE EFFECT

Table 6.1 provides a non exhaustive list of published works that deal with wave breaking (mostly, spilling) over beaches.
The list is far from complete, but it is enough to note that most of the tests used for such calibration were carried out at rather small scale - the most common reference is Ting and Kirby's (Dynamics of surf-zone turbulence in a strong plunging/spilling breaker, 1995 -1996) set of published data - and even the few field experiments only consider small domains. Wave heights – or significant heights – used for calibration rarely reach up to 0.10 m implying low Reynolds numbers and thus presumably a low level of turbulence and a comparatively high influence of viscosity.
It is also interesting to see that also the calculations are generally carried out at model, or very reduced scale; the reasons for this choice is, on the one hand, the opportunity of reproducing the available experimental tests and, on the other hand, the necessity of keeping down the numerical viscosity by keeping the mesh size as small as possible. The rationale behind this is the universally acknowledge assumption that as, long as the Froude number Fr is kept constant, the non-dimensional results will hold, regardless of other effects. The availability of well tested numerical techniques provides, now, a useful tool to improve the understanding of this kind of problems by numerically investigating on the effects of geometrical scale, e.g. by changing Re while keeping Fr constant.
This is not a trivial task because it mostly implies analyzing in detail the influence of viscosity and turbulence; as the dimensions go up (higher Re) the influence of viscosity decreases, but, at the same time the numerical viscosity associated with the calculation grid can increase, thus masking the former effect. On the other hand, the transition to turbulence - which might have an important effect on velocity profiles and impact - requires an effective simulation of the transition, difficult task for standard models. In this chapter the technique is applied to provide a useful insight of the effects of scale changes in wave breaking over shallow slopes.

Table 6.1: Some published work on wave breaking over beaches with Numerical NS/VOF integration

Year	Authors	Numerical method	Wave characteristics	Typical mesh side
1998	Liu P.L.F., Lin P.	RANS+VOF/ K-ε	H=0.125 T=2	dx=0.025 dz=0.006 n=69300
1999	Liu P.L.F., Lin P., Chang K.A., Sakakiyama T.	RANS+VOF/ K-ε	H=0.105 T=1.4	dx=0. 01 dz=0.007 n=28325
2000	Bradford S.C.	RANS+VOF/ K-ε+RNG (*FLOW3D*)	H=0.125 -0.128 T=2-5	dx=0. 02 dz=0.0075 n=64000
2001	Christensen E.D., Deigaard R.	RANS+VOF/ LES	H=0.08 T=1.4	dx=var dz=0.01 n=96000 3D=140*40*50
2002	Hsu T.J., Sakakiyama T., Liu P.L.F.	VARANS+VOF/ K-ε	H=0.182, 0.265	dx=0.02 dz=0.01 n=165000
2003	Karim M.F., Tanimoto K., Hieu P.D.	VARANS+VOF/ LES	H=0.07 T=1.6	dx=0. 02 dz=0.01 n=56400
2004	Hieu P.D., Katsutoshi T., Vu Thanh Ca	RANS+VOF/ SGS	H=0.125 T=2	dx=0.02 dz=0.01 n=202500
2004	Zhaoa Q., Armfield S., Tanimoto Q.	RANS+VOF/ SGS	H=0.125 T=2	dx=0.02 dz=0.008 n=100000
2004	N. Garcia, J.L. Lara, I.J. Losada	VARANS+VOF/ K-ε (*COBRAS*)	H=0.07 T=1.6	dx=0.04-0.01 dz=0.01 n=130000
2004	Lubin P., Vincent S., Caltagirone J., Abadie S.	NS/ LES	H/L = 0.13 con L=0.1	250 x 100 x 25 points
2005	Hieu P.D., Katsutoshi T.	RANS+VOF/ SGS	H=0.125/0.092 T=2 /1.6	dx=0.02 dz=0.01 n=202500
2005	Losada I.J., Lara J.L., Christensen E.D, Garcia N.	VARANS+VOF K-ε + LES (*COBRAS*)	H=0.1-0.25 T=2-6	n=256*94*24

Year	Authors	Numerical method	Wave characteristics	Typical mesh side
2005	Peng Q., Yijun H.	RANS+VOF/ K-ε	H=0.102 -0.105 T=1.54	dx=0. 05 dz=0.05-0.03 n=12000
2006	Karim M.F., Tingsanchali T.	VARANS+VOF/ K-ε	H=0.03 to 0.12 T=1.2, 1.6, 2.0	dx=0.02 dz=0.01 n=60000
2006	Losada I.J., Lara J.L.,. Liu F. P.L.	VARANS+VOF/ K-ε (*COBRAS*)	H=0.05-0.15 T=2-4	dx=0.04-0.01 dz=0.01 n=100000
2006	Christensen E.D.	RANS+VOF/ LES	H=0.127, 0.089 T=2-5	curvilinear grid 320*48*32 cells.
2006	J.L. Lara, N. Garcia, I.J. Losada	VARANS+VOF/ K-ε (*COBRAS*)	H=0.1 Tp=2.4, 3.2	dx=0.04-0.01 dz=0.01 n=105124
2006	Lubin P., Vincent S., Caltagirone J., Abadie S.	NS/ LES	H/L = 0.10-0.13 con L=0.1	$\Delta x=\Delta z=\Delta y=4\times10^{-4}$ m 251 x 100 x 25
2006	Lubin P., Branger, Kimmoun O.	RANS+VOF/ LES	Hrsm=0.14m Tp=1.3s	
2007	Lin P., Karunarathna A.	VARANS+VOF/ K-ε	H=0.10	dx=0.05 dz=0.01 n=325000
2007	Freyermuth A.T., Losada I.J., Lara J.L.	RANS+VOF/ K-ε (*COBRAS*)	H=0.28-0.48 Tp=8.4-16	dx=0. 05-0.02 dz=0.02-0.01 n=203319
2008	Reeve D.E., Soliman A., Lin P.Z.	RANS+VOF/ K-ε	H=0.5-1.5 Tp=5-7	dx=0.25 dz=0.1 n=38400
2008	Losada I.J., Lara J.L., Guance R., Gonzalez-Ondina J.M.	VARANS+VOF/ K-ε (*COBRAS*)	H=0.1 T=1.7	dx=0.05-0.02 dz=0.03-0.01 n=2326
2008	Chopakatla S. C., Lippmann, T.C., Richardson, J.E.	RANS+VOF/ RNG (*FLOW3D*)	Hrsm=0.5-1.2 Tp=8	dx=0.5 dz=0.1 n=204000

Continued Table 6.1: Some published work on wave breaking over beaches with Numerical NS/VOF integration

6.1 HYDRAULIC SIMILITUDE THEORY

Laboratory physical models are a valuable tool for coastal and maritime engineers. Breaking processes and wave transformations have been studied extensively in the laboratory; most of the equations in use are based on laboratory experiments with limited or absent field verification.

In general, when an experimental test of a full-size prototype is either impossible or expensive, the only feasible option for attacking the problem is through model testing in the laboratory.

An obvious goal of any experiment is to predict prototype performance from model observations. To achieve this, the concept of similitude is often used, so measurements made on one system (in the laboratory system) can be used to describe the behaviour of other similar systems (in the field system). To have complete similarity between model and prototype, we must maintain geometric, kinematical and dynamic similarity between them; if subscripts r and m denote prototype and model, respectively, the scale ratios shall be defined as:

Table 6.2: Similarity ratios

Geometric Similarity	$\lambda = \frac{L_m}{L_r}$
Kinematical Similarity	$\upsilon = \frac{V_m}{V_r}$
Dynamic Similarity	$\varphi = \frac{F_m}{F_r}$

The common dimensionless parameters in fluid mechanics are:

Table 6.3: Dimensionless similitude parameters

Number	Formula	Ratio	Importance
Reynolds	$\mathrm{Re} = \frac{\rho V l}{\mu}$	inertia force and viscous force	flow around bodies
Froude	$Fr = V / \sqrt{gh}$	inertia force and weight	free-surface flows
Mach	$Ma = V / c$	inertia force and elastic force	aerodynamic problems
Weber	$We = \frac{\rho V l}{t}$	inertia force and surface tension	not in hydrodynamic phenomena

The Reynolds number and the Froude number are the dimensionless parameters most often used in fluid mechanics. For the steady flow of an incompressible fluid without free surfaces, dynamic and kinematic similarity will be achieved if a model and a prototype meet the requirements of both geometric similarity and Reynolds number similarity. If free surfaces are involved, Froude number similarity must also be maintained and surface tension can be ignored.

6.2 Limitations of Physical Modeling: the Scale Effects

According to what previously asserted, physical model tests are one of the most effective ways to understand breaking process so far.
However, it is subject to some drawbacks. Apart from being expensive and time consuming, small-scale laboratory tests suffer from scale effects, because most of the scale models cannot satisfy the similarity laws.

Scale effects occur in all physical models. Scale effects are related to the inability to scale all relevant forces from prototype to model scale. Model effects have to be quantified in order to correctly interpret model results.

For the complete force similitude of a hydraulic model (be it physical or numerical), both Froude Fr and Reynolds Re criteria should be satisfied simultaneously when both gravity (Fr) and viscous forces (Re) are important. However, for most of the hydraulic models, water is the only feasible fluid to use. In small scale models under the same gravity condition, we thus can only satisfy one criterion, Fr, most of the time. This will lead to large viscous forces in small scale models (Burcharth et al., 1999). The error resulting from imperfect modelling of the prototype is called scale effect.

In contrast to the scale-down laboratory tests, numerical models in principle do not suffer from scale effects. Once the numerical model is developed, it can be applied to different environmental conditions including those that could not be modelled under normal laboratory conditions. It has been widely accepted that a good numerical model can certainly be complementary to model tests and can assist design engineers in identifying the most crucial cases for which model tests may be conducted. The ultimate goal of numerical models will be to replace (at least partially) the costly physical model tests.
As it was remarked in the previous paragraph, also numerical simulation is often carried out at model scale; some of the consideration below also apply to CFD models.

6.3 THE IMPORTANCE OF SCALE EFFECTS ON EXPERIMENTAL RESULTS

Surface waves, wave run-up and wave overtopping are governed mainly by gravity forces which requires Froude's similitude law (Figure 6.1). This means that, all forces related to friction, viscosity and surface tension are neglected in a Froude model.

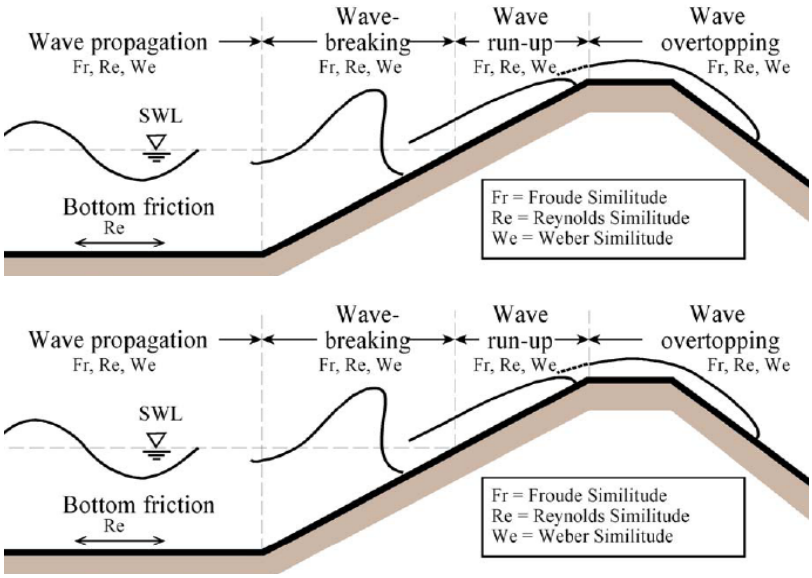

Figure 6.1: Processes and relevant similitude laws for wave motions

Scale effects have been investigated by various authors (de Rouck et al., 2005; Kortenhaus et al., 2004), and this has led to some practical rules that are usually observed in physical model studies.

Generally, water depths in the model should be much larger than h = 2.0 cm, wave periods larger than T = 0.35 s and wave heights larger than Hs = 5.0 cm to avoid the effects of surface tension; for rubble mound breakwaters the Reynolds number for the stability of the armour layer should exceed Re = 3x104; for overtopping of coastal dikes Re > 1x103; and the stone size in the core of rubble mound breakwaters has to be scaled according to the velocities in the core rather than the stone dimensions, especially for small models.

A method to achieved this is given in Burcharth et al. (1999); furthermore, critical limits for the influence of viscosity and surface tension are given in the follow table, more details can be found in Schüttrumpf and Oumeraci (2005).

Table 6.4: Processes, relevant similitude laws and critical limits for wave motions

Process	Relevant forces	Similitude law	Critical limits
Wave propagation	Gravity force	Fr_W,	
	Friction forces	Re_W,	$Re_W > Re_{W,crit}=1\cdot10^4$
	Surface tension	We	T>0,35s;d>2,0cm
Wave breaking	Gravity force	Fr_W,	
	Friction forces	Re_W,	$Re_W > Re_{W,crit}=1\cdot10^4$
	Surface tension	We	$T>0,35s;d_b>2,0cm$
Wave run-up	Gravity force	Fr_A, Fr_q	
	Friction forces	Re_q,	$Re_q > Re_{q,crit} = 10^3$
	Surface tension	We	$We > We_{crit} = 10$
Wave overtopping	Gravity force	Fr_A , Fr_q,	
	Friction forces	Re_q,	$Re_q > Re_{q,crit} = 10^3$
	Surface tension	We	$We > We_{crit} = 10$

With: $Fr_W=c/(g\cdot d)^{1/2}$; $Fr_A=v_A/(g\cdot h_A)^{1/2}$; $Fr_q=v_A/(2\cdot g\cdot A)$; $Re_W = c\cdot d/\nu$; $Re_q=(A-R_C)^2/(\nu\cdot T)$); $We=v_A\cdot h_A\cdot\rho_W/\sigma_W$

6.4 ANALYSIS ON THE SCALE EFFECT

During the work described in this thesis, the scale effect was investigated by conducting numerical experiments. Using the Froude law for scaling, numerical tests are performed in reduced numerical wave flumes. Each linear dimension, i.e. size of the computation domain, size of the beach and amplitude of the wave, is multiplied by factors 1/40 and 1/80. Since density and kinematic viscosity are kept constant, the Reynolds criterion is not satisfied in these tests.

The input data for these simulations were obtained by scaling all the necessary parameters in accordance with the Froude similarity. The duration of the simulation and the output intervals were also scaled down in order to produce comparable results for model and real case at any time step.

If prototype and model are scaled in length by λ and if the Froude number is kept constant, $\frac{Fr_m}{Fr_p} = \frac{V_m}{V_p}\frac{\sqrt{gh_p}}{\sqrt{gh_m}} = \lambda^{1/2}\tau^{-1} = 1$

the similitude ratios are:

length: $\lambda = \frac{L_m}{L_p} = \frac{1}{40} and \frac{1}{80}$

time: $\tau = \frac{t_m}{t_p} = \lambda^{1/2} = \sqrt{\frac{1}{40}} and \sqrt{\frac{1}{80}}$

mass: $\mu = \frac{m_m}{m_p} = \left(\frac{1}{40}\right)^3 and \left(\frac{1}{80}\right)^3$ if the fluid is the same in prototype and model

velocity: $\upsilon = \frac{V_m}{V_p} = \lambda\tau^{-1} = \sqrt{\frac{1}{40}} and \sqrt{\frac{1}{80}}$

turbulent kinetic energy: $\kappa = \frac{TKE_m}{TKE_p} = \lambda = \frac{1}{40} and \frac{1}{80}$

pressure: $\pi = \frac{P_m}{P_p} = \lambda = \frac{1}{40} and \frac{1}{80}$

discharge: $q = \frac{Q_m}{Q_p} = \tau^{-1}\lambda^3 = \frac{1}{40}^{\frac{5}{2}} and \frac{1}{80}^{\frac{5}{2}}$

Tirindelli et al. (2000) reviewed the relative influence of such diverse effects as viscosity, surface tension and compressibility; neglecting surface tension and compressibility in real life (and physical models) as scale (and therefore Reynolds number) goes down one should expect: a lower turbulence level and a strong effect of molecular viscosity.
The rationale behind accepting scale model results as valid for real life situation is that, as long as the Reynolds number is large enough, it does not affect the results. Before any conclusion is drawn, some care should be exercised, especially when considering very low scales, where the Reynolds Number is so low that the acceptability of the K – ε (or RNG) turbulence model itself could be questioned.

The following pictures show the numerical results, for different values of geometrical scale λ: wave height and horizontal velocities are reproduced remarkably well at model scale, (Figure 6.2 and 6.3).

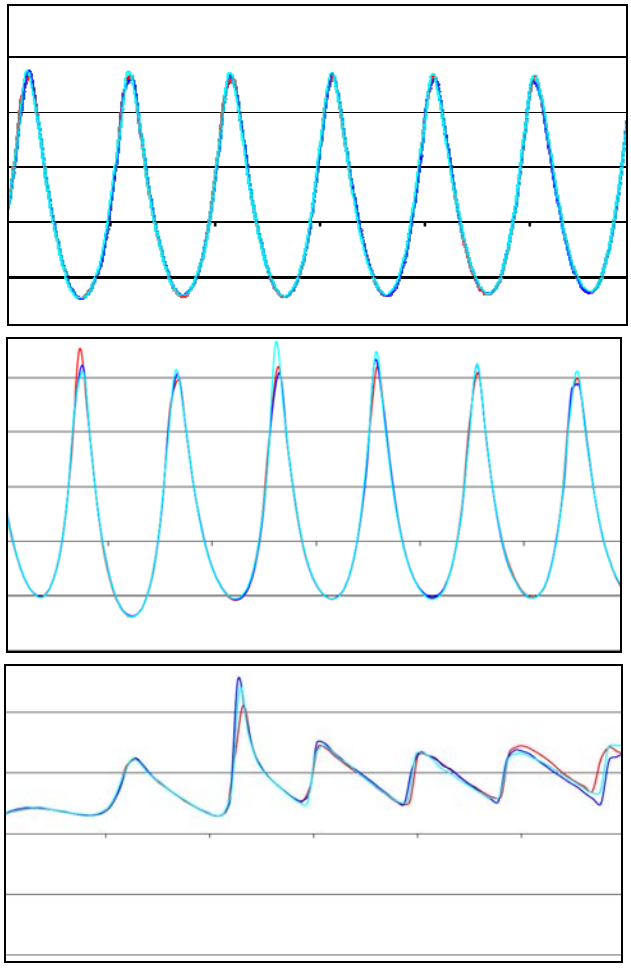

Figure 6.2: Scale effect on the wave height at different probes P1, P2 and P3: / full scale; / scale 1:40; / scale 1:80

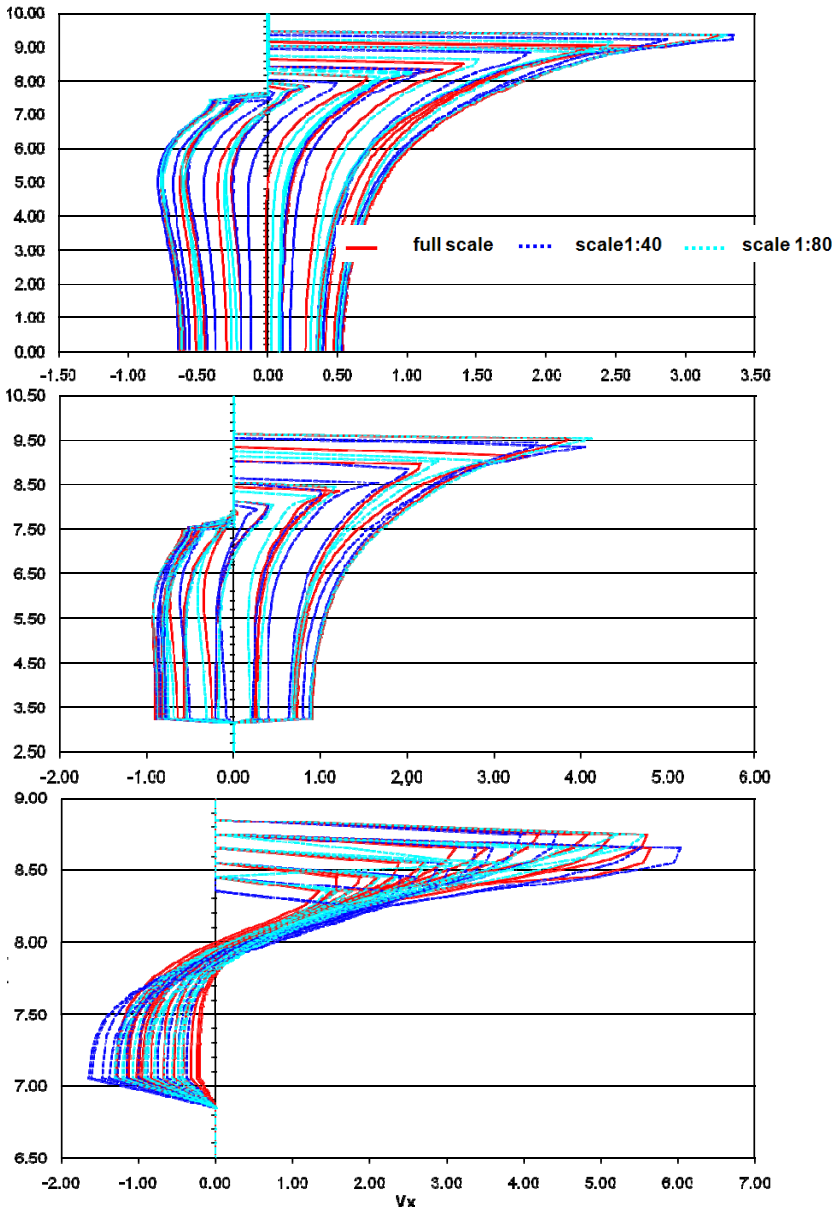

Figure 6.3: Scale effect on the horizontal velocity at different probes P1, P2 and P3

From Figure 6.4 to Figure 6.7, is appears that the TKE vertical distributions have similar trends as the scale varies, despite the considerable difference of the eddy (turbulent) viscosity, whose values in the figures are not scaled.

It should also be remembered that, as the scale goes down, also numerical viscosity becomes less important. Results thus are not highly dependent on viscosity – molecular, numerical or eddy – leading to the well known independence from Reynolds number. Full scale and model tests thus operate in same turbulence regime thereby generating values of height, velocity and turbulent kinetic energy almost coincident - up to a point.

Summarizing, the low scale – and therefore low Reynolds – calculation provides a much lower μt, as it is obvious, and at the smaller scale the value of the molecular viscosity starts being comparable with the eddy viscosity; an even smaller scale would lead to an even smaller turbulent effect. Pushing the calculation to that limit would mean to go far beyond the acceptable limits for current turbulence models, specially since no experimental data are available in that range.

A possible answer would be to move to LES (Lubin et al, 2006; Christensen, 2006) – independent as it is from the erratic ε variable; the applicability of LES to such large dimension and long time is however still beyond the computational capability – at least in the next future.

Some kind of low Reynolds Number model, such for instance as described by Bentaleb et al (2006) and Goldberg et al (1998) might provide some better insight in the short term.

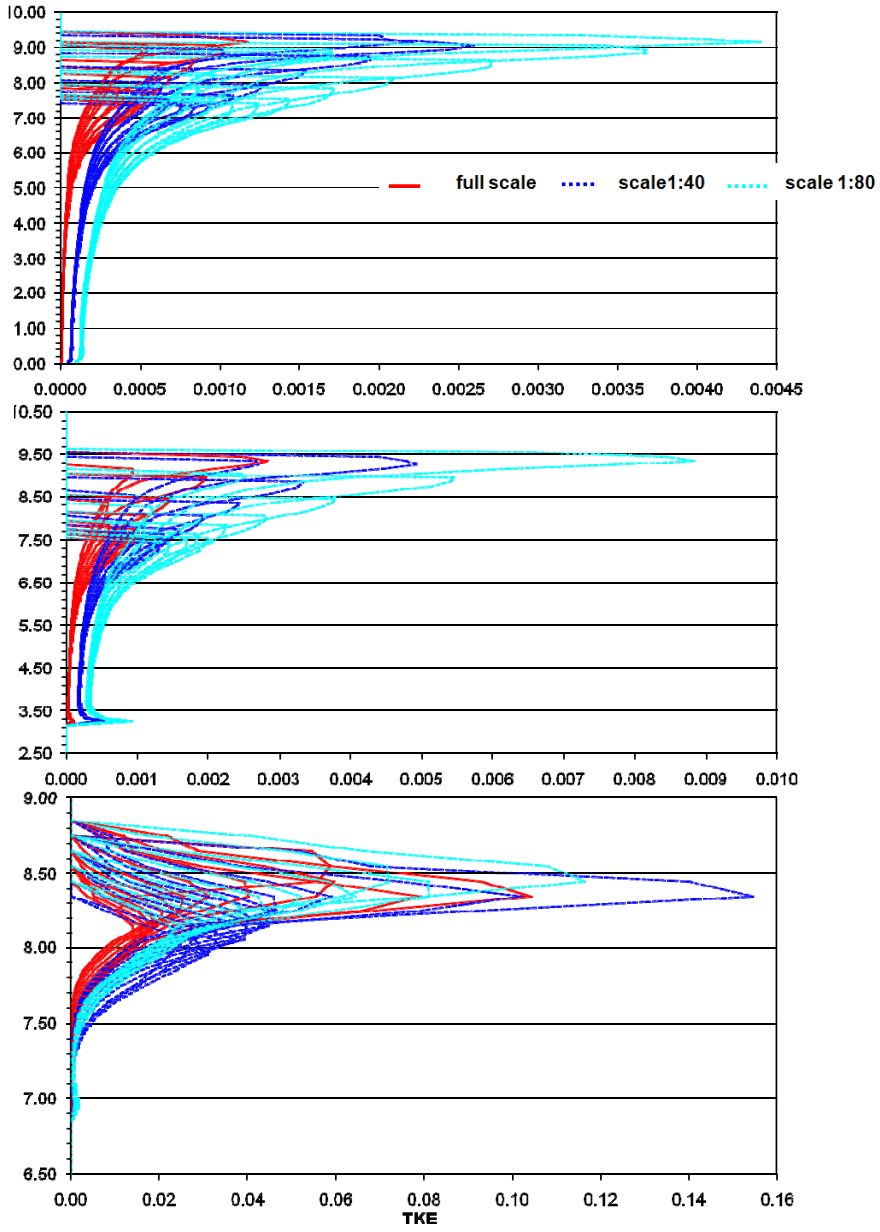

Figure 6.4: Scale effect on the turbulent kinetic energy at different probes

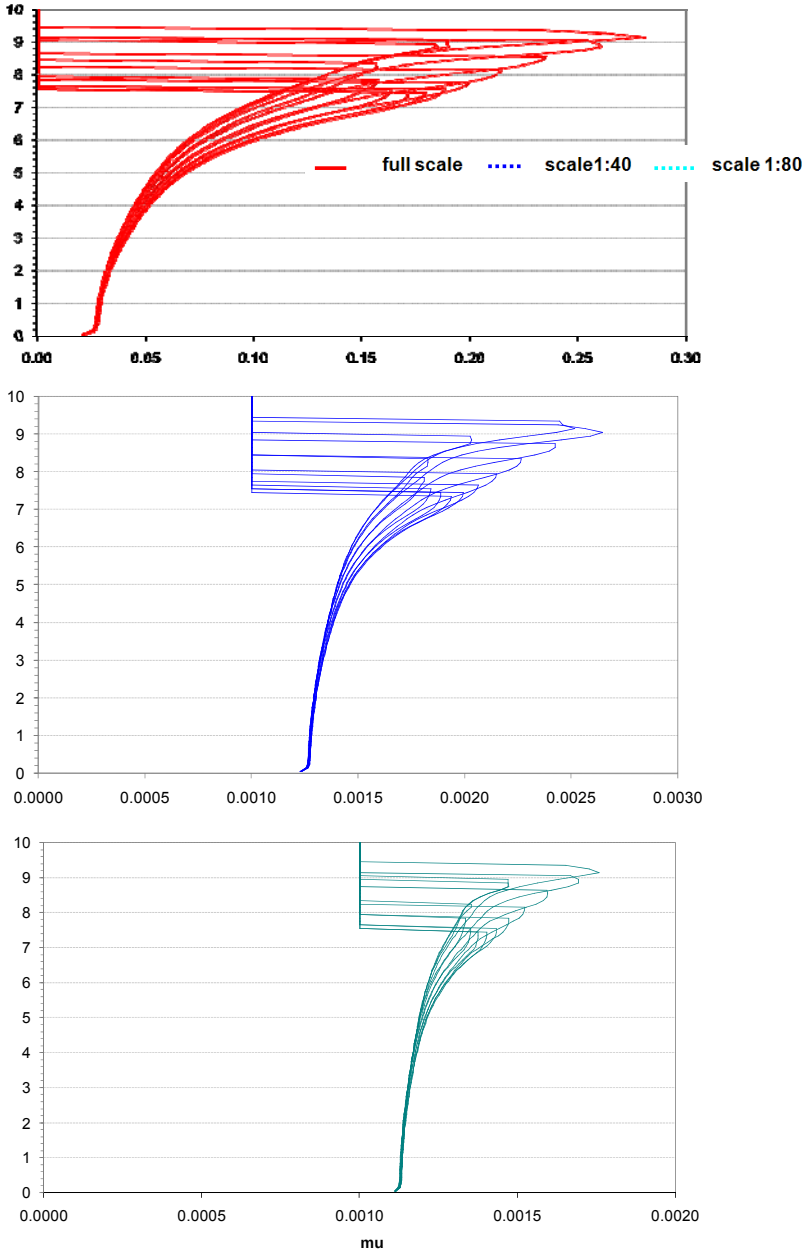

Figure 6.5: Scale effect on the eddy viscosity at probe P1

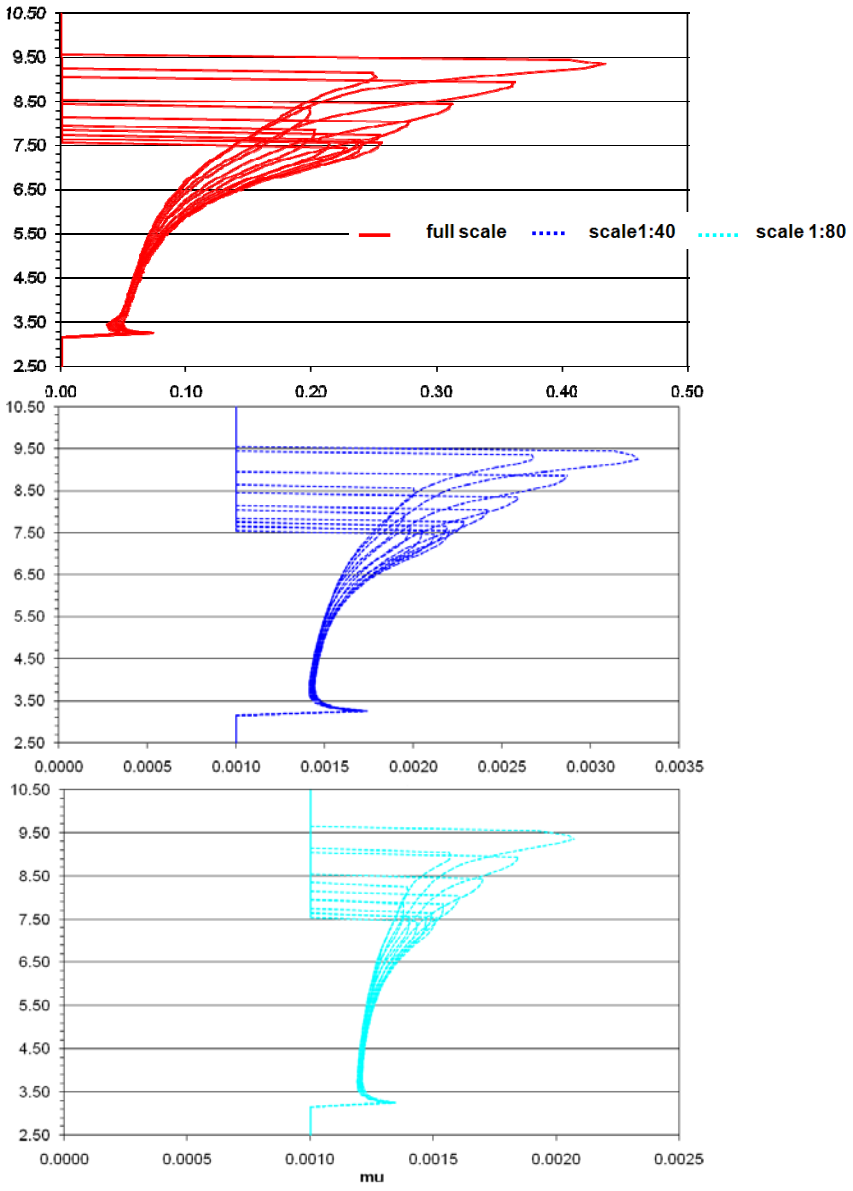

Figure 6.6: Scale effect on the eddy viscosity at probe P2

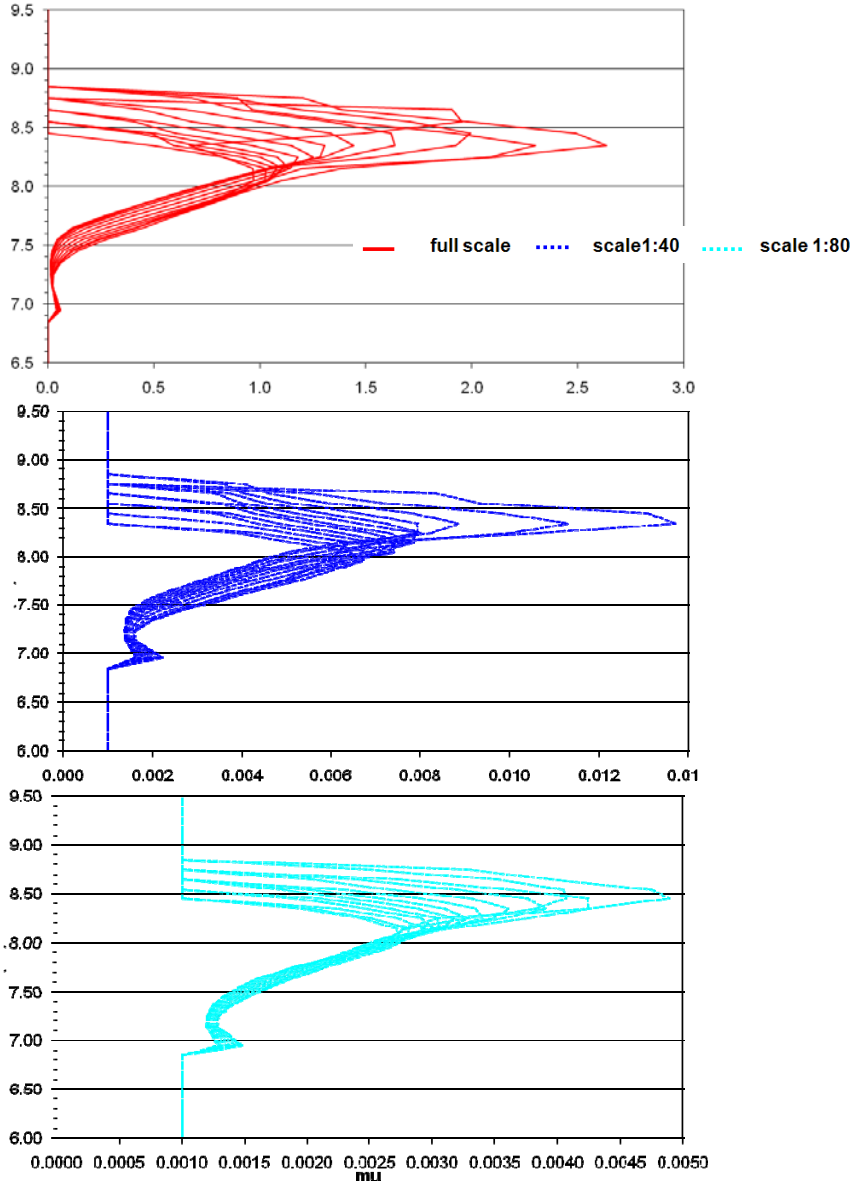

Figure 6.7: Scale effect on the eddy viscosity at probe P3

Also the average undertow profiles seem to be independent from the scale (Figure 6.8).

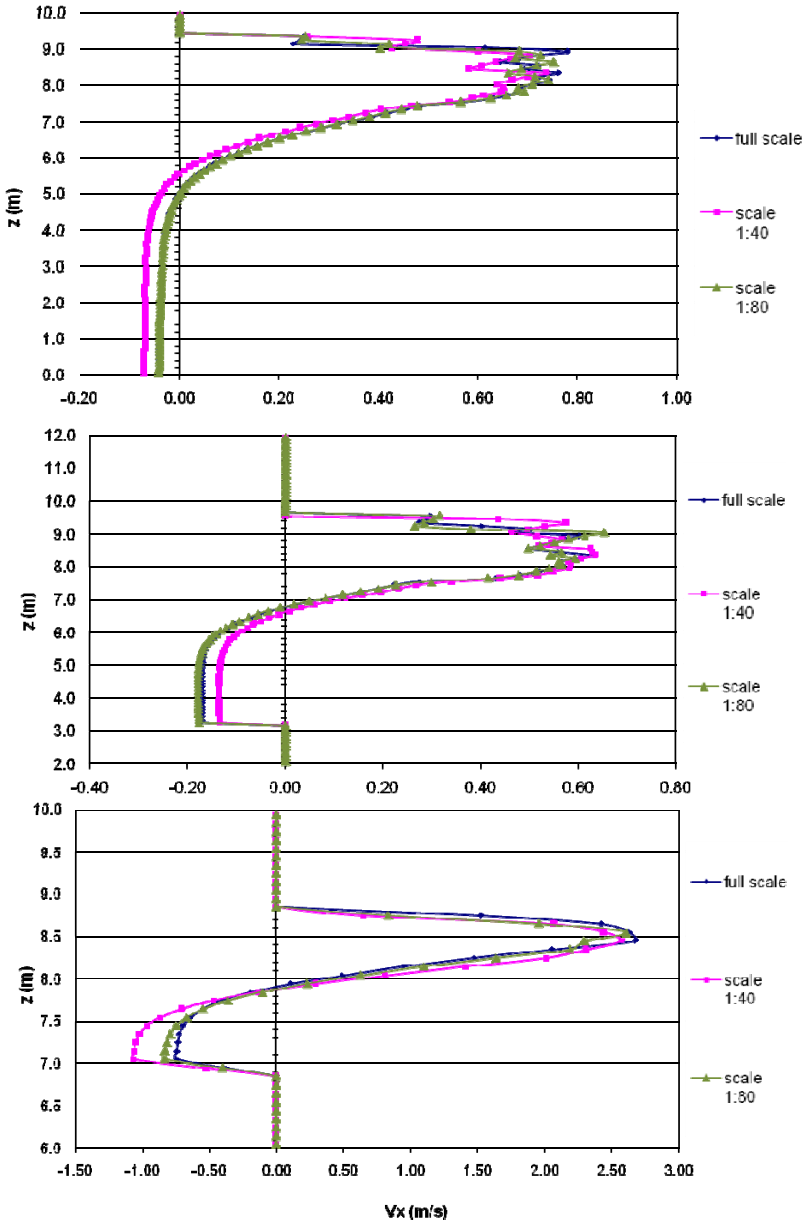

Figure 6.8: Scale effect on the undertow profiles at different probes

7 ENERGY AND MOMENTUM FLUX

The classical empirical method (Goda, Kamphuis) of describing wave transformation in the surf zone is based on the phase-averaged approach, variation of the wave height, the setup and the wave-induced current. Important quantities such as the wave celerity, the radiation stress and the energy flux are modeled by the use of sinusoidal theory.
The differences between breaking or broken waves and non-breaking ones is crucial to the breakwater design, and so a distinction should be made comparing the numerical results. In fact, for breaking waves and post breaking waves the wave loads are underestimated using linear wave theory, that doesn't consider the presence of the shallow water effects, as:

- the asymmetry of waves (elevation, velocity, . . .)
- the breaking waves (turbulence kinetic energy, impact forces, . . .)

In the precedent chapters we have seen that a RANS/VOF numerical model is able to describe free-surface elevation, pressure and velocity field within the surf zone. So, it allows the direct computation of relevant quantities in near-shore hydrodynamics (i.e., energy flux, momentum flux) using their complete formulation (no assumptions concerning the wave motion).

7.1 GENERAL FORMULAE FOR PROGRESSIVE WAVES

Wave energy is a quantity of primary interest, since it is a primary quantity that is transported with the wave trains. Many wave quantities like surface elevation and orbital velocity are oscillatory in nature with zero mean (within the framework of linear theory). In water waves, the most common energy parameter is the mean wave energy density per unit horizontal area; it is the sum of the kinetic potential and pressure energy density, integrated over the depth of the fluid layer and averaged over the wave phase.

In the rest of this chapter we shall deal only with progressive waves, i.e. with the waves which do not interact with structures.
Energy flux is the rate at which energy is transmitted in the direction of wave propagation.

Starting from the ideal fluid equation in Cartesian coordinates for a general three dimensional flow, we read:

$$grad\left[z+\frac{p}{\rho g}+\frac{1}{2g}\left(u_x^2+u_y^2+u_z^2\right)\right]=-\frac{1}{g}\frac{\partial\phi}{\partial t} \qquad (7.1)$$

where z is the height over the bed, p the pressure, ρ the water density, g the gravity acceleration, u_x and u_y the horizontal velocity components, u_z the vertical velocity component, Φ the velocity potential, and t the time.
Since the wave motion is assumed periodic, the last term of (7.1) vanishes, and the sum of the geometrical height, the mean pressure height term, and the mean velocity height term, is seen to be a constant for the entire flow.

The wave energy density is :

$$e(t)=\int_0^{d+\eta}\left[\rho gz+p+\frac{1}{2}\rho u^2\right]\cdot dz \qquad (7.2)$$

and the energy flux Fe (the rate of change of energy density) is:

$$Fe(t)=\int_0^{d+\eta}\left[\rho gz+p+\frac{1}{2}\rho u^2\right]\cdot u\cdot dz \qquad (7.3)$$

The time-averaged energy flux is:

$$Fe=\left\langle\int_0^{d+\eta}\left[\rho gz+p+\frac{1}{2}\rho u^2\right]\cdot u\cdot dz\right\rangle \qquad (7.4)$$

in which η is the surface elevation and d the water height.

Explicating the time averaging over a whole wave period, we have:

$$Fe = \frac{1}{T} \cdot \int_t^{t+T} \left[\int_0^{d+\eta} \rho \frac{u^2}{2} u \cdot dz + \int_0^{d+\eta} \rho g z u \cdot dz + \int_0^{d+\eta} p u \cdot dz \right] \cdot dt \qquad (7.5)$$

The total cross-shore wave averaged momentum flux is given by:

$$F_{qdm} = \frac{1}{T} \cdot \int_t^{t+T} \left[\int_0^{d+\eta} \left(p + \rho u^2 \right) \cdot dz \right] \cdot dt \qquad (7.6)$$

If no average current components are present, the F_{qdm} is equivalent at the radiation stress S_{xx}.

7.2 WAVE ENERGY FOR SMALL AMPLITUDE THEORY

Assuming linear theory, the average energy flux is given by (7.5) - where the integrand is of order H^2; so, for small amplitude, we can reduce the interval of integration from (0, d+η) to (0, d) making at the most an error of H^2 order. Therefore, we rewrite (7.5) in the form:

$$Fe(Airy) = \frac{1}{T} \cdot \int_t^{t+T} \left[\int_0^{d} \rho \frac{u^2}{2} u \cdot dz + \int_0^{d} \rho g z u \cdot dz + \int_0^{d} p u \cdot dz \right] \cdot dt \qquad (7.7)$$

According to linear wave theory, the average energy density per unit area of gravity waves on the water surface is proportional to the wave height squared (such in Boccotti and Foti):

$$E = \frac{1}{16} \rho g H^2$$

where E is the mean wave energy density per unit horizontal area (J/m2), sum of kinetic and potential energy density per unit horizontal area.
The potential energy density is equal to the kinetic energy, both contributing half to the wave energy density E.

As the waves propagate, their energy is transported. The energy transport velocity is the group velocity. As a result, the wave energy flux, through a vertical plane of unit width perpendicular to the wave propagation direction, is equal to:

$$Fe(Airy) = \frac{1}{8}\rho g H^2 \cdot C \cdot \frac{1}{2}\left[1 + \frac{2kd}{\sinh(2kd)}\right] = E \cdot Cg \qquad (7.8)$$

where C and Cg are the phase and group velocities, d is the mean depth, ϱ is the water density and g is the acceleration of gravity.

Due to the dispersion relation for water waves under the action of gravity, the group velocity depends on the wavelength L, or equivalently, on the wave period T.
Further, the dispersion relation is a function of the water depth d. As a result, the group velocity behaves differently in the limits of deep and shallow water:

$$Fe(Airy)_0 = \frac{1}{2}E_0 \cdot C_0 \qquad \text{(deep water)}$$

$$Fe(Airy) = E \cdot C \qquad \text{(shallow water)}$$

Using the following relations for water elevation, horizontal velocity and pressure, valid for linear wave, a comparison between the complete formula (7.5) and the simplified one (7.8) is carried out.

$$\eta = A \cdot \cos\left(\frac{2\pi x}{L} - \frac{2\pi t}{T}\right)$$

$$u = \frac{H}{2}\frac{gT}{L}\frac{\cosh\left[2\pi(z+d)/L\right]}{\cosh\left[2\pi d/L\right]} \cdot \cos\left(\frac{2\pi x}{L} - \frac{2\pi t}{T}\right)$$

$$p = \gamma\frac{H}{2}\frac{\cosh\left[2\pi(z+d)/L\right]}{\cosh\left[2\pi d/L\right]} \cdot \cos\left(\frac{2\pi x}{L} - \frac{2\pi t}{T}\right) - \gamma z$$

The results are summarized in the Table 7.1.

Table 7.1: Results for the comparison between the formulas

d	8.00			
H	0.20			
T	4.80			
Fe linear theory (7.8)	**215.36**			
dz - dt	0.001		0.0001	
upper limit of integration	D	d+eta	d	d+eta
flux Ep	6.467	6.705	3.8253e-008	3.9747e-008
flux Ec	0.001	0.001	3.3593e-012	3.5177e-012
flux P	220.12	227.29	215.37	222.54
Fe complete integral (7.5)	**226.59**	**234.00**	**215.37**	**222.54**

The linear approximation gets very close to the complete formulation as H→0 and for small discretization step. The remaining differences are due to the drift motions and to the upper limit of integration (d+eta).
Wave height, momentum flux, energy flux and its single parts are reported in Fig.7.1, for the wave described in previous table.

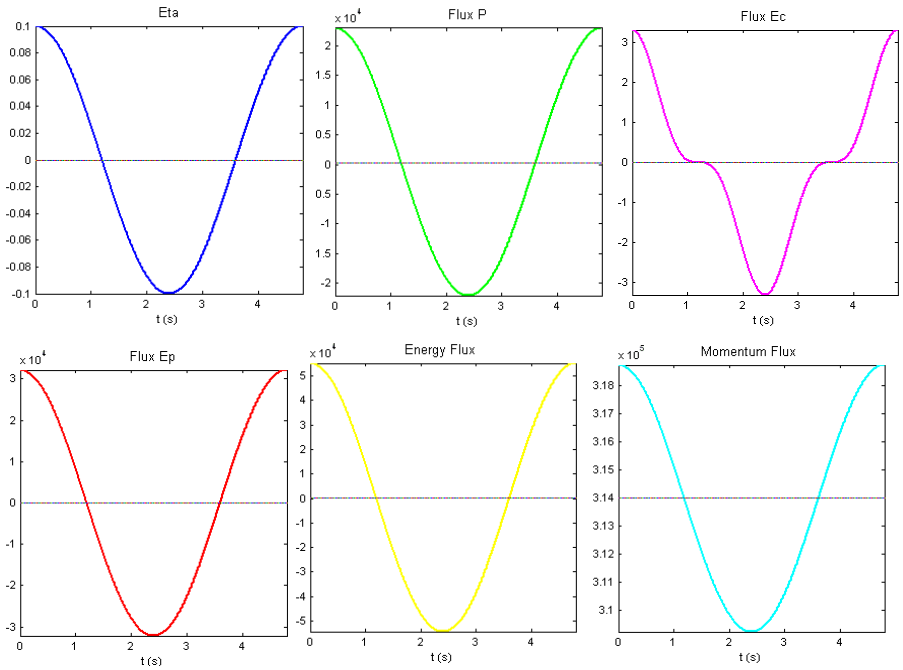

Figure 7.1: Flux for a sinusoidal wave

7.3 NUMERICAL APPLICATIONS TO NON-BREAKING, BREAKING AND REFORMED WAVE

The difference between breaking and non breaking waves is crucial in many aspects of the design of coastal works; such a difference is highlighted in some empirical formulas, but lies often undetected in engineering practice. It is indeed commonly often assumed that stability formulas, normally derived through experiment with non breaking waves can be transferred to shallow water situations where waves impact the construction after having broken – and that a correspondence can be made between such different situation by assuming that broken wave height and period can be safely used in the relevant formulas in place of the non breaking ones. Breaking wave height values are usually provided by formulas or models which describe the wave evolution on shallow bottom.
In this paragraph wave breaking effects on a slope (Figure 7.2) are analyzed in order to enquire about the reliability of these procedures. The simulations are carried out with regular input waves, thus highlighting hydrodynamic aspects that could be hidden when using random wave trains. The breaking therefore takes place localized in well determined points; as a result, from deep water to the swash zone, the wave height trend has a step shape, with leaps localized in the points where breaking conditions are reached.

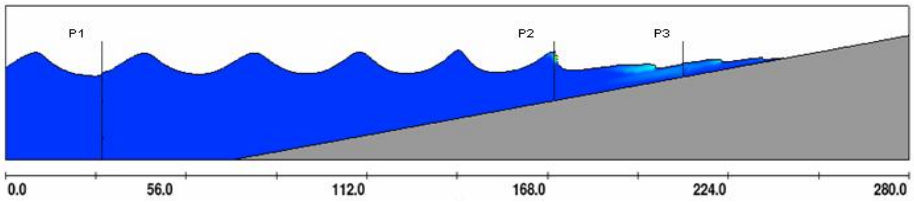

Figure 7.2: Numerical set-up

While the commonly accepted parameter for the intensity is the wave height, the most significant parameter associated with wave intensity is the momentum flux F_{qdm} transported by the wave, that is evaluated and represented in the following.

In the Figure 7.3, the F_{qdm} time behaviour is reported at the three probes P1, P2 and P3, (as in Figure 7.2), for H=2m and T=4.8s.

The first probe, P1, is in the constant depth zone (d=8m) where the waves are still sinusoidal; F_{qdm} fluctuations for both the numerically simulated wave and an Airy wave of the same height are practically the same. It also interesting to see that the kinetic term F_{qk} is relatively small so that the most important term of the momentum flux is the pressure.

For breaking waves (P2) and post-breaking or reforming waves (P3) the difference between the parameters for numerically simulated wave and those calculated according to the linear wave theory is much more important.

Also, the kinetic term for breaking and regenerated waves becomes the most important one in the momentum flux.
For the breaking wave (P2), the ratio:

$$r = \frac{F_{qdm}\, numerical}{F_{qdm}\, Airy}$$

between momentum flux numerically calculated and the same quantity evaluated for a correspondent Airy wave would be about 1.50.
The same parameter rises to 2 for post-breaking wave (P3).

Results so far show that while in the case of non-breaking waves the linear theory provides acceptable estimates of the momentum flux, and therefore possibly of the wave forces that would be exercised on a structure, for breaking and post-breaking waves the linear theory would strongly underestimate such a parameter.

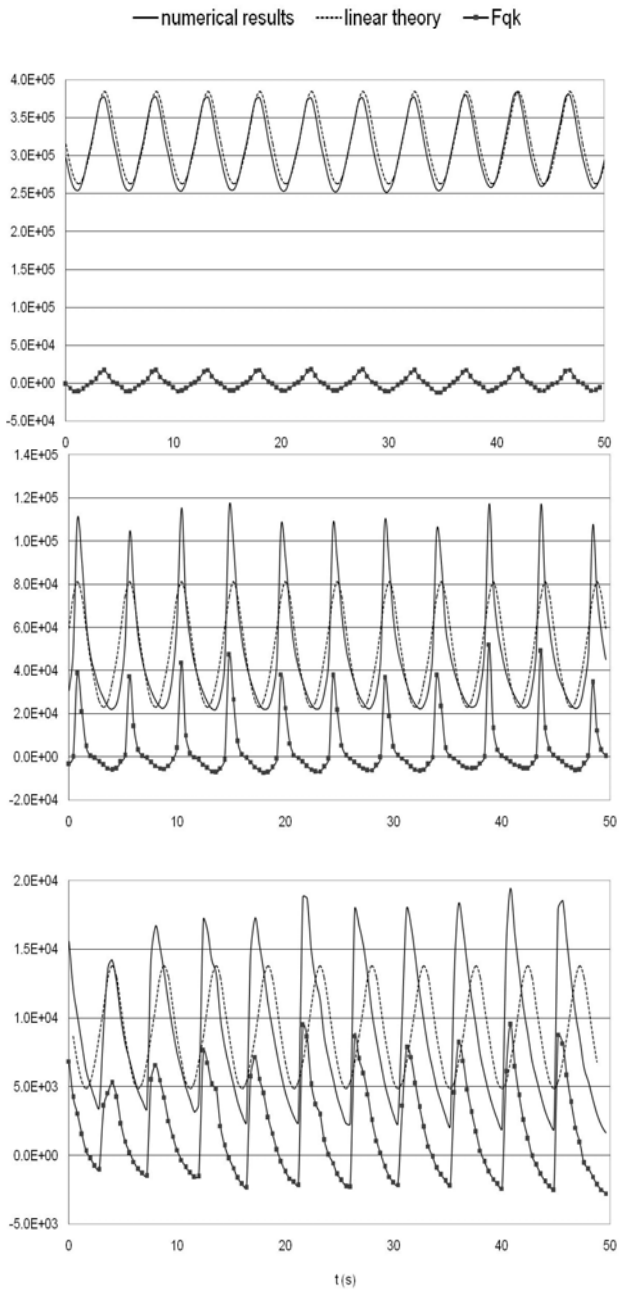

Figure 7.3: Time history of momentum flux in probe P1 (linear wave), P2 (breaking wave) and P3 (reformed wave)

The same simulations are thus repeated for different wave heights: in the Figures 7.4 and 7.5 a regular wave H=3 m, T=4.8 s is compared with a wave H=2m and same period, at various probes (P1 and P3).

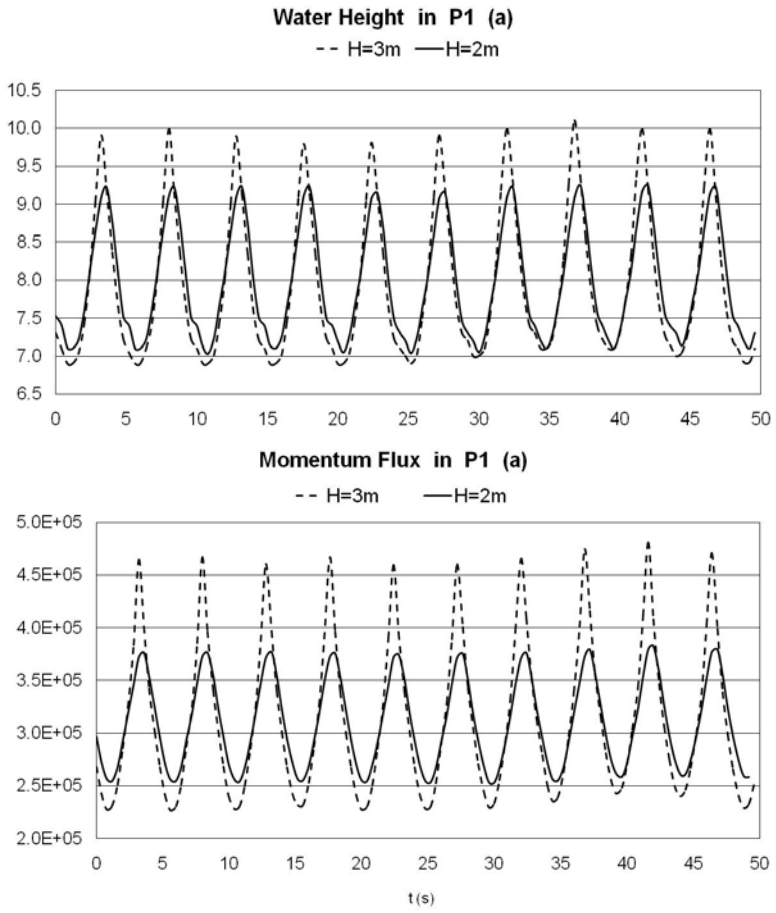

Figure 7.4: Wave height and momentum flux time histories in probe P1 for different H

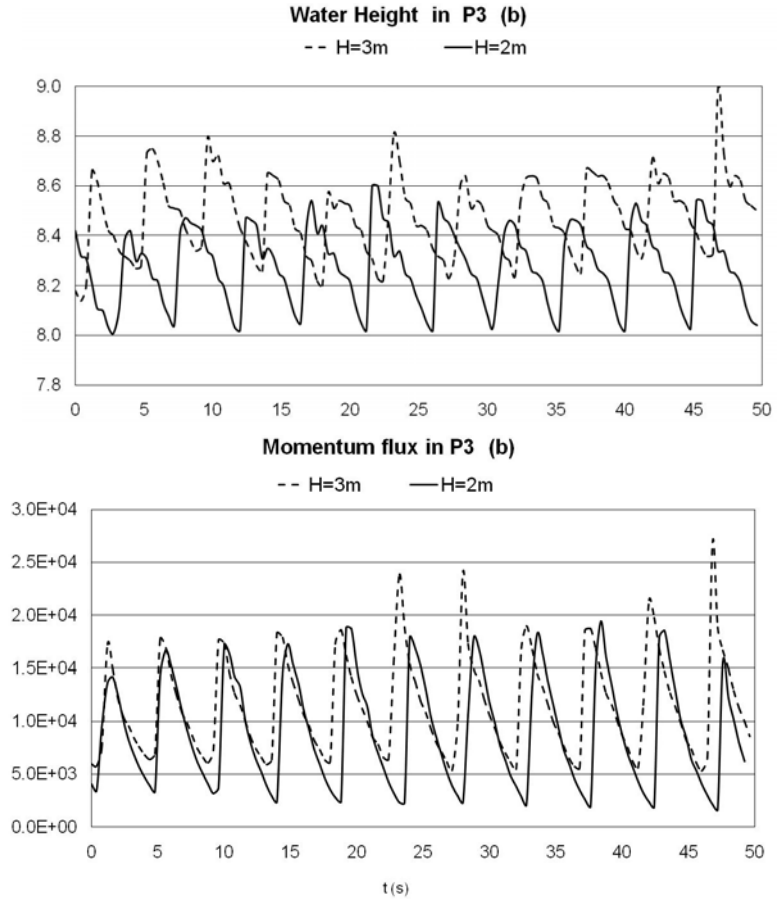

Figure 7.5: Water height and momentum flux time histories in probe P3 for different H

At probe P1 the differences in both water height and momentum flux between the waves are obvious. (Fig.7.4).

Moving along the slope, the higher wave train reaches probe P3 after its breaking point so, while the lower one (H=2) has not dissipated any energy yet (Fig.7.5) so their local wave heights and momentum fluxes are similar. The average water level (set up) is of course higher, as was to be expected.

7.4 WAVE ACTIONS ON A SCHEMATIC STRUCTURE

Wave breaking effects on a slope, and their relevance to wave actions on the wall, are analyzed by considering a schematic vertical wall founded at depth d_s on the previously considered sloping beach.

The tests were thus carried out with simple sinusoidal wave trains rather than with complex wave spectra since some hydrodynamic and numerical effects can be hidden by the random nature of the spectral wave generation. Equally, a purely schematic vertical wall is considered rather than a more complex structure such as an impermeable caisson installed on a rubble-mound foundation.

Two locations, and therefore two different values for d_s, are considered: the first (scheme A) by locating the wall at a distance of 170m from the wave generator (former position of probe P2) and the second (scheme B) at 210m (formerly probe P3).

In the first example waves break at about abscissa 192m, while in the first no breaking takes place before the wall: Figures 7.6 and 7.7 report results for water height and momentum flux at the wall.

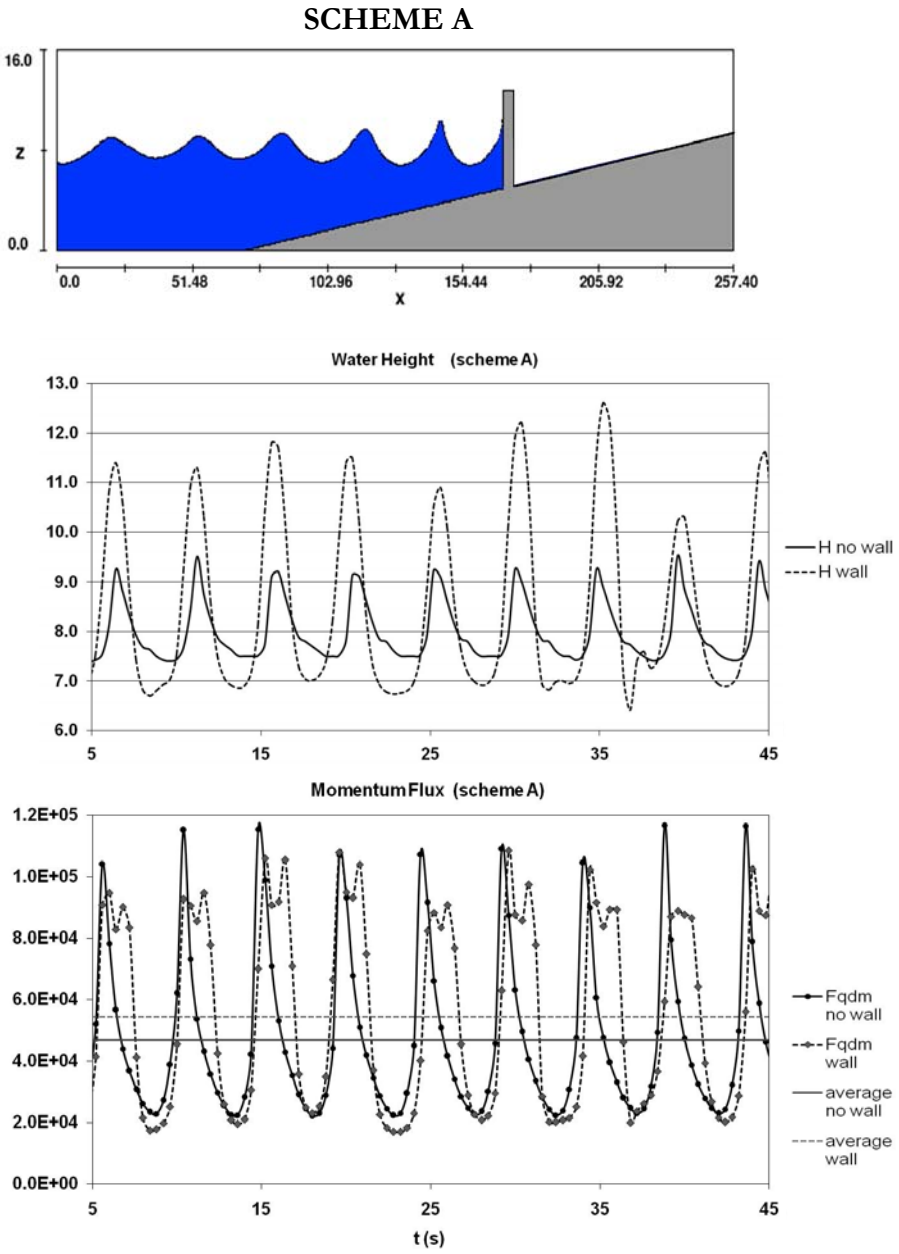

Figure 7.6: Numerical set-up with schematic structure, water heights and momentum fluxes at the wall as function of time: scheme A

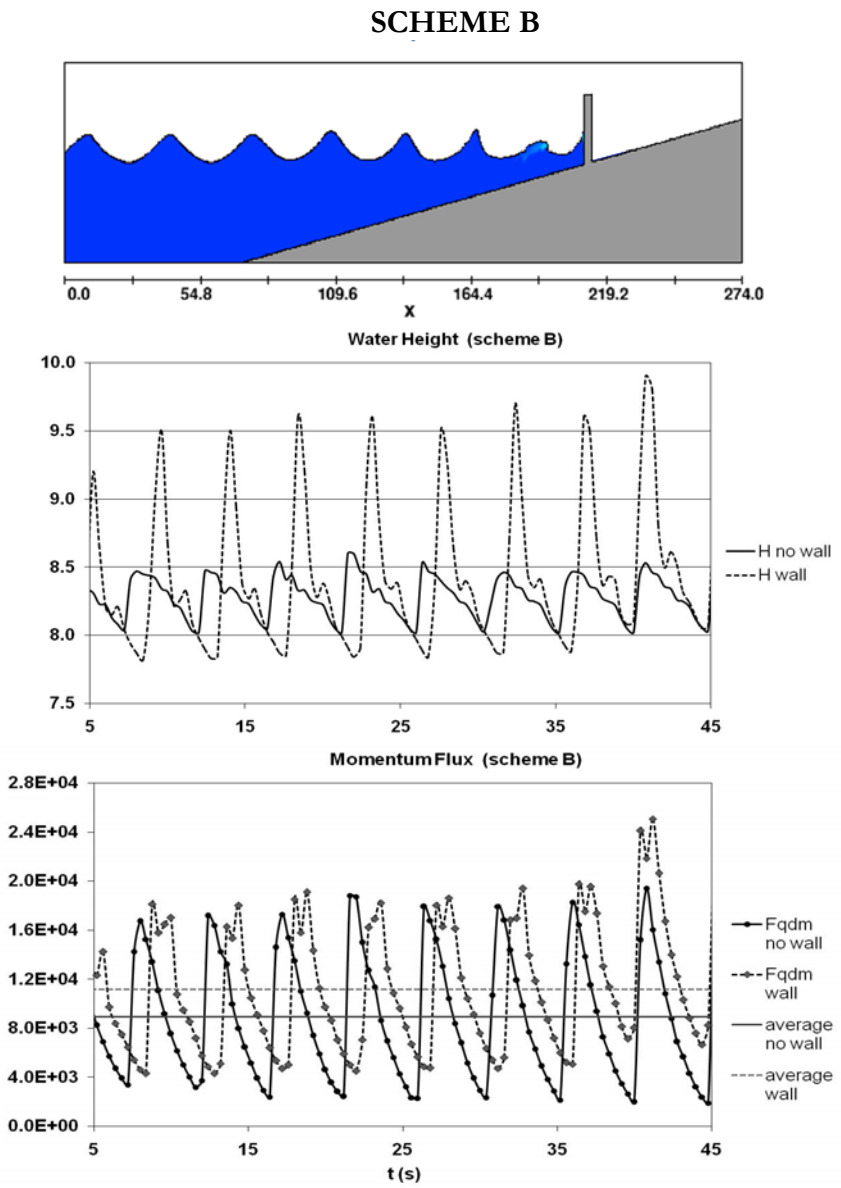

Figure 7.7: Numerical set-up with schematic structure, water heights and momentum fluxes at the wall as function of time: scheme B

As it was to be expected, the wave height is much greater when the wall is present, because of the reflection effects; it is remarkable however that the momentum flux (inclusive of the static pressure) does not change substantially.

The same calculations were carried out for different input waves in order to evaluate the influence of the offshore wave height as well as the effects of the wave breaking.

Figures 7.8 and 7.9 report resulting water height oscillations and momentum fluxes at the wall for scheme B with the following wave parameters: H=1, 2, 3 and 4 m, T=4.8 and 10 s.

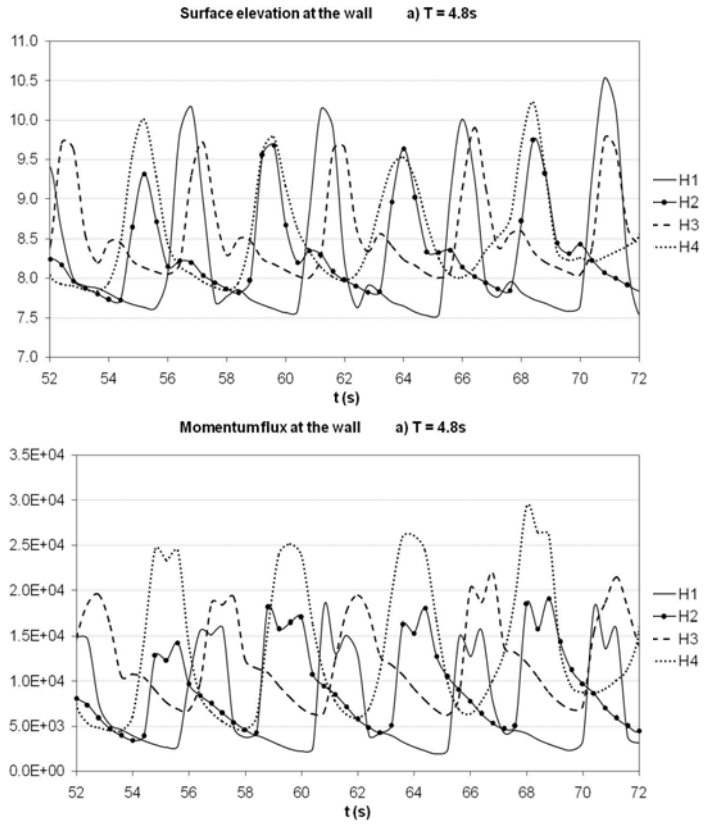

Figure 7.8: Surface elevations and momentum fluxes at the wall for different incident waves: a) T=4.8s

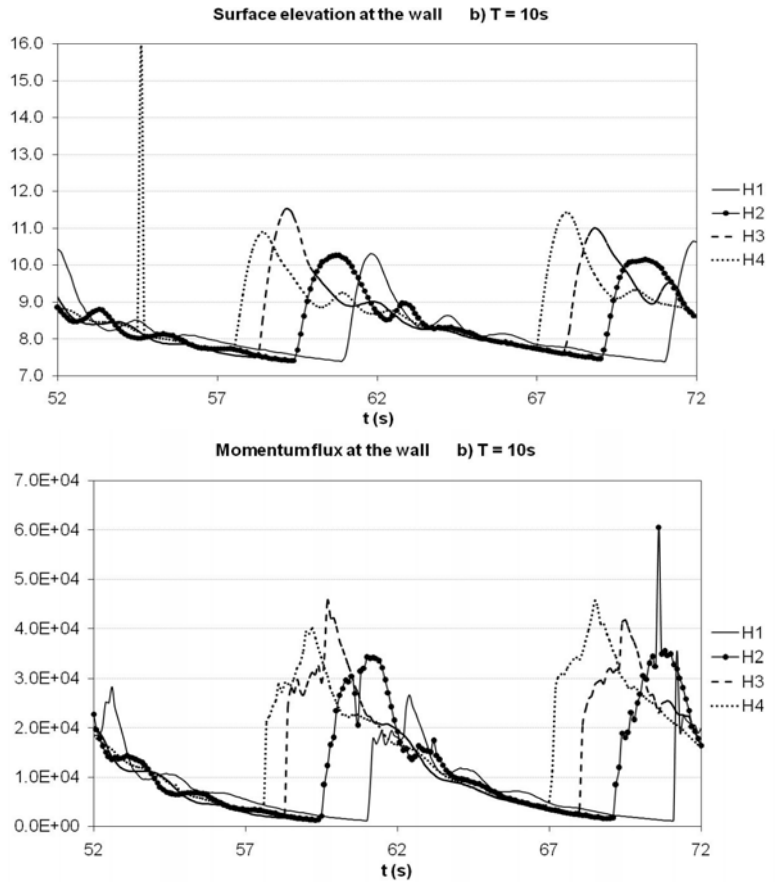

Figure 7.9: Surface elevations and momentum fluxes at the wall for different incident waves: b) T=10s

A clearer picture can be obtained by integrating the pressure at the wall over the whole water height for a whole period (Figures 7.10-11 and 7.12).

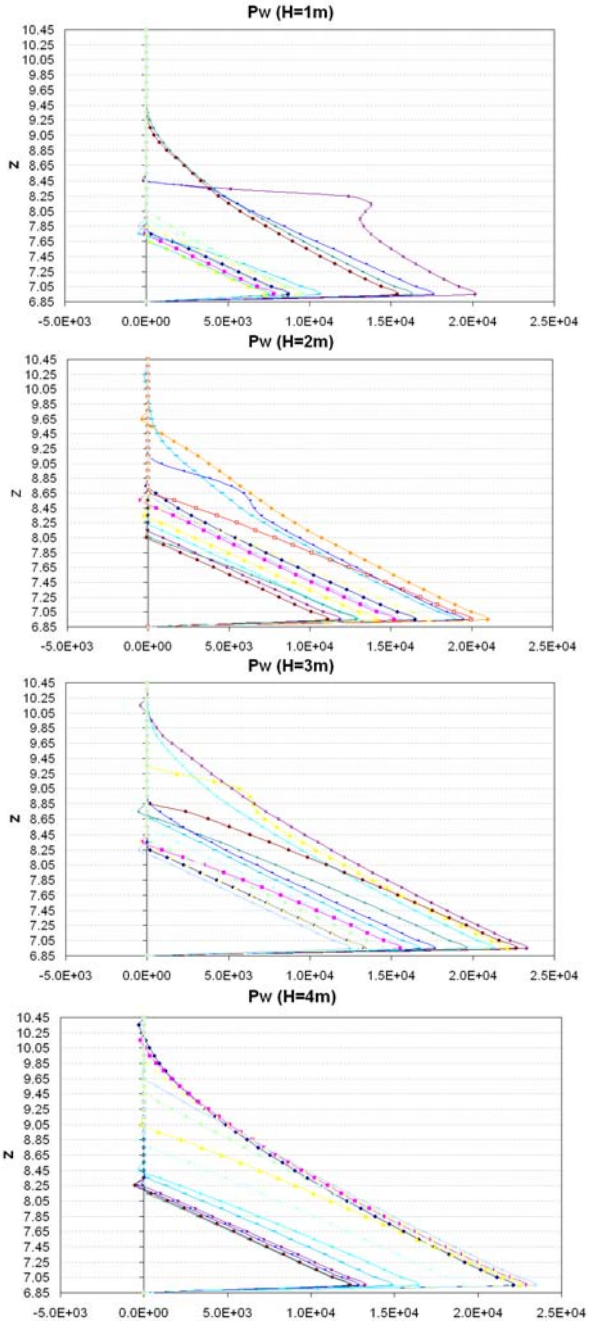

Figure 7.10: Pressure vertical profiles at the wall for different wave height (H=1, 2, 3, 4 m - T=4.8 s)

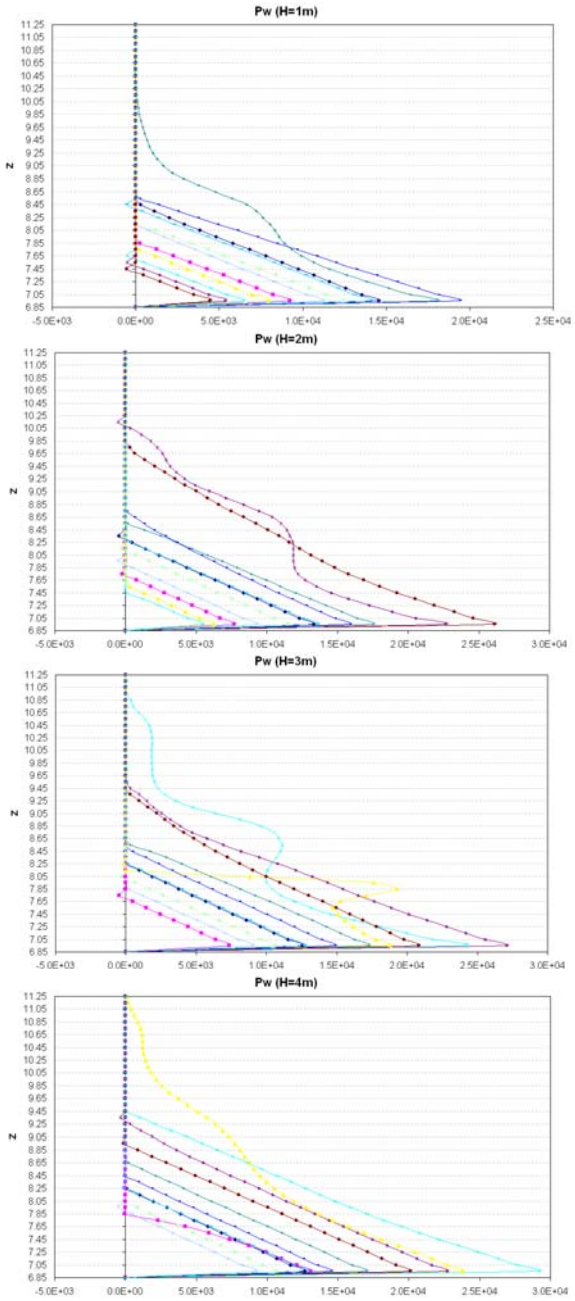

Figure 7.11: Pressure vertical profiles at the wall for different wave height (H=1, 2, 3, 4 m - T=10 s)

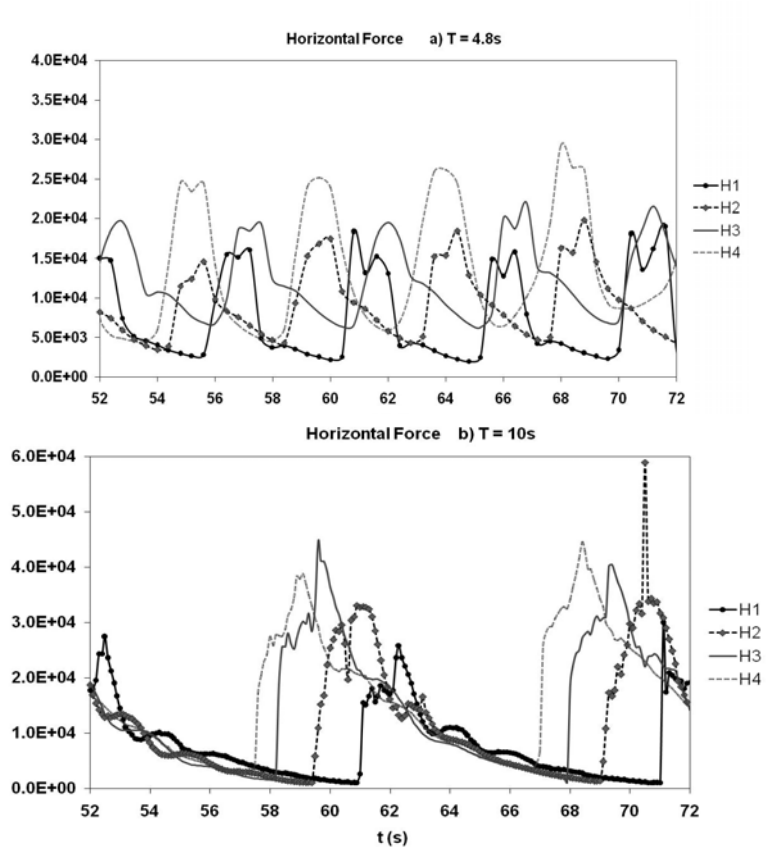

Figure 7.12: Horizontal force at the wall for different incident waves: a) T=4.8 s b) T=10 s

It is interesting to note that the lowest wave (H=1 m) yields water heights as high as the H=2 wave, which breaks before the wall; increasing wave heights yield increasing forces.

As it is well known to be expected by traditional procedures and engineering practice, a relatively constant value is reached when the beach slope is slight enough. This is confirmed by the numerical results, at least for longer waves (Figure 7.13).

8 WAVE ACTION ON VERTICAL STRUCTURES

8.1 HYDRAULIC PRESSURES ON STRUCTURES

Wave impacts on vertical breakwaters are among the most severe and dangerous loads this type of structure can suffer.
Whilst many design procedures for these structures are well established worldwide, a join research effort in Europe (PROVERBS Project - Probabilistic tools for vertical Breakwaters; Oumeraci et, 2001) showed that some of those design methods (Table 8.1) are limited in their application and may over- or under predict the loading under important conditions.

Within the PROVERBS project, a parameter map was developed, classifying different types of wave loading; input for this map are geometric and wave parameters which in combination yield an indication of a certain probability that one of the aforementioned breaker types will occur.

Table 8.1: Overview of design methods for wave loading (PROVERBS)

Author	Year	Pres-sures	Forces	Uplift	Comments
Quasi-Static Waves					
Sainflou	1928	yes	yes, but difficult	no	vertical wall, no berm
Miche-Rundgren	1944 1958	yes	yes	no	design curves from SPM, 1984
Goda	1985	yes	yes	yes	most-widely used design method
Impact Waves					
Hiroi	1919	yes	yes	no	vertical wall
Bagnold	1939	-	-	-	conceptual model only
Minikin	1963	yes	yes	no	sometimes incorrect dimen-sions!
Ito	1971	yes	yes	yes	
Blackmore & Hewson	1984	yes	yes	no	
Partenscky	1988	yes	not given	no	air content of wave needed
Kirkgöz	1990 1995	yes	yes	no	vertical wall only
Takahashi	1994	yes	yes	yes	extension of Goda model
Allsop et al.	1996	no	yes	yes	
Walkden et al.	1996	no	yes	no	relation of forces and rise time
Oumeraci & Kortenhaus	1997	yes	yes	yes	time-dependent approach!
McConnell	1998	no	yes	no	amendment of O&K, 1997
Hull & Müller	1998	yes	yes	no	amendment of O&K, 1997
Vicinanza	1998	yes	yes	no	amendment of O&K, 1997
Broken Waves					
SPM	1984	yes	yes	no	vertical walls only
Camfield	1991	yes	yes	no	amendment of SPM, 1984
Jensen	1984	yes	yes	yes	Crown walls
Bradbury & Allsop	1988	yes	yes	yes	Crown walls
Pedersen	1997	yes	yes	yes	Crown walls
Martin et al.	1997	yes	yes	yes	Crown walls

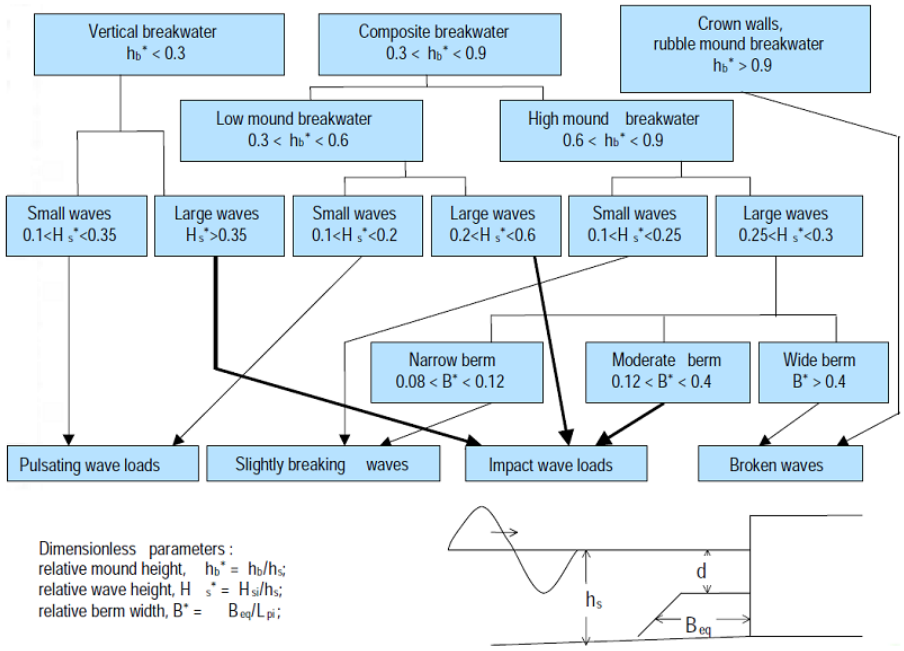

Figure 8.1: Proverbs Parameter Map

When waves approaching the shoreline hit a vertical wall structure, they are (partially) reflected. When the steepness or heights of the waves in front of the structure are relatively small, the pulsating wave pressures induce a similar response of the structure.

In other words, if small sinusoidal standing waves exist in front of a vertical reflective wall, they exert similar pressure fluctuations, which are sinusoidal in time (see Figure 8.2a). When waves translate in shallower water and come near breaking conditions, the shape of the waves and hence in a way the pressure-time history changes and becomes more asymmetric. Deformation due to the breaking process results in a steeper wave front and a more asymmetric pressure time history. Then the waves start to break (Figure 8.2b): a pressure peak can be seen to develop, due to the impact of the top of the wave. In some instances a very sharp peak (slamming) develops; the duration of such a shock pressure is much smaller than that of the so called quasi-static pressure exercised during the wave period (Figure 8.2c).

As fully broken waves hit the wall, the two pressure peaks (Figure 8.2d) are still apparent, their magnitude and duration depending on the distance between the breaking point and the upright section.

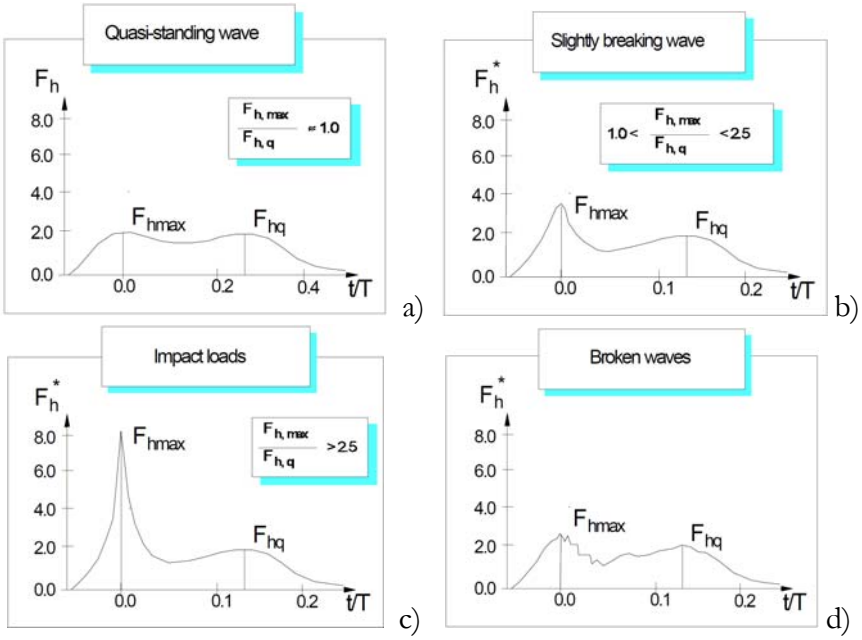

Figure 8.2: Identification of wave impact loading

According to the above mentioned PROVERBS programme, as well as to some previous pioneering work, such as the paper by Kirkgöz (1995), a distinction is thus to be made between quasi-static and dynamic loads. The quasi-static force varies in time in accordance to the water surface elevation, while the impact force, also called slamming (Wienke and Oumeraci, 2005) acts suddenly, and for a very short time.

Due to the short duration of such slamming loads, large-scale experiments combined with high sampling frequencies are required to get a sufficient resolution in time and space; RANS/VOF seems to be well suited to carry out this kind of analyses, as long as both computational and sampling steps are kept small enough.

The raising of such short duration impulses, linked as they are to compressibility effects, is however partially random in experiments as well as in practice, which reflects in high sensitivity to computational parameters.
Figures 8.3 and 8.4 provide an example, for a wave with H=2 m and T=4.8 s.

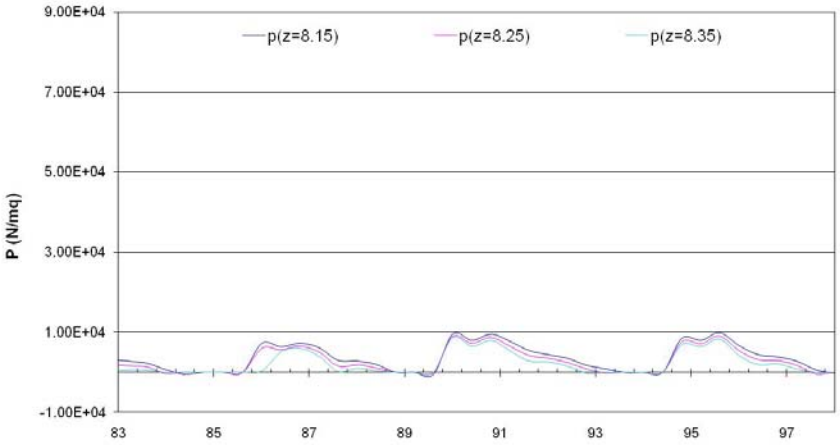

Figure 8.3: Typical slamming pressure as computed by RANS/VOF (dt=0.4 s; dz=0.1 m)

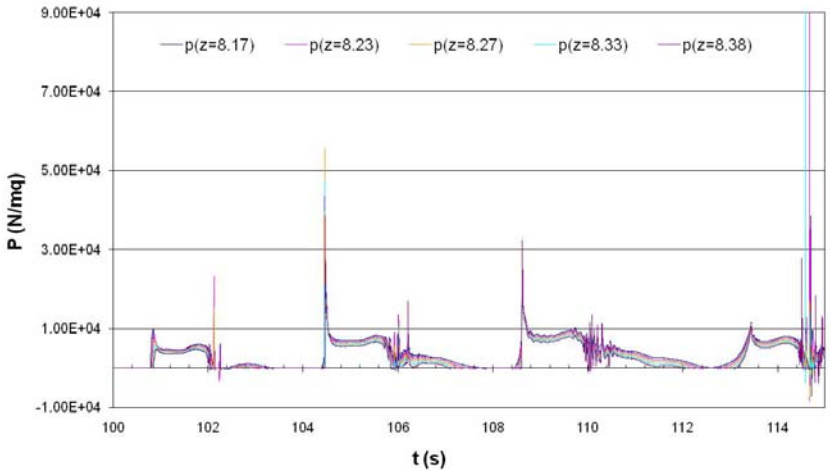

Figure 8.4: Typical slamming pressure as computed by RANS/VOF (dt=0.001 s; dz=0.05 m)

The quasi-static pressures are always in the order of ϱgH, but the impact pressures can be as much as 5 o 10 times higher.
The same calculations were carried out for different input waves (H=1, 2, 3 m – T=4.8 s) in order to evaluate the influence of the offshore wave height as well as the effects of the wave breaking on the slamming pressure. Results are summarized in Figure 8.5.

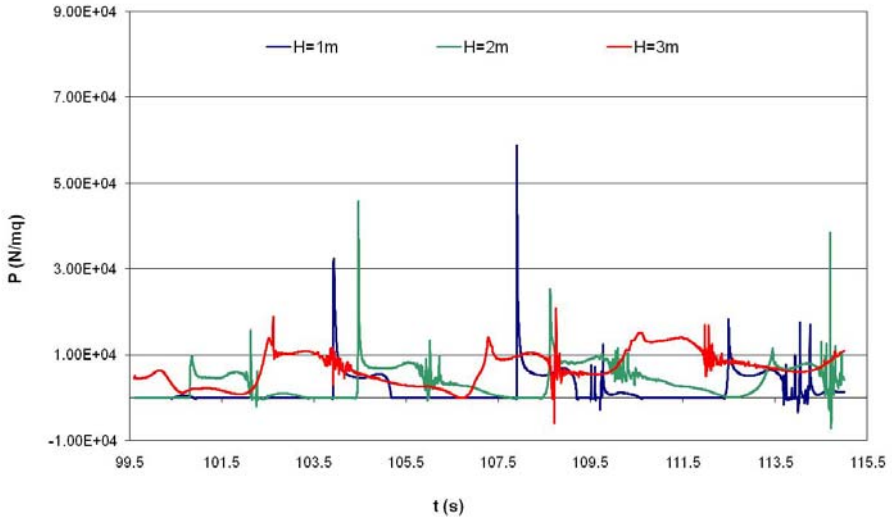

Figure 8.5: Slamming pressure comparison for different wave

In agreement with Figure 8.2, it is interesting to note that the lowest wave (H=1m) yields higher slamming pressures than the H=3m wave, which breaks long before the wall; the H=2m wave has an intermediate behavior between impact and broken wave.

8.2 IMPACT OF WAVES ON VERTICAL STRUCTURES

The computation of forces on the structure is based, generally, upon on classical approaches: restricting ourselves to the problem of a vertical structure on shallow water, formulas such as Takahashi (Takahashi et al, 1994) provide pressures and forces, as long as wave height is provided by semi-empirical methods (Nagai, 1968; Goda,1985; Kamphuis, 1991; Müller and Whittaker, 1996; Kobayashi et al, 2007).

APPENDIX I reports Takahashi's formula and its physical assumptions.

A weakness of such methods (in the following indicated as Goda/Takahashi GT) is that wave height in presence of a structure is bound to be modified by the presence of the structure itself (as simulated in the precedent chapter). Criteria for wave breaking in front of a vertical wall have been developed (Calabrese, 1999), but their applications are far from universal.

Although Goda's method is a valuable design method, field measurements of wave pressures and hydraulic model tests (Oumeraci et al., 1991) showed that wave forces under pulsating waves conditions on many structures were often larger than the ones predicted by simple prediction methods.
This can be ascribed to several uncertainties generated from two main sources:
- the uncertainty of the maximum individual wave height in a wave field;
- the model uncertainty in the wave force model (by Goda himself, or by Takahashi).

Some more useful information can be gained by plotting the results above (Figure 8.6).

Numerical RANS/VOF calculated pressures tend to exceed values calculated through the well tested procedure (GT Goda Takahashi) for longer periods, while they stay well below for lower periods.

As for global forces, a good fit is obtained for the lower period, while – again – for longer waves RANS/VOF considerably exceeds GT values.

This is no proof that empirical methods underestimate forces in some circumstances – it should not be forgotten that GT assumes a spectral distribution, while tests carried out within this work are based upon monochromatic waves; it does show however that RANS/VOF provides, for a vertical structure in shallow water, results that are comparable with available tests.

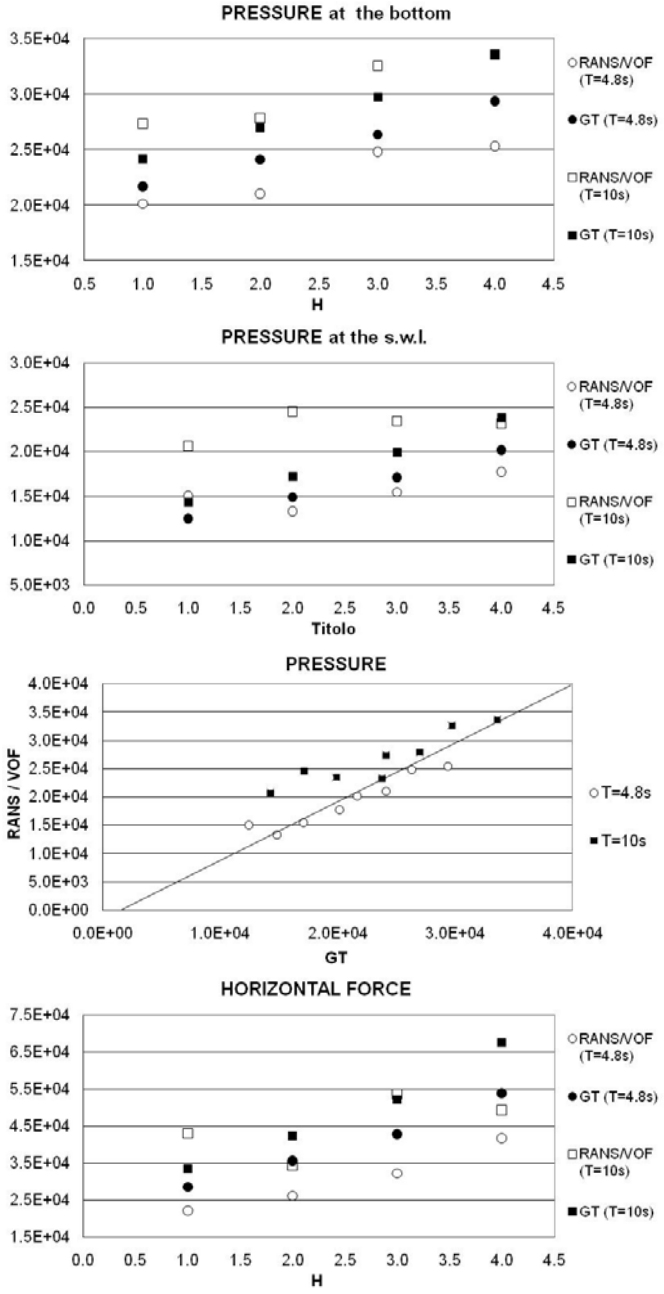

Figure 8.6: Pressures and forces at the wall
for different wave heights (H=1-2-3-4m) and periods (T=4.8s; T=10s)
RANS/VOF numerical simulation - GT Goda Takahashi procedure

9 CONCLUDING REMARKS

With the recent development of computer technology, CFD (computational fluid dynamics) methods have become an efficient tool to enquire into hydrodynamics of waves on shallow water; the numerical simulation of the free surface with a breaking wave is indeed not only an attractive research topic but an all-important task towards the full understanding of wave impact on structures, and particularly so on costal works. The quality of projects as well as the reliability of coastal risk evaluation very much depends on the availability of adequate numerical methods for coastal engineers.

The main numerical difficulty to be overcome was – and to some extent still is - the description of free surface shape and evolution. Numerical Navier Stokes integration with VOF surface algorithms, first developed by Lin and Liu's (1998,) has now evolved into a reliable technique (see for instance Christensen 2006, Dentale et al 2008). The method, however still needs to be thoroughly improved, calibrated and tested in order to extend its application to real cases.

The work presented here was aimed at critically analysing the influence of some key factors, such as scale of laboratory tests, boundary conditions, grid size and time steps, specially so in presence of sloping bottoms and shallow water obstacles, i.e. in the conditions of greatest importance towards coastal engineering and civil protection applications. Results were compared with laboratory measurements to evaluate the applicability of each approach in computing surf zone dynamics. In addition, simulations with different two equation turbulence models (K-ε and RNG) were evaluated and details of the wave propagation on shallow water and breaking wave properties were presented and discussed.

Scale effects are a key issue in hydraulic laboratory modeling and specially so in wave action studies. It is normally assumed that Froude number is the key parameter in wave laboratory experiments, so that results from a model can be safely scaled up if such a parameter is kept constant; this, of course, implies that the Reynolds number, strongly dependent as it is on the physical size of the experiment, only plays a minor role.

This assumption was properly verified by carrying out numerical tests at different scales and the present thesis has provided some insight in this regard. Results confirm that the rationale behind small scale laboratory modeling of spilling wave breaking is correct, and that important parameters are – within limits – not influenced by the scale; no final conclusion however could be reached about the lowest admissible limit for scale model testing, how i.e. what is the smallest scale at which viscosity becomes so important as to influence results. Indeed, as the scale, and therefore the Reynolds number, goes further down, the damping out of turbulence is not reproduced by current turbulence models. A need for a reliable Low Reynolds model is therefore evident. The answer might eventually come from the adoption of a specialized K-ε model or more probably from an improvement of current LES techniques.

Another point thoroughly analyzed in this thesis concerns the interaction between the waves and the structures in shallow water. The prediction of distributed pressures and waves forces on structures is not only very complex, but it depends upon such a variety of factors that traditional formulas and empirical approaches can be misleading.

For instance, the difference between breaking and non breaking waves is crucial in many aspects in the design of coastal works; such a difference is highlighted in some empirical formulas, but often still lies undetected in engineering practice.

Even though a significant progress has been made in the last few years towards a full understanding of wave impact on shallow water structures, stability formulas are still normally derived through experiment with waves which do not break before the actual impact; results from these experiments are then transferred to shallow water situations where waves break before making impact on the construction.

In this regard, the thesis presents the results of numerical simulation experiments on wave breaking effects in front of a vertical obstacle founded on a sloping bottom on shallow water, with the objective of clarifying physical issues which so far have remained undetected; tests were thus carried out with simple sinusoidal wave trains rather than with complex wave spectra since some hydrodynamic and numerical effects can be hidden by the random nature of the spectral wave generation. Equally, a purely schematic vertical wall was considered rather than a more complex structure such as an impermeable caisson installed on a rubble-mound foundation.
Water height and wave momentum parameters were considered for a slope with and without a vertical structure on shallow depth; the forces exerted on the structure were then evaluated for different foundation depths and wave heights
Results, for pressure and force on the structure, are shown to be comparable to those provided by existing and well proven empirical methods, while at the same time allowing the flexibility deriving from numerical simulation; a detailed picture of free-surface elevation, pressure and velocity field within the surf zone is thus now practically available.

RANS/VOF has thus proven to be to be an important design tool for structures in shallow water by to providing a 2D direct computation of relevant quantities in near-shore hydrodynamics, as long as proper care is placed upon numerically and experimentally verifying its parameters and its assumptions.

REFERENCES

- Battjes, J.A., (1988) "Surf-zone dynamics", Annu. Rev. Fluid Mech. 20, 257– 293.
- Benassai, E., (2006) "Le dighe maritime:progettazione-realizzazione-dissesti-manutenzione", Istituto italiano per gli studi filosofici.
- Bentaleb, Y., Schall, E., Koobus, B., Dervieux, A., Amara, M. (2006) "A numerical method for simulating turbulent shear flows with low Reynolds K−ε models", Monografías del Seminario Matemático García de Galdeano 33, 349–356.
- Boccotti, P., 2000 "Wave mechanics for ocean engineering", Elsevier Oceanography series, 64.
- Bovolin, V., Picciotti, M.V. (2004) "Numerical simulation of dynamic impact on structures", 4° Italy Japan Conference on Sediment Disaster Prevention Technology, Neaples 20-22 May 2004.
- Bradford, S.F. (2000) "Numerical simulation of surf zone dynamics, Journal of Waterway, Port, Coastal, And Ocean Engineering", Vol. 126, N. 1, Jan./Feb., 2000.
- Bullock, G.N., Crawford, A.R., Hewson, P.J., Walkden, M.J.A., Bird, P.A.D., (2000), "The influence of air and scale on wave impact pressures", Coastal Engineering vol. 42, pp. 291–312.
- Bullock, G.N., Obhrai, C., Peregrine, D.H., Bredmose, H., (2007), "Violent breaking wave impacts. Part 1: Results from large-scale regular wave tests on vertical and sloping walls", Coastal Engineering 54, pp. 602–617.
- Calabrese, M., (2000), "A breaking criterion for waves in front of simple vertical and composite breakwaters", Coastal Engineering, Elsevier, Amsterdam.
- Chiu, Y.F., Lin, J.G., Chang, S.C., Lin, Y.J., Chen, C.H., (2007), "An experimental study of wave forces on vertical breakwater", Journal of Marine Science and Technology, Vol. 15, No. 3, pp. 158-170.
- Chopakatla S.C., Lippmann, T.C., Richardson, J.E. (2008) "Field verification of a computational fluid dynamics model for wave

transformation and breaking in the surf zone", Journal of Waterway, Port, Coastal, and Ocean Engineering, vol. 134, n. 2.
- Christensen, E.D. (2006) "Large eddy simulation of spilling and plunging breakers", Coastal Eng., 53, 463–485.
- Christensen, E.D., Deigaard, R. (2001) "Large eddy simulation of breaking waves", Coastal Eng., 42, 53– 86.
- Ciardulli, F., (2009) " La Risposta Idraulica di Barriere Sommerse in Campo Non Lineare", Ph.D. thesys, Polo delle Scienze e delle Tecnologie - Facoltà di Ingegneria - Università Degli Studi Di Napoli "Federico II".
- Dalrymple, R.A, Rogers, B.D. (2006) "Numerical modeling of water waves with the SPH method", Coastal Engineering, 53, pp. 141–147.
- De Padova D., Darlymple R.A., Mossa M., Petrillo A.F. (2008b) "An analysis of the artificial viscosity in the SPH method modelling a regular breaking wave", Coastlab 08, Bari, Italy.
- De Padova, D. (2008a) "A numerical and experimental analysis of smoothed particle hydrodynamics in wave motion field", Doctoral Thesis, Technical University of Bari, Department of Environmental Engineering and Sustainable Development.
- De Serio, F., Mossa, M. (2006) "Experimental study on the hydrodynamics of regular breaking waves", Coastal Engineering, 53, pp. 99 – 113.
- Dentale, F., Monaco, M., Pugliese Carratelli, E. (2008) "A numerical assessment of scale effects on wave breaking modeling", 3rd SCACR International Short Course and Workshop on Applied Coastal Research, Lecce.
- Dentale, F., Pugliese Carratelli, E., Pane, S., (2009), "Modellazione numerica del moto ondoso su barriere frangiflutti sommerse porose", Studi Costieri, 2009, 16, pp. 89-106.
- Dentale, F., Russo, S.D., Pugliese Carratelli, E., (2010), "Innovative numerical simulation to study the fluid motion within rubble mound breakwaters and the armour stability", 17th Armourstone user meeting, Wallingford, UK.
- Dentale, F., Russo, S.D., Pugliese Carratelli, E., Messina B., Mascetti S., (2009), "Studio numerico avanzato sul moto di filtrazione in ambito marittimo", Analisi & Calcolo, Giugno 2009, pp. 42-45.

- Dong, C.M., Huang, C.J. (2004) "Generation And Propagation Of Water Waves In A Two-Dimensional Numerical Viscous Wave Flume", Journal Of Waterway, Port, Coastal And Ocean Engineering.
- Flow Science, Inc., 2009. FLOW-3D User's Manual.
- Foti, E., "Note di idraulica marittima e ingegneria costiera", Università degli Studi di Catania – Dipartimento di Ingegneria Civile ed Ambientale.
- Foti, E., Scandura, P., (2004) "A low Reynolds number k–e model validated for oscillatory flows over smooth and rough wall", Coastal Engineering 51 (2004) 173–184.
- Garcia, N., J. L. Lara, Losada, I. J., (2004) "2-D numerical analysis of near-field flow at low-crested breakwaters", Coastal Eng., 51, 991–1020.
- Gaunche, R., Losada, I.J., Lara, J.L., (2009), "Numerical analysis of wave loads for coastal structure stability", Coastal Engineering, vol. 56, pp. 543-558.
- Goldberg, U., Peroomian, O., And Chakravarthy, S. (1998) "A wall-distance-free K−e model with enhanced near-wall treatment", J. Fluids Engrg. 1998.
- Hieu, P.D., Tanimoto, K. (2006) "Verification of a VOF-based two-phase flow model for wave breaking and wave–structure interactions", Ocean Engineering, Vol.33 Issue: 11-12, pp: 1565-1588.
- Hieu, P.D., Tanimoto, K., Thanh Ca, V. (2004) "Numerical simulation of breaking waves using a two-phase flow model", Applied Mathematical Modelling, vol. 28, pp.983–1005.
- Hirt, C.W., and B.D. Nichols (1990) "Volume of fluid (VOF) method for dynamics of free boundaries", J. Comput. Phys., 39, 201– 225.
- Hsu, T.J., Sakakiyama, T., Liu, P.L.F., (2002); "A numerical model for wave motions and turbulence flows in front of a composite breakwater", Coastal Engineering vol. 46, pp. 25–50.
- Hu J.P., Yu Y.X., Zhu L.S., (2006), "Research on wave forces acting on the unit length of a vertical breakwater by tests and a numerical model", Journal of Hydrodynamics, Ser.B, 2006,18(5): 512-519.
- Hughes, S.A., 2004, "Wave momentum flux parameter: a descriptor for nearshore waves", Coastal Engineering 51 (2004) 1067– 1084
- Jonsson, I.J., 1998, "Wave action flux: a physical interpretation", J. Fluid Mech. (1998), vol. 368, pp. 155-164.

- Karim, M.F., Tanimoto, K., Hieu, P.D. (2003) "Simulation of Wave Transformation in Vertical Permeable Structure", Proceedings of The Thirteenth International Offshore and Polar Engineering Conference, Honolulu, Hawaii, USA, May 25–30, 2003.
- Karim, M.F., Tingsanchali, T. (2006) "A coupled numerical model for simulation of wave breaking and hydraulic performances of a composite seawall", Ocean Engineering , vol. 33, pp. 773–787.
- Kirkgöz, M.S., (1995), "Breaking wave inpact on vertical and sloping coastal structures", Ocean Engng., vol.22, n.1, pagg.35-48, Elsevier Science.
- Kobayashi, N., Meigs, L.E., Ota, T., Melby, J.A. (2007), "Irregular Breaking Wave Transmission over Submerged Porous Breakwater", Journal Of Waterway, Port, Coastal, And Ocean Engineering - Asce / March/April 2007
- Kortenhaus, A., Oumeraci, H., Allsop, N.W.H., Mcconnell, K.J., Van Gelder, P.H.A.J.M., Hewson, P.J., Walkden, M., Müller, G., Calabrese, M., Vicinanza, D., (2001), "CAP 5.1: Wave impact loads - pressures and forces", Proceedings Proverbs.
- Lara, J. L., Garcia, N., Losada, I. J. (2006a) "RANS modelling applied to random wave interaction with submerged permeable structures", Coastal Eng., 53, 395– 417.
- Lara, J. L., Losada, I. J., Liu, P. L. F. (2006b) "Breaking waves over a mild gravel slope: experimental and numerical analysis", J. Geophys. Res., 111, C11019.
- Larsen, J., Dancy, H. (1983) "Open boundaries in short-wave simulations - a new approach", Coastal Eng. 7, pp. 285–297.
- Lee, Y.G., Heo, J.K. (2005) "Simulating nonlinear waves on the free surface in surf zones with two-dimensional sloping beach", Ocean Engineering, vol.32, pp. 57–84.
- Liberatore, G., Petti, M. (1992) "Wave Transformations Over a Submerged Bar: Experiments and Theoretical Interpretations", Coastal Engineering 1992.
- Lin, P.(2008) "Numerical Modelling of Water Waves: An Introduction to Engineers and Scientists" - Taylor & Francis publisher.
- Lin, P., Karunarathna, S.A.S. (2007) "Numerical Study of Solitary Wave Interaction with Porous Breakwaters", Journal Of Waterway, Port, Coastal, And Ocean Engineering, ASCE - sept/oct 2007.

- Lin, P., Liu, P. L.F. (1998b) "Turbulence transport, vorticity dynamics, and solute mixing under plunging waves in surf zones", J. Geophys. Res., 103(15), pp. 677– 694.
- Lin, P., Liu, P.L.F. (1998a) "A numerical study of breaking waves in the surf zone", J. Fluid Mech., vol. 359, pp. 239-264.
- Lin, P., Liu, P. L.F. (1999) "Internal Wave-Maker For Navier-Stokes Equations Models", Journal Of Waterway, Port, Coastal, And Ocean Engineering / July/August 1999.
- Liu, P.L.F., Lin, P., Chang, K.A., Sakakiyama, T. (1999) "Numerical modeling of wave interaction with porous structures", Journal Of Waterway, Port, Coastal, And Ocean Engineering/ November/December 1999.
- Longo, S., Petti, M., Losada; I.J., (2002) "Turbulence in the swash and surf zones: a review", Coastal Engineering 45 (2002) 129–147.
- Losada, I. J., Lara, J. L., Christensen, E. D., Garcia N. (2005) "Modelling of velocity and turbulence fields around and within low-crested rubblemound breakwaters", Coastal Eng., 52, 887– 913.
- Losada, I.J., Lara, J.L., Guanche, R., Gonzalez-Ondina, J.M. (2008) "Numerical analysis of wave overtopping of rubble mound breakwaters", Coastal Engineering, vol. 55, pp.47–62.
- Lubin P., Branger H, Kimmoun O. (2006) "Large eddy simulation of regular waves breaking over a sloping beach", ICCE 2006 - Abstract 1005.
- Lubin, P., Vincent, S., Abadie, S., Caltagirone, J.P. (2006) "Three-dimensional Large Eddy Simulation of air entrainment under plunging breaking waves", Coastal Engineering 53 (2006) pp. 631–655.
- Lubin, P., Vincent, S., Caltagirone, J.P., Abadie, S. (2004) "Three-dimensional large eddy simulation of vortices induced by plunging breaking waves", ICCE 2004, Abstract 229.
- Lugni, C., Brocchini, M., Faltinsen, O.M., (2006), "Wave impact loads: The role of the flip-through", Physics Of Fluids 18, 122101.
- Martin, F.L., Losada, M.A., Medina, R., (1999), "Wave loads on rubble mound breakwater crown walls", Coastal Engineering37, pp.149-174.
- Monaghan J.J. (2005) "Smoothed particle hydrodynamics", Institute of Physics Publishing, Rep. Prog. Phys. 68, pp 1703–1759.

- Muller, G., Whittaker, T.J.T., (1996), "Evaluation of design wave impact pressures", Journal Of Waterway, Port, Coastal, And Ocean Engineering / January February 1996.
- Oumeraci H., A. Kortenhaus , W. Allsop, de Groot M., Crouch R. , Vrijling H., Voortman H. (2001) " Probabilistic Design Tools for Vertical Breakwaters", GPB Gorter bv, Steenwijk, The Netherlands.
- Peregrine, D.H. (1983) "Breaking Waves on Beaches", Ann. Rev. Fluid Mech. 15:149-78.
- Qi, P., Hou, Y. (2006) "A VOF—based numerical model for breaking waves in surf zone", Chinese Journal of Oceanology and Limnology, Vol.24, No.1, pp. 57-64.
- Reeve, D.E., Soliman, A., Lin, P.Z. (2008) "Numerical study of combined overflow and wave overtopping over a smooth impermeable seawall", Coastal Engineering, vol. 55, pp. 155–166.
- Shao, S. and Changming, J., 2006, "SPH computation of plunging waves using a 2-D sub-particle scale (SPS) turbulence model", Int. J. Numer. Meth. Fluids, 51:913–936.
- Shin, S., Cox, D.T., Kim, I.C., Yim, S., (2006), "Wave transformation, impact, and overtopping on a rubble mound breakwater: large scale measurements and numerical modeling", 30th International Conference on Coastal Engineering, San Diego.
- Suh, K.D., Park, W.S., Park, B.S. (2001), "Separation of incident and reflected waves in wave–current flumes", Coastal Engineering 43, pp.149–159.
- Takahashi, S. (1996) "Design of vertical breakwaters", Port and Harbour Research Institute.
- Ting, F. C. K., Kirby, J. T. (1995) "Dynamics of surf-zone turbulence in a strong plunging breaker", Coastal Eng., 24, 177– 204.
- Ting, F. C. K., Kirby, J. T. (1996) "Dynamics of surf-zone turbulence in a spilling breaker", Coastal Eng., 27, 131– 160.
- Tirindelli, M., Lamberti, A., Paphitis, D., Vidal, C., Hawkins, S., Morchella, P., Sanchez-Arcilla, A. (2000) "Wave action on rubble mound breakwaters: the problem of scale effect", DELOS EVK3-CT-2000-00041.
- Torres-Freyermuth, A., Losada, I. J., Lara, J. L. (2007) "Modeling of surf zone processes on a natural beach using Reynolds-Averaged Navier-Stokes equations", Journal of Geophysical Research, vol. 112.

- Viccione G., Dentale F., Bovolin V., Pugliese Carratelli E. (2008) "Simulation of Wave Impact Pressure on Vertical Structutes with the SPH Method", 3rd ERCOFTAC SPHERIC workshop on SPH applications, June 2008, Lausanne, Switzerland, pp 237-240.
- Wienke, J., Oumeraci, H. (2005), "Breaking wave impact force on a vertical and inclined slender pile - theoretical and large-scale model investigations", Coastal Engineering 52, pp. 435– 462.
- Zhao, Q., Armfield, S., Tanimoto, K. (2004) "Numerical simulation of breaking waves by a multi-scale turbulence model", Coastal Engineering 51, pp. 53–80.

APPENDIX I

Takahashi formula (extension of Goda model) established for all wave conditions (standing and breaking waves, crest wave and trough wave) the horizontal force distribution along vertical structures as well as the uplift pressure induced by the wave action along the caisson bottom.

Figure A.1 shows this pressure distribution.

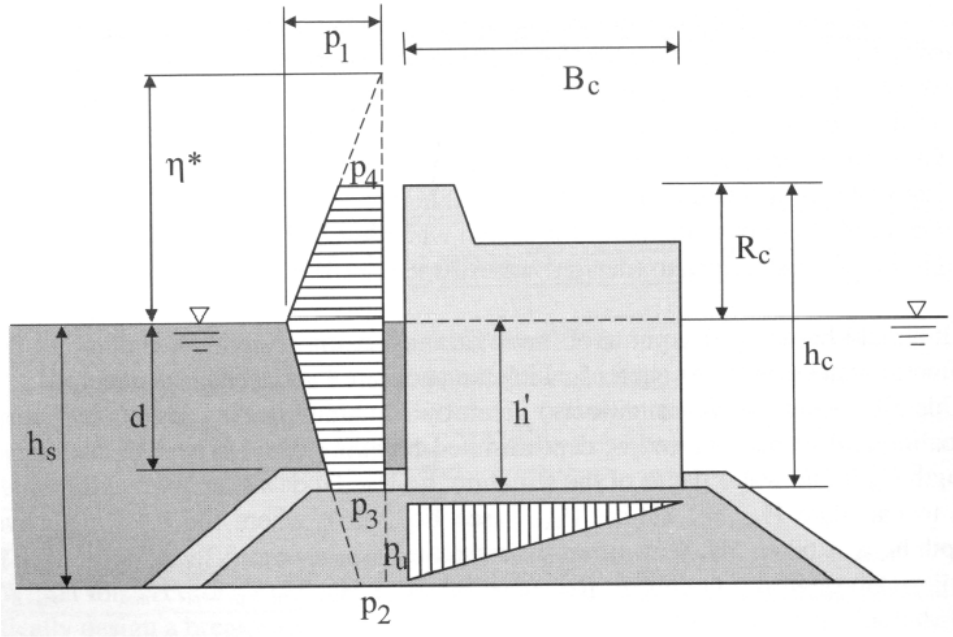

Figure A.1: Pressure distribution according to Takahashi (1994)

The Takahashi formula is written as:

$$\eta^* = 0.75(1+\cos\beta)H$$
$$p_1 = 0.5(1+\cos\beta)(\lambda_1\alpha_1 + \lambda_2\alpha^*\cos^2\beta)\rho g H$$
$$p_3 = \alpha_3 p_1$$
$$p_4 = p_1\frac{\eta^* - R^*_c}{\eta^*}$$
$$p_u = 0.5(1+\cos\beta)\lambda_3\alpha_1\alpha_3\rho g H$$

In which:

η: water elevation above the still water level;

H: incident wave height in front of the structure;

β: angle of incidence of the wave attack with respect to a line perpendicular to the structure;

$\alpha 1$, α^*, $\alpha 3$: multiplication factors dependent on the wave conditions and the water depth (see below);

$\lambda 1$, $\lambda 2$, $\lambda 3$: multiplication factors dependent on the geometry of the structure;

The α-factors are given by:

$$\alpha_1 = 0.6 + 0.5\left(\frac{4\pi h_s/L}{\sinh\left(4\pi h_s/L\right)}\right)^2$$
$$\alpha^* = \max\{\alpha_2, \alpha_I\}$$
$$\alpha_2 = \min\left(\frac{h_s - d}{3h_s}\left(H/d\right)^2, \frac{2d}{H}\right)$$

$$\alpha_I = \alpha_{I0} \cdot \alpha_{I1} \qquad \alpha_{I0} = \begin{cases} H/d & H \le 2d \\ 2 & H > 2d \end{cases}$$

$$\alpha_{I1} = \begin{cases} \dfrac{\cos\delta_2}{\cosh\delta_1} & \delta_2 \le 0 \\ \dfrac{1}{\cosh\delta_1 \cdot (\cosh\delta_2)^{0.5}} & \delta_2 > 0 \end{cases}$$

$$\delta_1 = \begin{cases} 20\delta_{11} & \delta_{11} \le 0 \\ 15\delta_{11} & \delta_{11} > 0 \end{cases} \qquad \delta_2 = \begin{cases} 4.9\delta_{22} & \delta_{22} \le 0 \\ 3.0\delta_{22} & \delta_{22} > 0 \end{cases}$$

$$\delta_{11} = 0.93\left(\frac{B}{L} - 0.12\right) + 0.36\left(\frac{h_s - d}{d} - 0.6\right)$$

$$\delta_{22} = -0.36\left(\frac{B}{L} - 0.12\right) + 0.93\left(\frac{h_s - d}{d} - 0.6\right)$$

$$\alpha_3 = 1 - \frac{h_s}{h'}\left(1 - \frac{1}{\cosh\left(2\pi h_s / L\right)}\right)$$

When the wave pressures are known, the wave forces are given by:

$$F_h = \frac{1}{2}(p_1 + p_4)R_c^* + \frac{1}{2}(p_1 + p_3)(d + d_c)$$

$$F_v = \frac{1}{2}p_u B_c$$